UNIVERSITY OF CALIFORNIA, SAN DIEGO

Elucidating Mechanisms of Neuronal Dysfunction Caused by Familial Alzheimer's Disease Mutations in iPSC Derived Neurons

A dissertation submitted in partial satisfaction of the requirements for the degree

Doctor of Philosophy

in

Biomedical Sciences

by

Grace Elaine Woodruff

Committee in charge:

Professor Lawrence S. B. Goldstein, Chair
Professor Arshad Desai
Professor Sylvia Evans
Professor Alysson Muotri
Professor Peter Novick

2015

The Dissertation of Grace Elaine Woodruff is approved, and it is acceptable in quality and form for publication on microfilm and electronically:

_____

_____

_____

_____

_____

Chair

University of California, San Diego

2015

DEDICATION

For my family

TABLE OF CONTENTS

LIST OF ABBREVIATIONS

APP. Amyloid Precursor Protein

AD. Alzheimer's Disease

Aβ. Amyloid-beta

Ca^{2+}. Calcium

CTF. C-Terminal Fragment

FAD. Familial Alzheimer's Disease

iPSC. Induced Pluripotent Stem Cell

LDL. Low Density Lipoprotein

LDLR. Low Density Lipoprotein Receptor

LRP1. Low Density Lipoprotein Receptor-Related Protein 1

SAD. Sporadic Alzheimer's Disease

PS1. Presenilin-1

PS1 ΔE9. Presenilin-1 Delta Exon 9 Mutation

PS2. Presenilin-2

γ-Secretase. Gamma-Secretase

β-Secretase. Beta-Secretase

α-Secretase. Alpha-Secretase

LIST OF FIGURES

LIST OF TABLES

ACKNOWLEDGEMENTS

I would like to thank my advisor, Dr. Larry Goldstein, for his support and guidance during my time in graduate school. Larry gave me a lot of freedom to explore different areas of research, which really promoted my growth as a scientist. He provided many insights into my results and helped with designing future experiments. Additionally, I thank Larry for encouraging participation in scientific meetings, which allowed me to travel and experience new cities, cultures, and scientific ideas. I came to graduate school knowing that I would grow as a scientist, but I truly believe that being a member of the Goldstein lab pushed me beyond what I would have accomplished in another laboratory, so I thank Larry for allowing me to be a member of his tremendous group of researchers.

I would like to thank the members of my thesis committee for their time and insight into my research. Dr. Alysson Muotri was always so encouraging and enthusiastic and really gave me a lot of confidence in my research. Dr. Arshad Desai, Dr. Peter Novick, and Dr. Sylvia Evans were very supportive and gave great feedback during my committee meetings. I really appreciate all of the members of my committee for taking the time to help me grow as a scientist.

I would also like to thank Dr. Nephi Stella and Dr. Richard Gardner who were my advisors as an undergraduate at the University of Washington. They both allowed me to have independent research projects as an undergraduate, which laid the foundation for all that I have been able to accomplish in graduate school. I am so

grateful that they both gave me the opportunity to work in their labs and took the time to impart knowledge to me.

I would like to thank all of the members of the Goldstein lab, past and present, who were friends, mentors and colleagues during my time in the lab. Specifically I would like to thank Cheryl Herrera, Jessica Young and Lauren Fong for being the best bay mates, friends and colleagues that I could hope to have. They really enriched my time in graduate school on both a scientific and personal level. I would like to acknowledge Sol Reyna for her work on various collaborative projects, her microscope and computer skills saved me endless amounts of frustration had I done those tasks myself. Angels Almenar-Queralt was a wonderful mentor and brilliant scientist who provided important insights into my research throughout my graduate career.

I would like to thank all of the wonderful people that I met in the BMS graduate program who provided friendship throughout my time in graduate school. The BMS program truly has exceptional individuals and I am thankful to have gotten to know so many of them. I would also like to acknowledge Adam Bastidas, who is my best friend, for his endless support. I am eternally grateful to the hours that Adam spent discussing science, lab, and many other topics and truly helped keep me motivated and for the most part, positive during my graduate career.

Last but definitely not least, I want to thank my family. I thank my Mom, Dr. Michelle Sexton, for encouraging me to join a lab as a freshman at the University of Washington. A big reason that I came to graduate school was because of the many hours that I spent in Seattle with my Mom both in the lab and at home discussing

research. Her encouragement and support throughout my academic pursuits are a huge reason that I have been successful and followed my dream of getting a PhD. I thank my Dad, Tom Woodruff, for all of his love and support throughout my academic journey. I really appreciate all of his encouragement and support over the years that I have been in graduate school. I thank my grandparents, Jim and Sue Sexton, for being wonderful human beings and for helping to shape me into the person that I am today. I thank my siblings, Jordan, Micahl, Naomi and Miriam, for all of their support and love. I thank my nephew, Levi, and nieces, Emery and Claire, for bringing me so much joy.

Chapter 2, in full, was published as The Presenilin-1 ΔE9 Mutation Results in Reduced γ-Secretase Activity, but not Total Loss of PS1 Function, in Isogenic Human Stem Cells. Woodruff G, Young JE, Martinez FJ, Buen F, Gore A, Kinaga J, Li Z, Yuan SH, Zhang K, Goldstein LS. The presenilin-1 ΔE9 mutation results in reduced γ-secretase activity, but not total loss of PS1 function, in isogenic human stem cells. Cell Rep. (2013) The dissertation author was the primary investigator and author of this work.

Chapter 3, in full, will be published in the near future with the tentative title of Reduced Endocytic Recycling and Transcytosis of APP and Lipoproteins Owing to Accumulation of APP β-CTFs in Familial Alzheimer's Disease Mutations. Reyna, S.M., Woodruff, G, Dunlap, M., Kloss, N. Goldstein, LS. The dissertation author was the primary researcher and author of this work.

VITA

Education

2015 Ph.D., Biomedical Sciences
University of California, San Diego

2009 B.S., Neurobiology
University of Washington, Seattle

Publications

Reyna, S.M., **Woodruff, G**., Dunlap, M., Kloss, N., and Goldstein, L.S. Reduced endocytosis and transcytosis of APP and lipoproteins owing to accumulation of APP β-CTFs in familial Alzheimer's disease mutations. (To be published)

Young, J.E., Boulanger-Weill, J., Williams, D.A., **Woodruff, G.**, Buen, F., Revilla, A.C., Herrera, C., Israel, M.A., Yuan, S.H., Edland, S.D., and Goldstein, L.S. (2015). Elucidating molecular phenotypes caused bye the SORL1 Alzheimer's disease genetic risk factor using human induced pluripotent stem cells. Cell Stem Cell. 16, 373-385.

Goldstein, L.S., Reyna, S., and **Woodruff, G**. (2015). Probing the secrets of Alzheimer's disease using human-induced pluripotent stem cell technology. Neurotherapeutics. 12, 121-125.

Liu, Q., Walts, S., **Woodruff, G**., Ouyang, J., Israel, M.A., Herrera, C., Sarsoza, F., Tanzi, R.E., Koo, E.H., Ringman, J.M., Goldstein, L.S., Wagner, S.L., and Yuan, S.H. (2014). Effect of potent γ-secretase modulator in human neurons derived from multiple presenilin-1 induced pluripotent stem cell mutant carriers. JAMA Neurol. 71, 1481-1489

Lu, P., **Woodruff, G**. Wang, Y., Graham, L., Hunt, M., Wu, D., Boehle, E., Ahmad, R., Poplawski, G., Brock, J., Goldstein, L.S., and Tuszynski, M.H. (2014). Long-distance axonal growth from human induced pluripotent stem cells after spinal cord injury. Neuron. 83, 4789-796.

Woodruff, G., Young J.E., Martinez, F.J., Buen, F., Gore, A., Kinaga, J., Li, Z., Yuan, S.H., Zhang, K., and Goldstein L.S. (2013). The presenilin-1 ΔE9 mutation results in reduced γ-secretase activity, but not total loss of PS1 function, in isogenic human stem cells. Cell Rep. 5, 974-985.

Sexton, M., **Woodruff, G**., Horne, E.A., Lin, Y.H., Muccioli, G.G., Bai, M., Stern, E., Bornhop D.J., and Stella, N. (2011). NIR-mbc94, a fluorescent ligand that binds to endogenous cB2 receptors and is amendable to high-throughput screening. Chem. Biol. 18, 563-568.

Marrs, W.R., Blankman, J.L., Horne, E.A., Thomazeau, A., Lin Y.H., Coy, J., Bodor, A.L., Muccioli, G.G., Hu, S.S., **Woodruff, G**., et al. (2010). The serine hydrolase ABHD6 controls the accumulation and efficacy of 2-AG at cannabinoid receptors. Nat Neurosci. 13, 951-957.

Sexton, M., **Woodruff, G**., Cudaback, E., Kreitzer, F.R., Xu, C., Lin, Y.H., Moller, T., Bai, M., Manning, C.H., Bornhop, D., and Stella N. (2009). Binding of NIR-conPK and NIR-6T to astrocytomas and microglial cells: evidence for a protein related to TSPO. PLoS ONE 4, e8271.

ABSTRACT OF THE DISSERTATION

Elucidating Mechanisms of Neuronal Dysfunction Caused by Familial Alzheimer's Disease Mutations in iPSC Derived Neurons

by

Grace Elaine Woodruff

Doctor of Philosophy in Biomedical Sciences

University of California, San Diego, 2015

Professor Lawrence S. B. Goldstein, Chair

Alzheimer's disease is a devastating neurodegenerative disorder with no clear etiology and no cure. Familial Alzheimer's disease is caused by mutations in the Amyloid Precursor Protein, Presenilin-1 and Presenilin-2, and mutations in Presenilin-1 are the most common cause of the familial form of the disease. Mouse and non-neuronal models of Alzheimer's disease do not fully recapitulate the disease that is seen in humans, which limits our understanding of the underlying cause of disease. Additionally, Presenilin-1 has many reported functions, but it is unclear which functions contribute to neuronal dysfunction and ultimately neuronal cell death in the

Alzheimer's brain. We developed an isogenic stem cell model of familial Alzheimer's disease to elucidate how Presenilin-1 mutations cause neuronal dysfunction. Using human neurons with a Presenilin-1 mutation, we have found that Preseniln-1 mutations are not simple loss-of-function mutations and that an increase in the more aggregation-prone amyloid-beta fragments does not necessarily lead to an increase in hyperphosphorylated tau. Furthermore, we have found that a Presenilin-1 mutation alters trafficking pathways of the amyloid precursor protein and lipoproteins, which could contribute to the phenotypes that are observed in Alzheimer's disease. These data implicate that the γ-secretase function of Presenilin-1 not only affects Amyloid Precursor Protein processing, but also affects trafficking and endocytosis of lipoprotein receptors and their cargo. Finally, we characterized an APP FAD mutation in both iPSC-derived neurons from patients and isogenic cells where the mutation was introduced into a control genetic background. We found that this APP mutation affects APP processing and tau accumulation, which is in contrast to a Presenilin-1 mutation. These data suggest that APP and Presenilin-1 mutations are not equivalent with respect to early detectable phenotypes.

Chapter 1

Introduction

Alzheimer's disease (AD) was first described in 1906 by Dr. Alois Alzheimer. AD is a chronic and fatal neurodegenerative disease with no cure, and is the most common cause of dementia. Currently, there are an estimated 36 million people worldwide with AD and that number is expected to quadruple in prevalence by the year 2050 (Brookmeyer, 2007). The most common initial symptom of AD is the inability to remember new information. As the disease progresses, cognitive and functional abilities decline, and the rate of decline varies between patients (Alzheimer's association, 2014). The primary pathologies found in the brains of AD patients postmortem are amyloid plaques and neurofibrillary tangles (NFTs). Amyloid plaques are extracellular and composed of amyloid-beta (Aβ) peptides that are generated from the full-length Amyloid Precursor Protein (APP). NFTs are intracellular and composed of hyper-phosphorylated tau protein. Another pathology reported in sporadic AD (SAD) patients and some patients with familial AD (FAD), is enlarged early endosomes (Cataldo et al., 2001). Additionally, brains of AD patients display massive synapse and cell loss particularly in the hippocampus and cortical areas.

1.1 Familial Alzheimer's Disease

Mutations that alter the processing of APP cause dominantly inherited AD, known as FAD. FAD is caused by autosomal dominant, highly penetrant mutations in three genes: APP, Presenilin-1 (PS1) and Presenilin-2 (PS2). A single extra copy of the APP gene also causes FAD (Rovelet-Lecrux et al., 2006). PS1 mutations are the most common cause of FAD with close to 200 mutations known to be pathogenic

(Bertram et al., 2010), APP mutations are less common, and PS2 mutations are the least common. Amyloidogenic APP processing generates the Aβ peptides that form the amyloid plaques and mutations in APP that cause FAD are clustered near the β and γ-secretase cleavage sites (Figure 1.2) PS1 and PS2 function as the catalytic core of the γ-secretase enzyme that generates the Aβ peptides and PS1 mutations are scattered throughout the PS1 gene (Figure 1.3). FAD is characterized by early disease onset before 65 years of age, but onset is often in the third or fourth decade of life (Kumar-Singh et al., 2006).

1.2 Sporadic Alzheimer's Disease

The vast majority of AD patients have SAD, where the precise cause of the disease remains elusive. The majority of SAD is also known as late onset AD (LOAD) as the age of onset occurs after 65 years of age. Recent genome wide association studies (GWAS) and other sequencing studies have identified many genes that are associated with SAD and it has been estimated that as much as 80% of AD risk is heritable (Gatz et al., 2006). The best-established genetic risk factor is the APOE gene, where the e4 allele of APOE increases the risk of AD 12-fold if two copies of e4 are present. Human APOE protein is an apolipoprotein and there are three major isoforms: APOE2, APOE3 and APOE4. Shortly after APOE4 was identified as the major genetic risk factor for SAD (Corder et al., 1993), APOE2 was found to be protective against SAD (Chartier-Hariln et al., 1994). Other risk factors identified by GWAS have much smaller effect sizes than APOE, typically between 1.1 and 1.3, whereas the

effect size for APOE4 is ~4 (Lambert et al., 2013). So far, all of the loci identified to date cluster in 3 major categories: immune function, cholesterol metabolism, and the endosomal system. This suggests that some or all of these pathways are important for developing AD and APP, the PS genes, and APOE all have reported function in these pathways.

1.3 Amyloid Precursor Protein Function

Human APP is a member of the APP family of proteins that also includes APLP1 (APP-like protein 1) and APLP2 (APP-like protein 2). Of these three proteins, APP is the only one with the Aβ domain, although APLP1 and APLP2 also undergo proteolytic processing. APP is a type 1 transmembrane protein with a small transmembrane and cytoplasmic domain and a large N-terminal extracellular domain. APP is expressed throughout the body in most tissues, but is highly expressed in the brain, especially in neurons (Zhang et al., 2014). Clues to the function of APP in mammals come from knockout studies in mice. Mice lacking any one APP family member are viable, but APP/APLP2 and APLP1/APLP2 double knockouts are embryonic lethal as are APP family member triple knockout. APP knockout mice are viable, but have reduced body weight, reduced locomotor activity, altered forelimb strength and gliosis (Zheng et al., 1995). These relatively mild phenotypes suggest that other APP family members can compensate for loss of APP. Studies from organisms with a single APP family member point to roles in development and axonal transport. For example, in *Caenorhabditis elegans*, APL-1 knockout results in embryonic lethality due to a molting defect (Hornsten et al., 2007). In *Drosophila,* overexpressing

APPL or human APP induces axonal transport defects that are independent of Aβ (Gunawardena and Goldstein, 2001; Torroja et al., 1999). In addition to these functions, it has also been proposed that APP controls lipoprotein metabolism via interactions with lipoprotein receptors (Kounnas et al., 1995).

1.4 APP Trafficking and Cleavage

APP is present in both the somatodendritic region and axon of human neurons. In axons, APP undergoes fast axonal transport with the majority of APP traveling in the anterograde direction (Rodrigues et al., 2012). APP is reported to reach the axon by at least two pathways: 1) direct delivery from the transgolgi compartment and 2) indirect delivery where first APP travels to the somatodendritic compartment, undergoes endocytosis and then is transcytosed to the axon (Niederst et al., 2014). APP undergoes complex and extensive proteolytic processing, which suggests that various proteolytic fragments could carry out APP functions. Proteolytic processing events are proposed to occur after APP is synthesized and transported to the cell surface. At the plasma membrane APP is cleaved by α-secretase, which generates the sAPPα and α-CTF (or C83) fragments, this proteolytic pathway is known as the non-amyloidogenic pathway as the initial cleavage by α-secretase abolishes the Aβ peptide (Figure 1.1). ADAM10 is proposed to be the major α-secretase in neurons (Kuhn et al., 2010). Additionally, ADAM10 mutations are associated with late-onset AD (Kim et al., 2009). The α-CTF is then endocytosed and undergoes further cleavage by γ-secretase which generates the APP intracellular domain (AICD) and p3 fragments. γ-secretase cleavage of α-CTF could occur in late endosomes, the ER, or both

compartments. Full-length APP undergoes the amyloidogenic pathway when APP is endocytosed and then cleaved by the β-secretase. The β-site APP-cleaving enzyme 1 (BACE-1) is the major β-secretase. β-secretase cleavage could occur in early endosomes, but the pH optimum for β-secretase is lower than the typical pH for an early endosome raising the possibility that β-cleavage actually occurs in more acidic organelles such as late endosomes (Takahashi et al., 2002; Vieira et al., 2010). Cleavage by β-secretase generates sAPPβ and the β-CTF (or C99) fragments (Figure 1.2). The β-CTF is further cleaved by γ-secretase, which generates the AICD and Aβ fragments. Aβ fragments can range in length, and many FAD APP mutations increase longer forms of Aβ (Moore et al., 2015). Recent data suggests that the majority of endogenous Aβ is generated in the somatodendritic compartment in a pathway that is dependent on endocytosis (Niederst et al., 2014).

1.5 APP FAD Mutations

Mutations in 18 of the 770 amino acids in APP cause inherited FAD and over 30 mutations are known. Most FAD mutations are close to α-, β-, and γ-secretase cleavage motifs and affect the proteolytic processing of APP (Figure 1.2). Additionally, duplication of the APP gene also causes dominantly inherited AD (Rovelet-Lecrux et al., 2006). In human neurons, APP mutations near the γ-secretase cleavage site increase the ratio of Ab42/40 peptides and also seem to affect β-secretase cleavage (Muratore et al). A mutation near the α-secretase cleavage site, K687N, makes APP a poor substrate for α cleavage (Citron et al., 1992). The APP Swedish mutation (K670N/M671NL), next to the β-cleavage site, has been shown to promote

β-cleavage of APP thereby increasing the β-CTF and Aβ peptides (Citron et al., 1992). Thus, most APP mutations seem to shift APP cleavage to the amyloidogenic route or to increase longer forms of Aβ peptides. Further evidence that enhanced β-cleavage is directly related to AD comes from recent identification of a protective APP mutation that seems to act by decreasing β-cleavage of APP (Jonsson et al., 2012). Finally, APP duplication also causes FAD and increases all full-length APP and likely all of the APP cleavage fragments. It should be noted that in addition to affecting APP processing, APP FAD mutations might also alter sorting pathways or signaling at endosomal and other vesicular intermediates. For example, APP duplication both in Down's Syndrome and FAD has been shown to increase the size of early endosomes (Cataldo et al., 2003; Israel et al., 2012), and presently the cause of such changes are unknown, but could contribute to AD pathology.

1.6 Presenilin-1 Function

The presenilin family of proteins consists of PSEN1 and PSEN2. Presenilins are multipass transmembrane proteins and function as the catalytic core of the γ-secretase complex and have reported γ-secretase independent functions. PSEN1 knockout mice are embryonic lethal, which highlights a role for PSEN1 in development and also suggests that PSEN1 has functions that cannot be compensated for by PSEN2. PSEN2 knockout mice are viable and considered normal other than discrete lung fibrosis (Herreman et al., 1999). Studies in flies mice and worms all point to a crucial role for PSEN1 in Notch signaling and Notch is a γ-secretase substrate. PS1/PS2 double knockout mice are embryonic lethal and have severe somite

segmentation defects and neural tube malformations (Donoviel et al., 1999). The γ-secretase complex is composed of four different subunits including PS1 or PS2, Pen-2, APH1 and Nicastrin with all subunits present in a 1:1:1:1 stoichiometry (Sato et al., 2007). The majority of known γ-secretase substrates are type 1 transmembrane proteins such as Notch and APP, and there are currently around 100 known substrates (Haapasalo and Kovacs, 2011). γ-secretase substrates have roles in a wide variety of functions including transcriptional regulation, regulation of cell death, regulation of cell fate, neuritis outgrowth and cell adhesion, and others (Haapasalo and Kovacs, 2011). Therefore, aberrant γ-secretase activity could lead to a wide variety of phenotypes. In addition to γ-secretase dependent functions of PS1, there are many examples of γ-secretase independent functions as well. For example, PS1 has been reported to be involved in the maturation and trafficking of various membrane proteins including Nicastrin and TrkB (Leem et al., 2002; Naruse et al., 1998). PS1 has been shown to be involved in Wnt signaling through destabilization of B-catenin. More recently, a role for PS1 in lysosomal acidification was described (Lee et al., 2010), although this finding has so far failed to be replicated by another group (Coen et al., 2012). Finally, presenilins have been reported to form low-conductance divalent cation channels, and in knockout cells these channels were reported to account for 80% of calcium leak from the endoplasmic reticulum (Tu et al., 2006). Presenilins may also have a role in lysosomal Ca^{2+} levels (Coen et al., 2012). All of these finding highlight a diverse role for presenilins and disruption of all or any of these functions could contribute to the neurodegeneration that is observed in the patients with presenilin mutations.

1.7 Presenilin FAD Mutations

Mutations in PS1 are the most common cause of FAD with almost 200 mutations reported to be pathogenic (Wu et al., 2012). The majority of PS1 mutations are single nucleotide substitutions, but inframe deletions and insertions have also been described (Figure 1.3). Thus far, null PS1 mutations have not been reported to co-occur with AD, but rather cause a skin disorder known as Familial Acne Inversa (Wang et al., 2010). Patients with PS1 mutations present with all of the typical signs of AD, but the neuropathology can differ somewhat from sporadic or APP mutations. For example, patients with mutations affecting exons 8 and 9 are associated with cotton wool plaques, which are devoid of a dense amyloid core. These patients also often present with other clinical phenotypes such as spastic paraparesis (Dumanchin et al., 2006). In general, it should be noted that there is considerable neuropathological heterogeneity across different APP and PS mutations (Larner and Doran, 2006).

A central question in the study of PS1 mutations has been whether these mutations cause disease through a gain or loss-of-function mechanism. It seems that there is now somewhat of a consensus that PS1 mutations impair γ-secretase activity, because many different PS1 mutations display accumulation of γ-secretase substrates such as Notch, APP CTFs, or N-cadherin CTFs (Bentahir et al., 2006; Chávez-Gutiérrez et al., 2012). However, it should also be noted that accumulation of γ-secretase substrates could also occur due to decreased degradation in the autophagy/lysosomal system where PS1 has also been implicated independent of γ-secretase activity (Lee et al., 2010; Neely et al., 2011). The first evidence of FAD

mutations impairing PS1 function came from studies in C. *elegans*. Loss-of-function mutations in the C. *elegans* PS homolog, SEL12, was shown to be rescued by PS1 and PS2, but not by six different FAD mutations (Levitan et al., 1996). Another primary argument for PS1 mutations acting as loss-of-function comes from conditional PS1 knockout mice in which PS are inactivated in the adult cerebral cortex. These mice develop neurodegeneration and similar pathology to AD including synaptic loss, neuronal death and tau hyper phosphorylation (Saura et al., 2004). A recent study that made knock-in mice harboring two different FAD mutations found that these mice shared similar phenotypes to the PS1 conditional knockout mice, which led the authors to conclude that FAD mutations are loss-of-function (Xia et al., 2015). Future studies investigating the cause of PS-mediated neurodegeneration will require careful interpretation of results as well as careful elucidation of which functions of PS1 are disrupted. Importantly, looking at both γ-secretase dependent and γ-secretase independent functions of PS1 will allow determination of which PS functions are disrupted and allow conclusions about whether FAD mutations are truly complete loss-of-function. Given the heterogeneity of clinical phenotypes that can accompany PS1 mutations, it seems unlikely that all mutations will fall into a single category of gain or loss-of-function.

1.8 Mouse Models of AD

There are many different genetic mouse models of AD, but perhaps the most important feature of these models is that none of them fully recapitulate all of the features that are seen in humans. Furthermore, many of the models overexpress APP

and PS1 mutations at levels that far exceed what is seen in patients. Given that a single extra copy of the APP gene in humans is sufficient to cause disease, models of gross overexpression may not be ideal to dissect early pathological changes. A full review of AD mouse models can be found here (Hall and Roberson, 2012), and below some of these models will be highlighted. APP mouse models of AD overexpress the Indiana (V717F), Swedish (KM670/671NL) or London (V7171) mutations (Calhoun et al., 1998; Games et al., 1995; Rockenstein et al., 2001). PS1 mouse models overexpress the M146L, ΔE9, and P246L mutations in addition to human APP with the Swedish mutation. Most of the models exhibit cognitive deficits and amyloid plaques, but tangles are generally only present when human tau with mutations that cause frontotemporal dementia (FTD) are also expressed. It is important to note that tau mutations do not cause AD, therefore the utility of models expressing FTD tau mutations probably does not represent what occurs in AD. The 3xTg model, which expresses human APP with the Swedish mutation, human tau with the P301L mutation and PS1 M146V mutation, develops plaques before tangles as is seen in human AD (Oddo et al., 2003). As mentioned above, the e4 allele of APOE is the strongest genetic risk factor for AD and APOE mouse models of AD also exist.

1.9 Stem Cell Models of AD

Human induced pluripotent stem cells (aspics) (Takahashi et al., 2007a) are a powerful tool for modeling human disease in cell types like neurons and cardiomyocytes that are not readily accessible cell types. In years since aspics were first published many exciting studies have published successful recapitulation of

disease phenotypes from a variety of diseases including AD. The first study to use iPSC-derived neurons to model AD used fibroblasts from 2 non-demented controls (NDCs), 2 patients with SAD, and 2 patients with FAD caused by a duplication of the APP gene (Papp) (Israel et al., 2012). This study reported that the 2 APPdp patients and one of the SAD patients exhibited increased Ab40 and an increased ratio in the level of phosphorylated tau to total tau (p-tau/t-tau) at the T231 phosphorylation site. Therapeutic insight came from the finding that β-secretase inhibitors, but not γ-secretase inhibitors, decreased the p-tau/t-tau ratio, which suggests that excess β-CTF of APP is directly related to phosphorylated tau and not Aβ. Since this first study, many others have also modeled FAD caused by APP mutations. One study generated neurons from APP E693delta and APP V717L patients (Kondo et al., 2013) and found that E693delta neurons had decreased total Aβ while V717L neurons exhibited an increase in the Aβ 42/40 ratio. They also reported that E693delta neurons accumulated intracellular Aβ oligomers and that one patient with SAD also shared this phenotype. They did not report any measurements of phosphorylated or total tau. A more recent paper generated neurons from patients with the APP V717I mutation ((Muratore et al., 2014) and reported an increase in the Aβ 42/40 ratio and also reported an increase in the amount of sAPPβ. In addition to the changes in APP processing, they also reported increased levels of total and phosphorylated tau, and at later time points, an increase in the p-tau/t-tau ratio.

In addition to iPSC models of FAD APP mutations, there have also been several studies with PS1 and PS2 FAD mutations. Mutations analyzed include the PS1 A246E, PS1 A79V, PS1 M146L, PS1 H163R and PS2 N141I (Koch et al., 2012; Liu

et al., 2014; Sproul et al., 2014; Yagi et al., 2011). All of these studies have reported an increase in the Aβ 42/40 ratio. Interestingly, all of the studies failed to find or report any changes in abundance of phosphorylated or total tau.

Finally, in addition to the above studies that reported SAD phenotypes from a limited number of patients, one study investigated a risk factor for AD in a large number of individuals (Young et al., 2015). This study looked at SNPs in the gene SORL1, which has consistently been associated in GWAS with AD (Rogaeva et al., 2007). They found that individuals that were homozygous for SNPs associated with AD risk were unable to induce expression of SORL1 upon addition of the growth factor BDNF, while individuals with protective variants induced SORL1 expression and consequently reduced Aβ levels. Another study investigated 3 SAD patients with an APOE3/4 genotype and reported that 2 of the SAD patients had increased Ab 42/40 ratio (Duan et al., 2014).

Although iPSC technology, especially for use with brain cell types, is still in its infancy, the studies published to date highlight the possibility that this system can provide new insights to a complex disease. The early work has been valuable in providing mechanistic insights into FAD pathology, and work with neurons from SAD patients is just getting underway. Moving forward, models with more complex culture systems in which more cell types from the brain can interact will be valuable in advancing this growing field. Additionally, larger studies of sporadic patients will allow dissection of how complex genetic background can give rise to AD. The Young et al, study is an exciting example of how iPSC-derived neurons can be used to stratify patients that might respond to a particular therapeutic and studies from FAD patients

where reproducible AD-related phenotypes are present is a system in which drug screening could be carried out. Going forward, studies utilizing iPSC-derived neurons to probe mechanisms of disease beyond the Aβ and tau pathways will provide important insights to this complex disease.

1.10 Amyloid Cascade Hypothesis

The prevailing hypothesis in the AD field is called the "Amyloid Cascade Hypothesis". This hypothesis proposes that Aβ peptides aggregate into toxic oligomers, which initiates hyper phosphorylation of tau and ultimately synapse loss and cell death. The Amyloid Cascade theory is not without its problems, the most significant of which is that extensive amyloid deposits can be found in the brains of elderly individuals who do not have signs of dementia (Bennett et al., 2006). Further problems with this hypothesis stem from drug trials aimed at reducing Aβ. A stage III clinical trial that blocks production of Aβ was halted because patients were not improving and in some cases their symptoms were worsening (Schor, 2011). As new research and models of AD emerge, our understanding of its cause will evolve.

1.11 Questions and Goals of the Thesis

The first major goal of the thesis was to generate an isogenic stem cell model of FAD caused by a PS1 mutation. Previous work from the Goldstein lab and others highlighted the need to have an isogenic system in which to study FAD mutations. The AD-related phenotypes that were measured from NDCs, SAD and FAD patients previously (Israel et al., 2012) can be quite variable due to individual genetic variation

or to variability in the iPSC generation process or subsequent differentiations. Once an isogenic stem cell model was generated, the first question to be answered was whether PS1 mutations are gain or loss-of-function.

Another major question to be answered was how a PS1 mutation affects trafficking of various proteins including APP. There are many reports in the AD literature of PS1 having a role in the trafficking of membrane proteins and how disruption of these pathways could cause some of the defects found in AD. An advantage to the iPSC system is that protein trafficking can be investigated in the absence of overexpression of PS1 mutations or APP and in human neurons.

Finally, the other major goal of the thesis was to investigate differences between PS1 and APP mutations again utilizing an isogenic IPSC system. It is unknown whether various APP and PS1 mutations have similar or different initiating events that cause AD. To begin answering this question, these studies measured APP processing and total tau protein levels as well as phosphorylated tau levels and compared a PS1 and APP mutation.

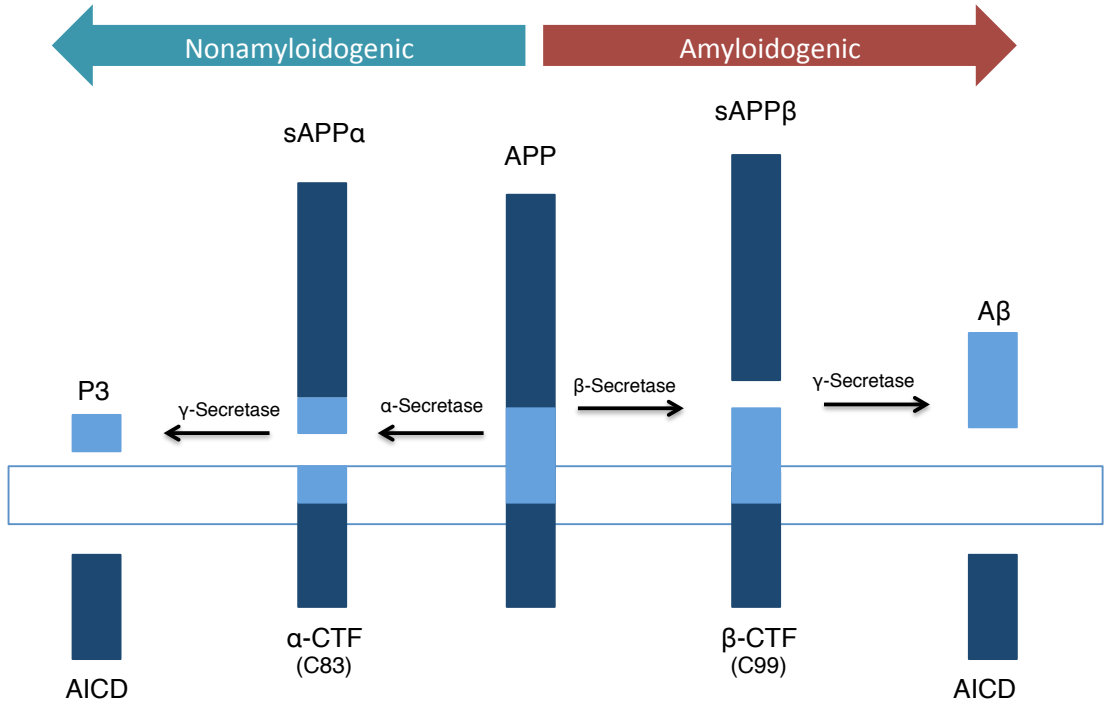

Figure 1.1. APP Processing. Full-length APP undergoes proteolytic processing by two different pathways: Nonamyloidogenic and Amyloidogenic. In the nonamyloidogenic pathway, full-length APP first gets cleaved by α-secretase, which generates the sAPPα and α-CTF (also known as C83) fragments. The α-CTF is then further cleaved by γ-secretase, which generates the P3 and AICD fragments. In the amyloidogenic pathway, full-length APP is first cleaved by β-secretase, which generates the sAPPβ and β-CTF (also known as C99) fragments. The β-CTF is then cleaved by γ-secretase, which generates Aβ peptides and the AICD fragment. Aβ peptides can range in length, but Aβ40 is the most abundant and most forms of FAD increase longer forms of Aβ, specifically Aβ42.

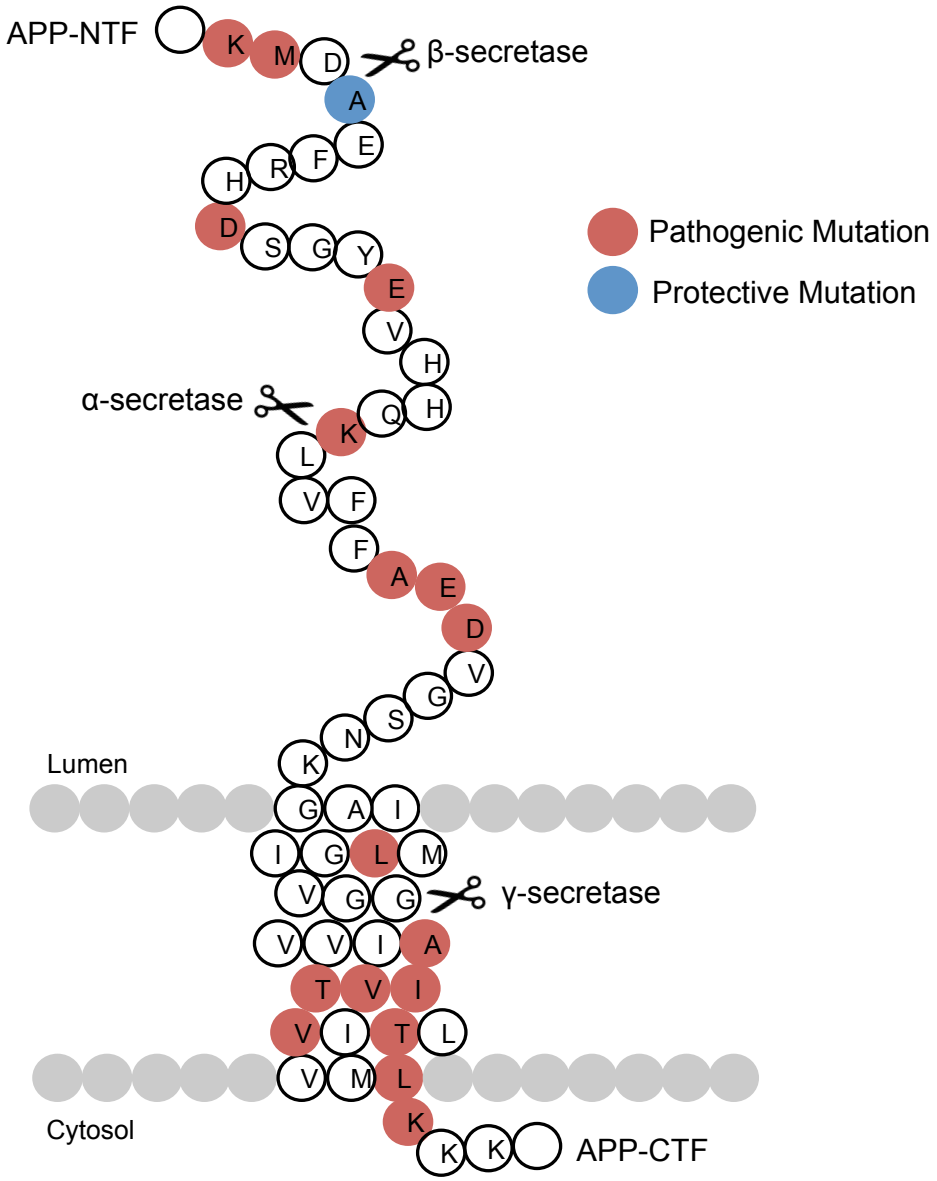

Figure 1.2. APP Mutations. Diagram of the region of APP that undergoes processing and where pathogenic mutations have been identified. Red circles indicate a pathogenic mutation at that amino acid. The blue circle indicates a site where a protective mutation has been identified at that amino acid. As can be seen in the diagram, most mutations are clustered around the various cleavage sites.

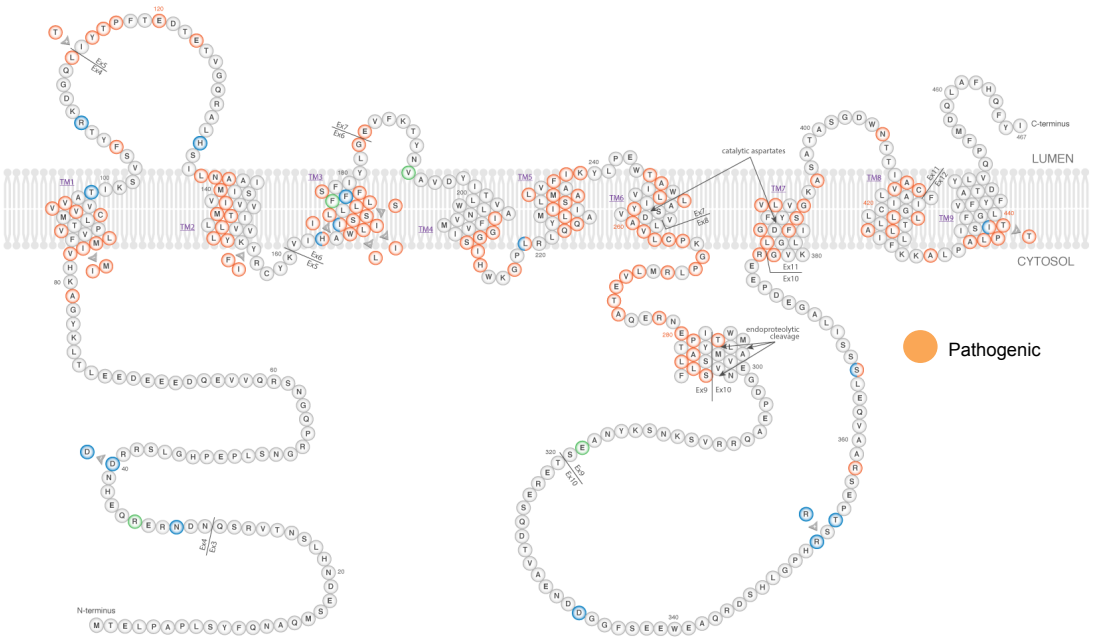

Figure 1.3. PS1 Mutations. Diagram of the PS1 gene and where pathogenic mutations have been identified. Orange circles indicate a pathogenic mutation at that amino acid. As can be seen in the diagram, mutations that cause FAD are spread throughout the PS1 protein.

Chapter 2

The Presenilin-1 ΔE9 Mutation Results in Reduced γ-Secretase Activity, but not Total Loss of PS1 Function, in Isogenic Human Stem Cells

2.1 Introduction

Alzheimer's Disease (AD) is a progressive neurodegenerative disease that is the most common cause of dementia (Barnes and Yaffe, 2011). Pathologically, AD is characterized by amyloid plaques consisting of Amyloid-beta (Aβ) peptides and neurofibrillary tangles composed of hyper-phosphorylated tau protein. While the precise mechanism that causes AD is still under investigation, key proteins involved in the disease have been identified. The Amyloid Precursor Protein (*APP*) and the presenilin genes (*PSEN1* and *PSEN2*) are all implicated in AD because mutations in these genes cause dominantly inherited forms of the disease. Presenilin 1 (PS1) is a multipass transmembrane protein with multiple biological functions. PS1 undergoes proteolytic processing (Thinakaran et al., 1996) to form N and C-terminal fragments, which then associate with Nicastrin, APH-1 and PEN-2 to form the γ-secretase complex (Edbauer et al., 2003). PS1 functions as the catalytic core of γ-secretase, which cleaves type 1 transmembrane proteins such as APP, Notch and cadherins. When APP is cleaved by γ-secretase, the Aβ fragment, a main component of senile plaques, is generated. In addition, PS1 has γ-secretase independent functions such as maturation and trafficking of transmembrane proteins, including Nicastrin and TrkB (Leem, et al., 2002; Naruse, et al., 1998), and down-regulation of Wnt signaling through destabilization of β-catenin (Killick et al., 2001). More recently, PS1 has also been shown to control lysosome acidification (Lee et al., 2010; Wolfe et al., 2013).

Mutations in PS1 are the most common cause of FAD, with over 100 mutations reported to be pathogenic (http://www.molgen.ua.ac.be/ADMutations, (Bertram et al., 2010). The dominant amyloid cascade hypothesis posits that FAD mutations act by increasing the formation of toxic Aβ fragments of APP, which are generated by sequential cleavage of APP by β-secretase and then by γ-secretase. The most abundant form (ca. 85%) of the Aβ peptide contains 40 amino acid residues (Aβ40), with a minority (ca. 15%) of an alternative species containing 42 amino acids, Aβ42. FAD PS1 mutations generally increase the proportion of the Aβ42 peptide, which is thought to be the key agent that causes the pathological changes in FAD (Scheuner et al., 1996). Whether PS1 mutations cause increases in Aβ42 and therefore FAD by a gain or loss-of-function mechanism remains controversial. Controversy persists because virtually all previous studies probing the nature of FAD PS1 mutations have relied on experimental manipulations that overexpress PS1 and PS1 mutants in mouse and/or non-neuronal systems (Bentahir et al., 2006; Chávez-Gutiérrez et al., 2012; Kumar-Singh et al., 2006) or that express mutant forms of PS1 in competition with wild-type forms in cell types that may not have normal levels of expression of other key genes. For example, studies of cultured neurons completely lacking PS1 results in near absence of Aβ generation suggesting that FAD PS1 mutations cause a gain-of-function (Simons et al., 1998). Paradoxically, removal of PS1 from neurons in the adult mouse brain causes neurodegeneration with aspects of neuropathology similar to that seen in AD (Saura et al., 2004). This result led to the suggestion that FAD PS1 mutations generate loss-of-function of PS1. Similarly, studies using overexpression of PS1 FAD mutations are difficult to interpret, primarily

because overexpression of FAD PS1 mutants do not accurately recapitulate normal activity and function of the PS1 protein, and because these studies are done in non-neuronal cell types that do not express the same amounts of key PS1 interacting proteins as in neurons. Finally, since mouse models of FAD do not fully recapitulate the pathologies seen in human patients (Ashe and Zahs, 2010; Games et al., 1995; Radde et al., 2008), differences between mouse and human responses to FAD PS1 mutations may be important.

In view of the persistent controversy about the mechanism of dysfunction caused by FAD PS1 mutations we set out to test whether a key and representative FAD PS1 mutation, PS1 Δe9, expressed at endogenous levels in human neurons and in an isogenic genetic background, is similar to or different from targeted PS1 haploinsuficiency. To achieve this goal we used induced pluripotent stem cell (iPSC) technology (Takahashi, et al., 2007), which provides the opportunity to study bona fide human neuronal cells that express normal levels of neuronal genes, proteins, and pathways. To compare the effects of specific mutations in a controlled isogenic genetic background, we used genome-editing technology with TAL Effector Nucleases (TALENs) (Miller et al., 2011; Sander et al., 2011) to generate and study an allelic series of PS1 mutations including the FAD PS1 ΔE9 mutation. This mutation lacks the PS1 endoproteolysis site, thus preventing normal PS1 cleavage during maturation, which facilitates precise quantitative determination of the level of mutant protein in neuronal cells. We compared the phenotypic consequences of FAD PS1 ΔE9 mutations to heterozygous PS1 null mutations, which enabled us to rigorously

conclude that the PS1 ΔE9 mutant acts as a dominant gain-of-function mutation by poisoning intact γ-secretase enzyme complexes in human neuronal cells.

2.2 Results

Generation of isogenic iPSC lines carrying different PS1 mutations with TALENs

There are several genome-editing methods that have been used to edit iPSCs, zinc finger nucleases (ZFNs) (Soldner et al., 2011), TALENs (Hockemeyer et al., 2011) and more recently the CRISPR/Cas9 system (Mali et al., 2013). We compared both ZFNs and TALENs (Figure 2.1) and used TALENs for our genome-editing strategy. We designed TALENs to target the PS1 gene in the genome of iPSCs derived from J. Craig Venter (Gore et al., 2011), whose genome has been sequenced and is publicly available (Levy et al., 2007). The FAD PS1 ΔE9 mutation is a point mutation in the splice acceptor consensus sequence of intron 8 that causes in-frame skipping of exon 9 (Perez-Tur et al., 1995). To introduce the ΔE9 point mutation, we used single stranded oligodeoxynucleotides (ssODNs) (Chen et al., 2011) as the repair template with 60bp of PS1 homology on either side. We recovered and screened 192 clonal iPSC lines using allele specific PCR to identify lines that had the ΔE9 mutation. From 192 candidate lines, 14 lines amplified in the allele specific PCR. We cloned and sequenced the PCR products to test whether candidate lines had incorporated 1 or 2 copies of the ΔE9 mutation and whether candidate lines had any disruption of the PS1 gene (i.e., insertions or deletions). This analysis resulted in recovery of an allelic series of PS1 mutations in otherwise isogenic iPSCs (Table 2.1 and Figure 2.2 A). Although our strategy was not designed to detect iPSC lines with disruption of the PS1 locus, we

obtained 1 line with disruption of 1 PS1 allele (wt/null) caused by insertion of one nucleotide in exon 9. This single nucleotide insertion interrupts the PS1 open reading frame, causes a premature stop codon, and likely induces nonsense mediated decay of the PS1 mRNA templated by this allele (Figure 2.2 B). In total, we generated 3 lines with 1 copy of the ΔE9 mutation (wt/Δe9), and 2 lines that were homozygous for the ΔE9 mutation (Δe9/Δe9), 2 lines with 1 allele containing the ΔE9 mutation and the other allele an insertion in exon 9 that disrupts the PS1 gene (Δe9/null).

Since γ-secretase activity is key to many developmental pathways(Herreman et al., 1999), we tested whether introducing the FAD PS1 ΔE9 mutation, or disrupting one copy of the PS1 gene affects pluripotency. Staining of iPSC lines with a typical cell surface pluripotency marker, Tra-1-81, revealed no obvious differences between mutant and control lines (Figure 2.1 F). To test neuronal differentiation, we generated neural progenitor cells (NPCs) from the isogenic iPSCs. Two NPC lines per genotype were generated, with the exception of the wt/null genotype where we only obtained 1 iPSC line (Table 2.1). We used the PA6 coculture differentiation protocol previously used in our lab (Yuan et al., 2011) along with dual SMAD inhibition (Chambers et al., 2009)to generate NPCs. After the 12-day differentiation period, we FACS purified the NPCs (Yuan, et al., 2011) to remove undifferentiated cells and contaminants. We found no significant differences in the percentage of NPCs marked by cell surface markers between the different genotypes (Figure S2A).

TALEN-targeted iPSC lines harbor few new protein coding mutations

Recent studies suggest that reprogrammed iPSC lines can accumulate elevated frequencies of genetic and epigenetic changes potentially owing to reprogramming and subsequent selection during culture and expansion (Gore et al., 2011; Hussein et al., 2011; Lister et al., 2011). Similarly, a concern with using genome-editing strategies such as TALENs or ZFNs is the occurrence of off-target effects, in particular DSBs, which may generate insertions or deletions in protein-coding regions other than those intended for targeting. Because targeted iPSCs were subcloned after genome-editing with the TALENs in order to generate clonal cell lines, detecting mutations due to off-target genome editing is complicated by the potential mutational effects of the subcloning process itself.

To address these concerns, we performed whole-exome sequencing on our TALEN-modified iPSC lines and the parent iPSC line, and compared the resultant mutational load to that found between non-modified iPSC subclones and human embryonic stem cell (hESC) subclones and their iPSC and hESC parent population. We generated three single-cell subcloned lines each for two iPSC lines (CVB and CVI) and one hESC line (Hues 9). We analyzed the mutational load of the protein-coding regions of the genome by performing exome sequencing on these nine subcloned lines, the six TALEN-edited lines, and the parent iPSC and hESC lines. We observed a very low frequency of protein-coding mutations (0-3) in each of the subcloned lines. Additionally the number of acquired mutations did not differ between the iPSC and hESC lines. The mutational load found in each of the non-modified iPSC and hESC subclones (Table 2.2) when compared to their mixed parent population was statistically very similar to the mutational load found in the TALEN-edited subclones

(Table 2.3) when compared to their mixed parent population (p=0.13), indicating that TALEN-based genome editing does not introduce an additional point mutational load over subcloning. Additionally, the edited subclones did not possess a detectable increase in indel count, indicating that insertions and deletions due to off-target DSBs did not seem to occur. Furthermore, the edited subclones did not possess any chromosome-level shifts in allele ratios at known SNP sites, indicating that the edited lines are not aneuploid. Taken together, these findings have led us to conclude that subcloning of iPSCs is not inherently highly mutagenic and that modification with TALENs is unlikely to cause any significant off-target effects.

Interestingly, recent work from Ding, et al., reports TALEN modification of Hues1 hESCs. In this paper, TALEN-modified subclones also demonstrated a low number of off-target effects as analyzed by whole exome and whole genome sequencing. However, across the subclones this group found 24 single-nucleotide variants in coding regions, approximately 10 times more than we found in our experiment. The reason for this difference is puzzling, but could possibly be due to differences in the number of passages the clones underwent prior to subcloning, differences in the maintenance of the cells (i.e. feeders vs. feeder-free conditions), or differences inherent to the particular cell line used. One possibility to circumvent this discrepancy and ensure truly isogenic cell lines would be to first subclone iPSCs or hESCs prior to genome-editing with TALENs.

PS1 mRNA is substantially reduced by null but not FAD ΔE9 PS1 mutations

To test whether the TALEN-induced mutations had the expected molecular effects on PS1 mRNA abundance, we harvested RNA from NPCs of each PS1 genotype and performed qRT-PCR analysis. We found that the wt/null line exhibited decreased PS1 mRNA to ca. 50% of normal (Figure 2.2 B), which confirmed that the nucleotide insertion in exon 9 results in loss of PS1 mRNA, likely due to nonsense mediated decay of the PS1 message. We also observed that the wt/ΔE9 lines and the ΔE9/ΔE9 lines did not significantly differ from wt/wt lines for PS1 mRNA, while ΔE9/null had ca. 50% of normal levels of PS1 mRNA (Figure 2.2 B). To evaluate PS1 mutant effects on PS1 protein abundance, we took advantage of the finding that PS1 undergoes endoproteolysis to generate a 26-27 kDa N-terminal fragment and a 16-17 kDa C-terminal fragment (Thinakaran, et al., 1996). Part of the endoproteolysis site is in exon 9 of PS1 and thus an important feature of the ΔE9 mutation is that the endoproteolysis site is destroyed. Therefore, lines containing 1 copy of ΔE9 are predicted to generate 50% of the cleaved product and 50% of the full-length (~44 kDa), while cells containing two copies of ΔE9 should not generate any of the cleaved products. Western blot analysis using a c-terminal antibody (Figure 2.2 C,D and E) revealed that these lines all behaved as predicted with wt/ΔE9 producing 50% of the uncleaved fragment, ΔE9/ΔE9 producing 100% of the uncleaved fragment and ΔE9/null producing only uncleaved fragment, but at 50% the level of ΔE9/ΔE9. To further confirm that the null mutations were indeed a true null allele and not a truncated protein with residual function, we also performed a western blot with an N-terminal antibody (Figure 2.1 G,H and I). Using an N-terminal antibody we also observed significantly decreased protein from cell lines harboring null PS1 alleles.

Thus, based on PS1 mRNA and protein production, we concluded that PS1 mutants induced in isogenic iPSC lines generated the expected effects on PS1 mRNA expression, protein production, and endoproteolysis.

The PS1 ΔE9 mutation increases the Aβ42/40 ratio in human neurons by decreasing Aβ40

APP normally undergoes several proteolytic processing events to generate a collection of soluble APP fragments including the APP intracellular domain (AICD) and Aβ peptides. Aβ peptides are generated when APP first undergoes cleavage by β-secretase and then by cleavage with γ-secretase. FAD mutations in APP, PS1, and PS2 have been shown to alter processing of Aβ, with most mutations reported to increase the Aβ42/40 ratio when expressed under a variety of conditions (Kumar-Singh et al., 2006; Qiang et al., 2011). Since APP processing in human neurons that generates Aβ peptides, in particular Aβ42, plays a key role in AD pathogenesis we tested for changes in APP processing in purified human neurons generated from isogenic human NPC lines with different PS1 mutations. Purified neurons were generated by differentiating NPCs for 3 weeks followed by FACS purification (Yuan, et al., 2011). We found no significant differences in the percentage of neurons generated between the different genotypes (Figure 2.4 B). We used a highly sensitive assay (Israel, et al., 2012) to measure Aβ 38, 40 and 42 species from purified cells and progenitors. We found that cell lines harboring one copy of ΔE9 significantly increased the secreted Aβ42/40 ratio, by two-fold, compared to the wt/wt lines (Figure 2.3 A and B). Two copies of ΔE9 increased the 42/40 ratio 3-fold over wt/wt lines, and similarly,

ΔE9/null lines also tripled the 42/40 ratio over wt/wt. Interestingly, wt/null was not significantly different from wt/wt, demonstrating that loss of one copy of PS1 does not mimic the ΔE9 mutation.

We used purified neurons to investigate whether the ΔE9 mutation increases the Aβ42/40 ratio by decreasing Aβ40, increasing Aβ42, or both. We observed that the wt/null genotype was not significantly different from wt/wt for Aβ40 (Figure 2.3 C). However, all genotypes containing even a single copy of Δe9, wt/Δe9, Δe9/Δe9 and Δe9/null, had significantly decreased Aβ40 (Figure 2.3 C). There were no significant differences between wt/null and wt/Δe9 in the amount of Aβ42, however, Δe9/Δe9 and Δe9/null genotypes displayed significantly increased amounts of Aβ42 (Figure 2.3 D). Therefore, we conclude that PS1 ΔE9, expressed at endogenous levels in human neurons, increases the Aβ42/40 ratio by decreasing Aβ40 and increasing Aβ42. Additionally, we determined that loss of one PS1 allele does not significantly alter Aβ production and in particular did not affect the Aβ42/40 ratio.

Finally, to test whether PS1 ΔE9 affects tau phosphorylation, the other major pathological hallmark of AD, we measured phospho-tau at site Thr231, a site that correlates with neurofibrillary tangle number (Buerger et al., 2006). We did not observe any significant differences in the ratio of P-tau/T-tau between any of the PS1 genotypes (Figure 2.4 D).

The PS1 ΔE9 mutation impairs γ-secretase-dependent functions of PS1

To determine directly whether the ΔE9 mutation impairs γ-secretase mediated processing of different protein substrates, we measured the cleavage of the C-terminal

fragments (CTFs) of APP and N-cadherin, both of which are γ-secretase substrates. Ordinarily, APP first undergoes cleavage by α and β secretases, which yield α and β CTFs, and then γ-secretase further cleaves the α and β CTFs. Similarly, N-cadherin undergoes an initial proteolytic processing event, which generates a CTF that is also cleaved by γ-secretase. Therefore, if the ΔE9 mutation impairs γ-secretase activity, we would expect to see an increase in APP and N-cadherin CTFs. All lines containing at least one copy of ΔE9 had significantly increased APP CTFs over wt/wt (Figure 2.5 A and B). We also quantified full-length APP and observed no significant differences between genotypes (Figure 2.4 A). This suggests that the ΔE9 mutation does impair γ-secretase cleavage of APP CTFs. Similarly, we were unable to detect any N-cadherin CTF for wt/wt, wt/null and wt/ΔE9 genotypes, but did observe obviously elevated levels of CTFs in Δe9/Δe9 lines and Δe9/null lines (Figure 2.5 C). Collectively, these data demonstrate that the ΔE9 mutation expressed at endogenous levels in a normal genetic background in human neurons impairs γ-secretase activity.

Previous studies reported that low doses of γ-secretase inhibitors that moderately impaired γ-secretase function increase the Aβ42/40 ratio in a variety of cell types (Sato et al., 2003; Shen and Kelleher, 2007). Thus, as an additional test of whether the ΔE9 mutation decreases γ-secretase activity in purified euploid human neurons, we compared the effects of the ΔE9 mutation to a low dose of the γ-secretase inhibitor, Compound E. Similar to previous reports, we found that a high dose of γ-secretase inhibitor (200nM) completely inhibits all Aβ production (data not shown) in all genotypes. Strikingly, a low dose (5nM) of Compound E substantially increases the Aβ42/40 ratio in wt/wt, wt/null, and wt/ΔE9 neurons, but not in ΔE9/ΔE9 or ΔE9/null

(Figure 2.5 D). Thus, the ΔE9 mutation has a similar phenotypic impact on Aβ processing as direct and low level inhibition of γ-secretase. Surprisingly, the ΔE9 mutation appears to confer resistance to low dose inhibition of γ-secretase activity by Compound E.

The PS1 ΔE9 mutation does not impair γ-secretase independent functions of PS1

To further probe whether the ΔE9 mutation acts as a loss or gain-of-function, we asked whether the ΔE9 mutation interferes with a γ-secretase independent function of PS1, Nicastrin maturation. Wild-type PS1 has been reported to facilitate Nicastrin maturation by acting as a chaperone in early biosynthetic compartments (Leem, et al., 2002). Thus, we quantified the relative amounts of mature and immature Nicastrin in purified neurons with various PS1 genotypes by quantitative western blot (Figure 2.6 A and B). We found that the ratio of mature/immature Nicastrin was significantly decreased compared to wt/wt only in cell lines that harbor a PS1 null mutation (wt/null and Δe9/null). There were no significant differences in mature/immature Nicastrin between wt/wt, wt/Δe9 and Δe9/Δe9 genotypes. This result suggests that the ΔE9 mutation does not impair all γ-secretase independent functions of PS1 since it generates a phenotypic effect that is clearly different from a null allele (Figure 2.6 C).

2.3 Discussion

Based on direct quantitative biochemical comparisons, our results demonstrate that the phenotypic effects of a proven null PS1 mutation and an FAD PS1 ΔE9 mutation are not equivalent in isogenic euploid purified human neurons. In

addition, the ΔE9 allele inhibits aspects of γ-secretase activity while maintaining normal activity for at least one γ-secretase independent function, nicastrin maturation. Thus, by using carefully genetically engineered human cells, this series of experiments reveals that some, and we propose, by extension, all PS1 FAD mutations are not simple loss-of-function alleles with respect to the biochemical pathway that generates key phenotypes associated with the initiation and development of AD.

Previous experiments probing whether the PS1 ΔE9 mutation changes the Aβ42/40 ratio by increasing Aβ42, decreasing Aβ40, or both have been reported multiple times with contradictory results (Chávez-Gutiérrez, et al., 2012; Kumar-Singh, et al., 2006). This issue is important since determining how the FAD PS1 ΔE9 mutation changes the ratio of Aβ species in euploid human neurons may help to elucidate AD mechanisms and inform development of effective AD drugs. By taking advantage of the allelic series we generated in a controlled genetic background in purified human neurons we were able to determine that the ΔE9 mutation increases the Aβ42/40 ratio in a gene dosage dependent manner by significantly decreasing the amount of Aβ40 while moderately increasing the amount of Aβ42. Our results are in contrast to some but not all previous attempts to clarify this issue. For example, a number of previous analyses of FAD PS1 mutations used mouse embryonic fibroblasts (MEFs) or HEK cells overexpressing PS1 ΔE9; some experiments incorporated additional overexpression of human APP and APP mutations. These studies are complex to interpret since it is unknown whether overexpression of PS1 ΔE9 results in biochemical data accurately representing the normal activity of PS1. An alternative approach is defined by early studies in *C.elegans,* which suggested that

FAD PS1 mutations encode PS1 proteins with decreased activity compared to wt PS1 (Shen et al., 1997). Early studies in HEK cells treated with antisense PS1 RNA showed increased secretion of Aβ42 (Refolo et al., 1999), which also supported the idea that PS1 mutations are simple loss-of-function. Later studies from knockout mice suggested that PS1 mutations are gain-of-function because complete loss of PS1 resulted in severely decreased overall Aβ production, unlike PS1 mutations. More recent studies propose that many PS1 mutations have decreased γ-secretase activity (Bentahir et al., 2006; Heilig et al., 2010; Koch et al., 2012) A common issue among these studies is that evaluation of Aβ production in non-human and/or non-neuronal cells may not be ideal because Aβ production and factors influencing Aβ production vary significantly among cell types (Qiang, et al., 2011; Israel, et al., 2012) and in comparison to neurons, which are the primary cell type affected in AD. Although these differences among cell types and systems might not have large scale effects, AD itself and AD phenotypes can be generated by relatively minor changes in expression of key genes, e.g., a 50% dosage increase of APP itself is sufficient to generate severe early-onset FAD (Rovelet-Lecrux, et al., 2006). Our system using genetically manipulated isogenic iPSC-derived neurons avoids these problems, allows effects of relatively minor magnitude to be evaluated, and in principle avoids problems of uncontrolled dosage at other key loci.

We note that until the work reported here, a complete and direct comparison of γ-secretase dependent and independent functions generated by an FAD PS1 mutation and a null allele has not been reported. Strikingly, PS1 haploinsuficiency had no significant effect on the Aβ42/40 ratio or total levels of Aβ40 and Aβ42, which again

demonstrates that PS1 loss-of-function and PS1 ΔE9 are not equivalent with respect to Aβ production and CTF processing. Thus, our finding confirms that the ΔE9 mutation is not simply a complete loss of PS1 function because the ΔE9 mutation has decreased γ-secretase activity compared to wt PS1 and heterozygous null allele, but has no affect on Nicastrin maturation, a γ-secretase independent function of PS1. In fact, we found impaired Nicastrin maturation only in cell lines that harbored a PS1 null mutation, which further confirms that PS1 ΔE9 maintains at least some normal PS1 functions. Furthermore, we found that PS1 haploinsuficiency had no detectable effect on APP or N-cadherin cleavage, again suggesting that PS1 haploinsuficiency and PS1 ΔE9 do not have the same effect on γ-secretase activity. Our findings also suggest that under the physiological conditions of our studies, and with respect to the phenotypes measured, γ-secretase activity is available in excess, because loss of one PS1 allele did not significantly alter γ-secretase cleavage of APP or N-cadherin.

In addition to testing how total levels of Aβ and the Aβ 42/40 ratio responded to different PS1 genotypes, we also measured phosphorylation of tau at Thr231. We did not observe any significant differences in the ratio of tau phosphorylated at Thr231 relative to total tau, when any of our PS1 mutants or combinations were compared to wt PS1, even in cell lines that were homozygous for the ΔE9 mutation and had significantly increased Aβ42. This result is similar to recent studies of neurons made from IPSCs carrying two different presenilin mutants, PS1 A246E and PS2 N141I (Yagi et al., 2011) but is in contrast to previous studies of iPSC-derived neurons from FAD caused by an APP duplication (Israel, et al., 2012) or trisomy 21 (Shi et al., 2012), both of which reported an increase in the ratio of phosphorylated tau relative to

total tau. An intriguing possibility is that FAD caused by an extra copy of APP and FAD caused by PS1 mutations differ in the earliest phenotypes and mechanisms by which they cause disease and thus differ in their induction of abnormal levels of phospho-tau. In this context, there is evidence that different FAD mutations result in positional and temporal differences in tau phosphorylation and accumulation. Specifically, analyses of post-mortem AD tissue revealed that different PS1 mutations (Shepherd et al., 2004) affect tau deposition and phosphorylation differentially with mutations in PS1 exons 8 and 9 having less hyperphosphorylated tau than mutations in exons 5 and 6. Further studies in iPSC-derived neurons, either with genome modifications or derived from patients with specific FAD mutations will clarify the nature of tau phenotypes in different FAD mutants.

A major focus of AD therapeutics has been γ-secretase inhibition, which has thus far failed to perform as hoped in clinical trials (Opar, 2008). In some cases, γ-secretase inhibition has even accelerated cognitive decline (Extance, 2010). Our data suggest that γ-secretase inhibition could worsen patients either by increasing the proportion of Aβ42 or by increasing the amount of APP CTFs, which have been proposed to play a role in AD pathogenesis (Jiang et al., 2010; Rodrigues et al., 2012). Interestingly, our recent work in an IPSC derived human neuronal system (Israel, et al., 2012) suggested that the β-CTF of APP is toxic in purified FAD neurons since treatment with a β-secretase inhibitor, rather than a γ-secretase inhibitor reduced abnormal phospho-tau levels in these FAD neurons. Since the FAD PS1 ΔE9 mutation decreases the amount of Aβ40 in our system and increases the APP CTFs, it is possible that this class of FAD mutation confers its toxic properties, in part, by the

accumulation of other pathogenic APP fragments such as the APP CTF. Thus a potentially important therapeutic implication from our work is that γ-secretase modulation that restores the Aβ ratios and/or restores γ-secretase function to normal levels or character could be more beneficial for AD treatment. Future studies characterizing other PS1 functions that may be affected by drugs and mutations will also be important for designing AD therapeutics.

A final important implication emerging from the work we report here concerns the question of whether TALENs introduce significant off-target mutations in iPSCs. By performing exome sequencing on genome-edited and subcloned iPSC lines we found that the genome-edited lines did not have a significantly higher number of unique mutations beyond what we observed in simple IPSC or hESC subcloning experiments. Thus, the introduction of TALENs does not appear to cause major off-target mutagenic effects. Another recent publication (Ding et al., 2013) reported that exome and whole genome sequencing on TALEN-targeted hESC lines revealed mutations unique to different subclones, although at an apparently higher frequency than we report here, possibly due to inherent differences in the particular cell line used or in the number of passages the clones underwent prior to subcloning. Taken together these data suggest that it may be impossible to derive completely isogenic cell lines. However, the relative number of single nucleotide variants between TALEN-targeted lines is still apparently less than what would be observed between different individual human genomes. Finally, as we report here, the generation of an allelic series and the analysis of multiple independent lines allows for careful evaluation of phenotypic effects in a bona fide, euploid, cell-type representative human model.

2.4 Experimental Procedures

iPSC Culture

iPSCs were generated as previously described (Gore, et al., 2011; Israel, et al., 2012). iPSCs are cultured on an irradiated MEF feeder layer generated in-house. Cells are grown in medium containing KO DMEM (Gibco), 10% Plasmanate (Talecris Biotherapeutics), 10% KO Serum Replacement (Gibco), 20mM GlutaMax (Invitrogen), 20mM NEAA (Invitrogen), 20mM Pen/Strep (Invitrogen) and 20ng/uL FGF (Millipore). Cells were passaged by dissociation with Accutase (Innovative Cell Technologies).

Isogenic iPSC Generation

iPSCs were pretreated with 10uM Rock Inhibitor (Ascent Scientific) for 1 hour prior to nucleofection. Cells were dissociated using accutase and passed through a 100uM filter to obtain single cells. Two million iPSCs were nucleofected using Amaxa Human Stem Cell Nucleofector Kit 1 (Lonza), with 7.5ug of each TALEN-encoding plasmid, 2ug of pmaxGFP (Lonza) and 30ug of ssODN (Integrated DNA Technologies). Cells were maintained in iPSC culture conditions with 10uM Rock inhibitor for 72 hours followed by FACS sorting (FACS Aria, BD Biosciences) for GFP+ cells. GFP-expressing cells were plated a $1x10^4$ cells per 10cm plate in the presence of Rock Inhibitor. Thereafter, media was changed every other day until isolated colonies grew. Isolated colonies were manually picked and grown in 96-well plates. Once cells were confluent, cells were split into a duplicate well and grown until

confluent at which point they were harvested for DNA using DNA QuickExtract (Epicentre). DNA was amplified using allele specific primers to detect the ΔE9 point mutation using Jump Start PCR Ready Mix (Sigma). Cell lines that amplified using the allele specific PCR were then digested with EcoRI to further confirm insertion of the ssODN. To sequence the PCR products, we cloned them using the Zero Blunt PCR Cloning Kit (Invitrogen).

Exome Sequencing

Exome sequencing was performed as previously described (Gore, et al., 2011). Briefly, genomic DNA from each sample was sheared and ligated to barcoded Illumina sequencing adaptors. DNA was then hybridized using the Roche NimbleGen SeqCap EZ Exome library to capture exomic regions. Exome regions were captured with streptavidin-coated beads and then PCR-amplified with Illumina sequencing adaptors. The resulting libraries were sequenced on an Illumina Genome Analyzer IIx or Illumina Hiseq. Reads were mapped to the whole genome using BWA, and a consensus sequence was generated using GATK (Broad Institute best practices). Consensus sequences between the progenitor cell lines and subcloned cell lines were compared to look for candidate novel mutations. Candidate variants that occurred at locations present in the dbSNP database or that showed any presence in the progenitor line were removed. Identified candidate mutations were validated by Sanger sequencing.

Statistical Analysis of Mutation Counts

To determine if TALEN modification resulted in an increased off-target point mutational load, the number of mutations in the TALEN-modified subcloned iPSC lines was compared to the number of mutations in the unmodified subcloned pluripotent stem cell lines. In order to analyze the potential mutational load introduced by the TALEN process itself and exclude any normal culture mutations, the number of mutations acquired after subcloning was analyzed rather than any overall iPSC mutations acquired due to reprogramming or post-reprogramming culture. Because of the varied culture history of each progenitor line and subclone, it was difficult to construct a hypothetical mutational distribution for each line. Thus, the nonparametric Mann-Whitney test was used to compare the median number of mutations in each subclone group. The test revealed that TALEN-modified and unmodified subclones had a similar median number of mutations; no significant difference could be determined ($p=0.13$). This indicates that TALEN-modified lines do not acquire any additional mutational load over that expected during normal culture and subcloning.

NPC Differentiation, Purification, and Culture

iPSCs were differentiated to NPCs as previously described (Yuan, et al., 2011). Briefly, $1x10^5$ iPSCs were seeded onto PA6 cells in PA6 differentiation medium: Glasgow DMEM, 10% KOSR, 1mM Sodium Pyruvate, 0.1mM Nonessential Amino Acids and 0.1 mM β-Mercaptoethanol (all from Invitrogen). For the first 6 days media was not changed and also contained 500 ng/ml Noggin (R&D Systems) and 10 μM SB431542 (Tocris). After the first 6 days, medium was changed every other day until

day 12. On day 12, cells were dissociated and stained with, CD184, CD44, CD271 and CD24 (all from BD Biosciences). CD184 +, CD24+, CD44-, CD271- cells were sorted (FACS Aria, BD Biosciences). NPC cultures were cultured on 20 µg/ml poly-L-ornithine and 5 µg/ml laminin (both from Sigma) coated plates in medium containing: DMEM:F12 + Glutamax, 0.5X N2, 0.5X B27 (both from Life Technologies), 1X P/S, and 20 ng/ml FGF (Millipore). Media was changed every other day.

Neuron Differentiation, Purification, and Culture

NPCs were expanded to 10cm plates and grown to confluency (3-4 days) at which point FGF was removed from the media. The medium was changed twice per week and the cells were differentiated for 21 days. After the 3 week differentiation, neurons were purified as previously described (Yuan, et al., 2011). Briefly, cells were dissociated using Accutase and Accumax (both from Innovative Cell Technologies) and then stained with CD184, CD44 and CD24 (all from BD Biosciences). CD184-, CD44-, CD24+ cells were sorted (FACS Aria, BD Biosciences) and then plated on poly-ornithine/laminin coated plates in NPC media + 0.5mM dbCAMP (Sigma), 20ng/uL BDNF and 20ng/uL GDNF (both from Peprotech).

Gene Expression Analysis (qRT-PCR):

For mRNA expression analysis, total RNA was prepared using RNeasy kit (Qiagen). The RNA was DNase treated (Ambion) and first-strand cDNA synthesis was performed with Superscript (Invitrogen). qPCR was done on a Applied Biosystems 7300 real time PCR system using FastStart Universal SYBR Green Master

(Roche). Results were quantified using the $\Delta\Delta C_t$ method. PS1 levels were normalized to the house-keeping genes TATA-binding protein (TBP) or the ribosomal protein RPL27. Primers for PS1 spanned exons 4 and 5. Forward Primer: TGACTCTCTGCATGGTGGTGG; Reverse Primer: TCTCTGGCCCACAGTCTCGGT

Aβ Measurements

NPCs were plated at a density of $5x10^5$ in 12 well plates. Media was changed 24 hours after plating and replaced with 0.5mL of NPC media + FGF. After 48 hours, media was harvested and stored at -80 and protein was harvested for normalization purposes. Neurons were plated at density of $1.5x10^5$ per 96 well in a 100uL volume of glial conditioned media. Media was harvested from purified neurons after 2 weeks. Glial conditioned medium was made by putting NPC media onto glia (Lonza) for 24 hours. Aβ from the media was measured with MSD Human (6E10) Abeta3-Plex Kits (Meso Scale Discovery). For experiments with γ-secretase inhibitor, all media was changed on day 3 and replaced with 100uL of media either with Compound E or DMSO (vehicle). All media was harvested on day 5. Compound E (EMD Chemicals) was used at concentrations of 5nM and 200nM. 3-6 independent measurements were made per line. Each NPC line was differentiated twice in independent experiments for purified neurons.

Gel Elctrophoresis and Western Blot

Tissue culture lysates were prepared using RIPA lysis buffer (Millipore) supplemented with protease (cocktail set I, Calbiochem) and phosphatase (Halt, Pierce) inhibitors. The BCA assay (Pierce) was used to estimate the protein content. Equal protein amounts were separated in MES buffer alongside Novex Sharp prestained markers (Invitrogen) on NUPAGE 4–12% Bis-Tris precast gels (Invitrogen) and then transferred to polyvinylidene fluoride (PVDF) or nitrocellulose (0.45 μm pore size Immobilon Millipore). Membranes were blocked in 5% BSA in tris buffered saline with 0.1% Tween-20 or Odyssey Blocking Buffer (Li-Cor). Primary antibodies (Presenilin 1 c-loop 1:1000 Chemicon; Presenilin 1 N-term 1:1000 Santa Cruz; APP C-terminus 1:1000 Calbiochem; N-cadherin C-terminus 1:1000 BD Biosciences; Nicastrin 1:1000 Affinity BioReagents; Actin C4 1:100,000 Chemicon; Tubulin-alpha DM1A 1:50,000 Sigma) were prepared in 5% BSA. Fluorescent secondary antibodies (LiCor) were diluted 1:5000. LiCor Odyssey infrared imager was used to measure pixel intensities of bands at detector settings set at the maximum or one half unit below saturation. For each protein band, background subtracted integrated intensity values were calculated using the Odyssey software. Since absolute integrated intensity values vary for the same samples on different blots, samples within a blot were plotted relative to control and these normalized values were used to average replicates from separate blots. To show protein bands in the conventional manner with dark bands on a light background, grayscale images were inverted in the figures. HRP-conjugated secondary antibodies (Invitrogen) were diluted 1:5000. Blots were developed using ECL Western Blotting Kit (Pierce).

Statistical Methods

All data was analyzed using GraphPad Prism Software (GraphPad). Statistical analysis comparing different genotypes was performed by Tukey's multiple comparison test. Drug responses were compared to controls by Dunnett's test.

Chapter 2, in full, was published Woodruff, G., Young J.E., Martinez, F.J., Buen, F., Gore, A., Kinaga, J., Li, Z., Yuan, S.H., Zhang, K., and Goldstein L.S. (2013). The presenilin-1 ΔE9 mutation results in reduced γ-secretase activity, but not total loss of PS1 function, in isogenic human stem cells. Cell Rep. 5, 974-985. The dissertation author is the primary investigator and author of this work.

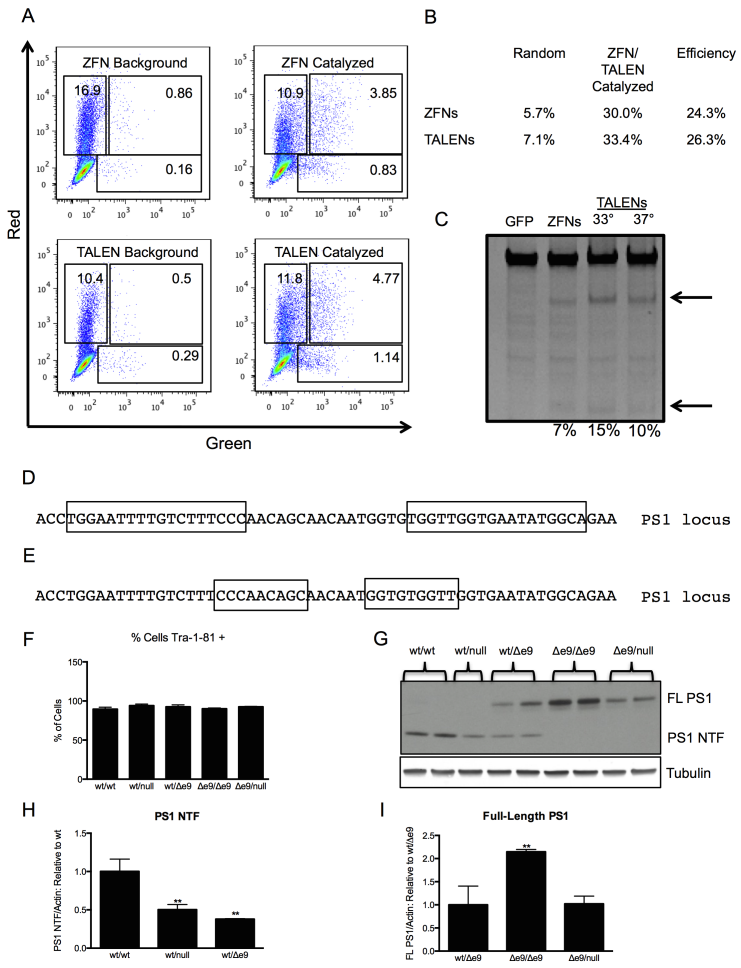

Figure 2.1. Comparison of ZFNs and TALENs by Episomal Assay and Surveyor Assay, (A) FACS plots demonstrating background and ZFN or TALEN-catalyzed recombination. (B) Calculated background and ZFN or TALEN-catalyzed recombination efficiency. (C) Screening of ZFNs and TALENs directed against the PS1 locus. Disruption of the PS1 locus was measured by the Surveyor assay. Black arrows indicate the expected Surveyor nuclease digest products. TALENs were tested in cells grown at 33 and 37 degrees and the frequency of disruption of the ZFNs or TALENs is indicated below each lane. (D) TALEN binding sites at the PS1 locus. Boxes indicate the TALEN binding sites. (E) ZFN binding sites at the PS1 locus. Boxes indicate the ZFN binding sites. (F) Insertion of the ΔE9 mutation or disruption of the PS1 gene did not significantly affect the percentage of cells that stained positive for the cell surface pluripotency marker Tra-1-81 as analyzed by FACS. (G) Western blot for PS1 protein using an N-terminal antibody from lysates from NPCs from each genotype. (H) Quantification of PS1 NTF with reference to tubulin and normalized to wt/wt levels. Error bars represent SEM from 3 biological replicates per line. (I) Quantification of FL-PS1 with reference to tubulin and normalized to wt/Δe9 levels. Error bars represent SEM from 3 biological replicates per line.

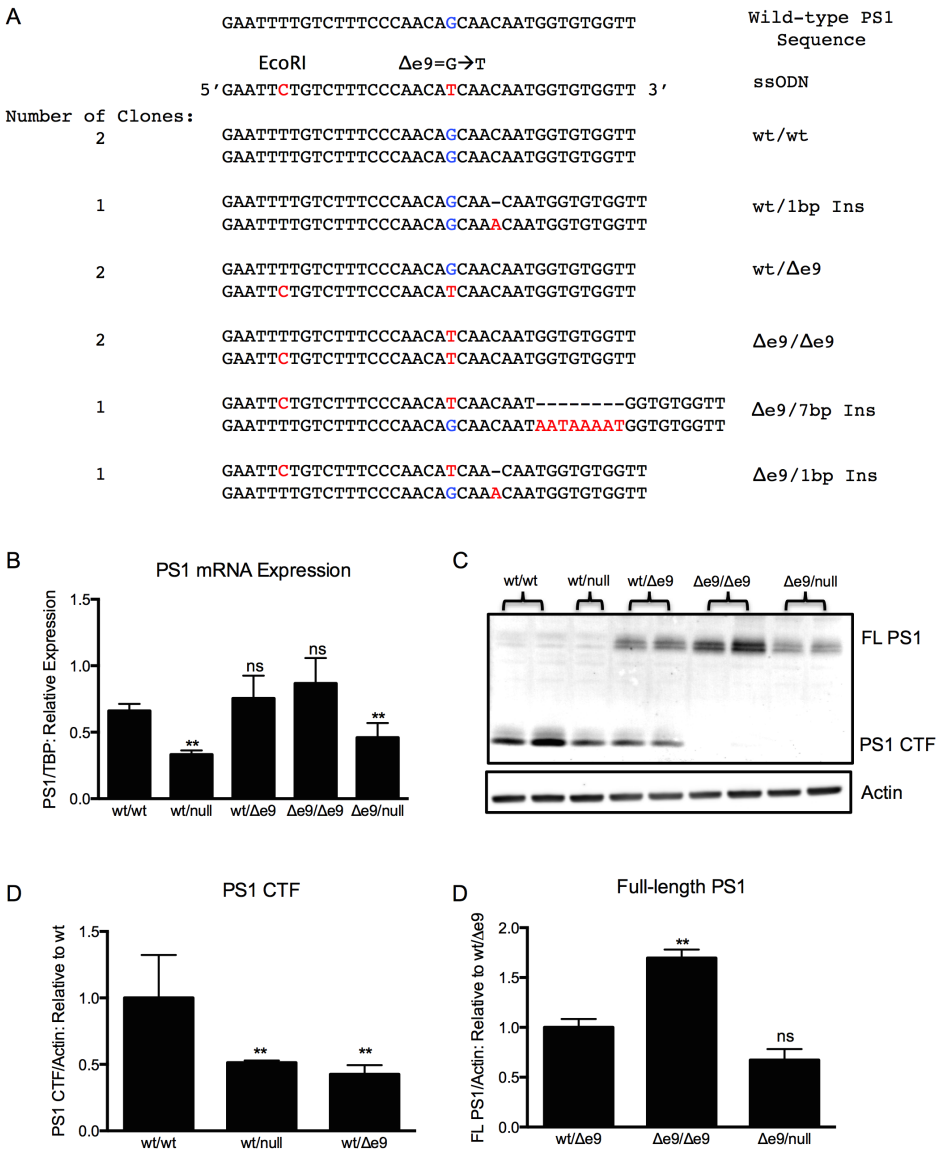

Figure 2.2. PS1 mRNA is reduced by null but not FAD PS1 ΔE9 mutations (A) Generation of isogenic iPSC lines harboring PS1 null and ΔE9 mutations. Insertions of the ΔE9 mutation or random nucleotide insertions that disrupt the PS1 gene are shown for each allele from each line. The wild-type nucleotide is depicted in blue and mutations or insertions are in red. (B) PS1 mRNA levels by qPCR from isogenic NPC lines normalized to TBP. The error bars represent SEM from experiments with technical replicates N=3. (C) Western blot for PS1 protein from lysates from each NPC line. (D) Quantification of PS1 CTF with reference to Actin and normalized to the levels in the wt/wt lines. Error bars represent SEM from biological replicates N=2. (E) Quantification of FL-PS1 with reference to Actin and normalized to the levels in the wt/Δe9 clones. Error bars represent SEM from biological replicates N=2.

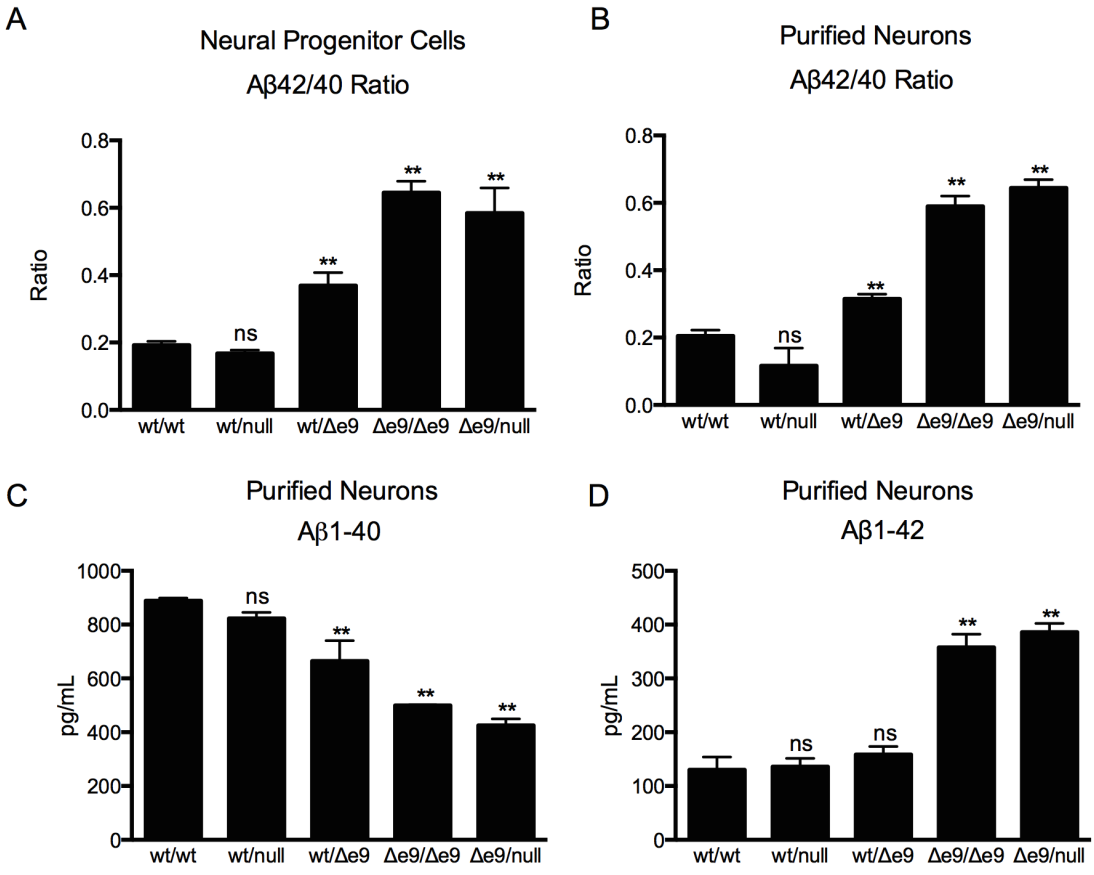

Figure 2.3. The PS1 Δe9 Mutation Increases the Aβ42/40 Ratio by Decreasing Aβ40

(A) Secreted Aβ42/40 ratio from NPCs. Bars represent measurements from 2 NPC lines per genotype with the exception of the wt/null genotype. Error bars represent SEM from 6 biological replicates per line. (B) Secreted Aβ42/40 ratio from purified neurons. Bars represent measurements from 2 lines per genotype with the exception of the wt/null genotype. Error bars represent SEM from 6 biological replicates per line. (C) Secreted Aβ40 from purified neurons. Error bars represent SEM from 6 biological replicates per line. (D) Secreted Aβ42 from purified neurons. Error bars represent SEM from 6 biological replicates per line.

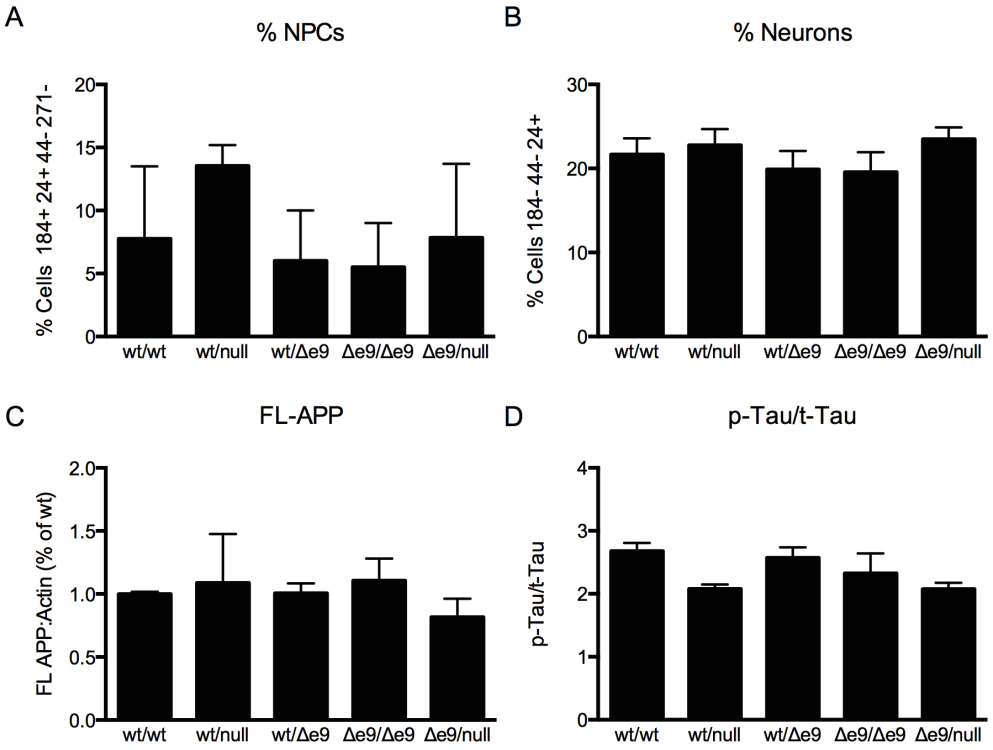

Figure 2.4. No Significant Differences in the Percentage of NPCs or Neurons, FL-APP or p-Tau/t-Tau Generated by Cell Lines Containing PS1 Null or Δe9 Mutations (A). Percentage of NPCs generated by each genotype as quantified by percentage of cells that stained for the NPC signature CD184+ CD24+ CD44- CD271. Bars represent measurements from 2 clonal lines per genotype with the exception of the wt/null genotype. Error bars represent SEM from 2 independent differentiations per line. (B) Percentage of neurons generated by each genotype as quantified by the percentage of cells that stained for the neuron signature CD184- CD44- CD24+. Bars represent measurements from 2 clonal lines per genotype with the exception of the wt/null genotype. Error bars represent SEM from 4-6 differentiations per line. (C) Quantification of FL-APP from lysates from neurons from each genotype. Bars represent measurements from 2 clonal lines per genotype with the exception of the wt/null genotype. Error bars represent SEM from 3 independent western blots. (D) No significant differences in the p-Tau/t-Tau ratio between genotypes. Bars represent measurements from 2 lines per genotype with the exception of wt/null. Error bars represent SEM from 3 biological replicates per line.

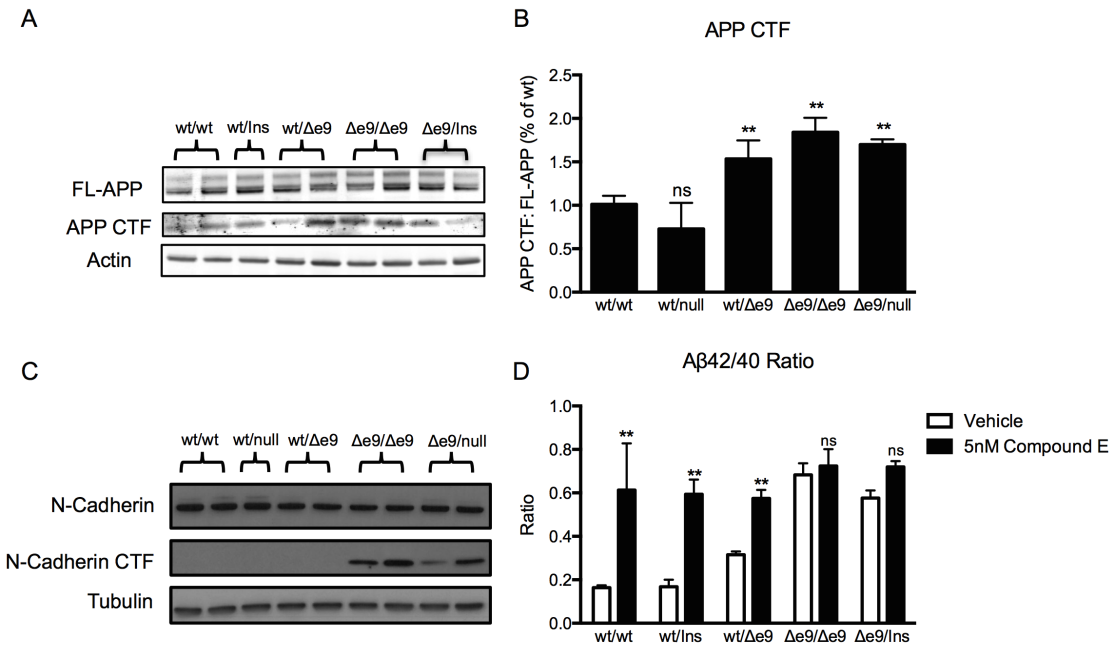

Figure 2.5. The PS1 ΔE9 mutation impairs γ-secretase activity. (A) Representative western blot of FL-APP and APP CTF. (B) Quantification of APP CTF with reference to FL-APP and normalized to levels in wt/wt. Each bar represents measurements from 3 biological replicates. Error bars represent SEM from 3 measurements per line. (C) Western blot of FL N-cadherin and N-cadherin CTF. (D) Secreted Aβ42/40 ratio from purified neurons treated with a γ-secretase inhibitor, Compound E, at 5nM. Error bars represent SEM from 4 biological replicates per line.

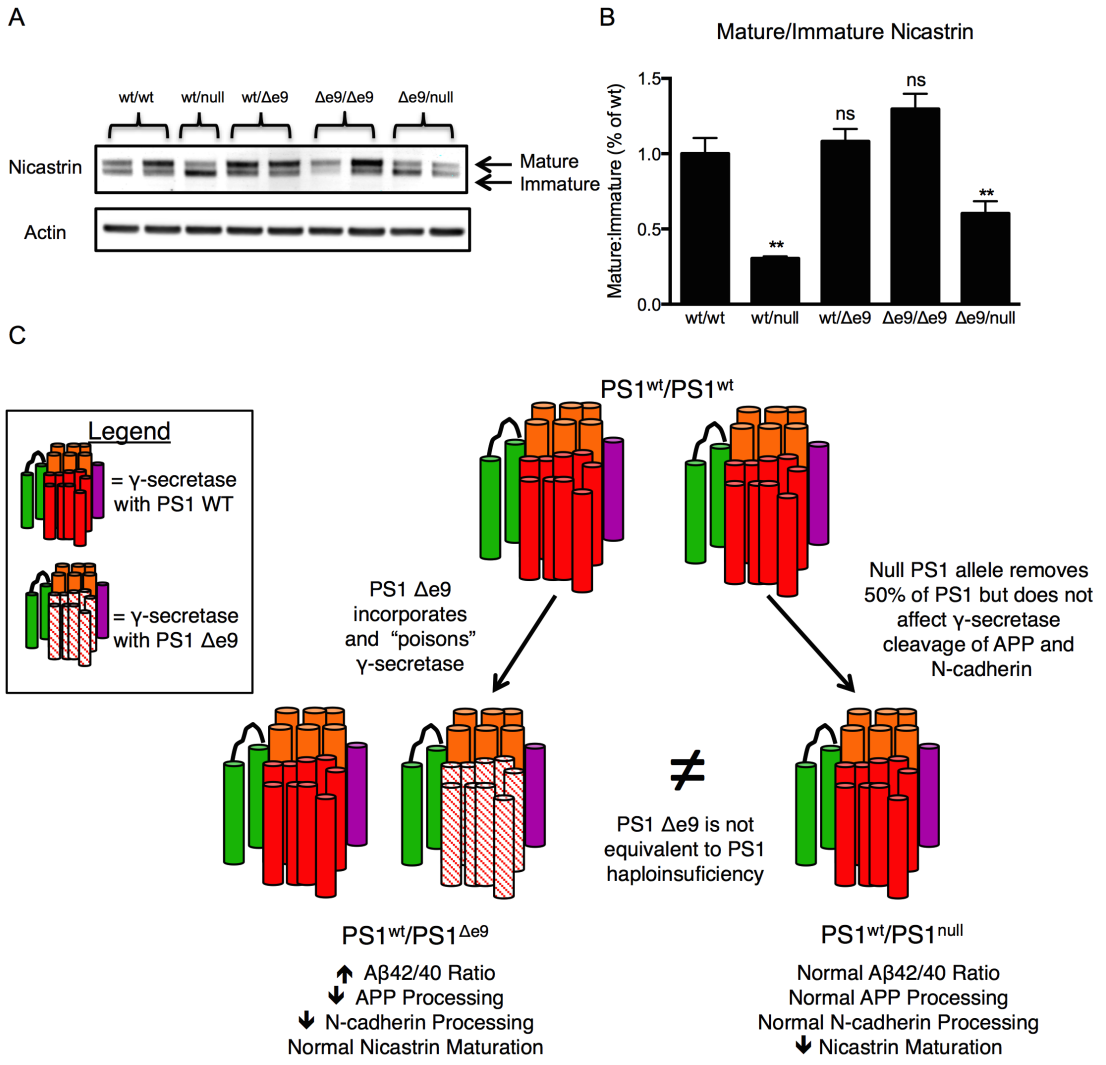

Figure 2.6. PS1 Null Mutations, but not the PS1 Δe9 Mutation, Impair Nicastrin Maturation (A) Representative western blot of Nicastrin from isogenic lines. Black arrows indicate mature and immature forms of the protein. (B) Quantification of mature and immature Nicastrin. Error bars represent SEM of 2 biological replicates per line. (C) Schematic summary of results

Table 2.1. Isogenic iPSC and NPC Lines

Genotype	Number of iPSC Clones[a]	Number of NPC Lines[b]
wt/wt	6	2
wt/null	1	1
wt/Δe9	3	2
Δe9/Δe9	2	2
Δe9/null	2	2

a. Number of iPSC clones is the total number of clones that received the indicated mutations.

b. Number of NPC lines is the number of iPSC clones that were used to make NPCs

Table 2.2. IPSC and hESC Subclones Have a Low Number of Protein Coding Mutation

Cell Line and Subclone	Unique Mutations[a]	Chromosome	Gene	Protein Change[b]	Mutation Type[c]	Prediction[d]
iPSC-CVB 1.7	0	N/A	N/A	N/A	N/A	N/A
iPSC-CVB 1.8	0	N/A	N/A	N/A	N/A	N/A
iPSC-CVB 1.9	3	2,2,8	ACSL3, CCDC108, DKK4	P129S V398F C166C	Non-Syn Non-Syn Syn	Tolerated Damaging N/A
iPSC-CVI 1.13	0	N/A	N/A	N/A	N/A	N/A
iPSC-CVI 1.14	0	N/A	N/A	N/A	N/A	N/A
iPSC-CVI 1.15	1	2	WDR33	P587S	Non-Syn	Tolerated
hESC-Hues9 1.7	0	N/A	N/A	N/A	N/A	N/A
hESC-Hues9 1.8	0	N/A	N/A	N/A	N/A	N/A
hESC-Hues9 1.9	1	8	POTEA	M299R	Non-Syn	Damaging

a. Number of mutations unique to this cell line compared to the parental iPSC or HUES cell lines

b. Indicates whether the detected mutation will change amino acids in the protein

c. Indicates whether the mutation is a synonymous or non-synonymous mutation

d. Indicates whether the mutation is predicted to be damaging to the protein or tolerated

Table 2.3. TALEN-targeted iPSC Lines Have a Low Number of Off Target Mutations

Genotype	Unique Mutations[a]	Chromosome	Gene	Protein Change[b]	Mutation Type[c]	Prediction[d]
wt/wt	0	N/A	N/A	N/A	N/A	N/A
wt/Δe9	1	8	CSMD1	I2038I	Syn	Tolerated
wt/Δe9	3	4,14,19	SYNE2	E795E	Syn	Tolerated
			ZNF225	V4668I	Non-Syn	Tolerated
			PDIA3	G466V	Non-Syn	Damaging
Δe9/Δe9	1	17	STAT3	R278H	Non-Syn	Tolerated
Δe9/Δe9	2	5	NUP155	S58Y	Non-Syn	Tolerated
			PCDH-GA10	A606S	Non-Syn	Tolerated
Δe9/null	1	15	PDIA3	S169S	Syn	Tolerated

a. Number of mutations unique to this cell line compared to the parental iPSC or HUES cell lines

b. Indicates whether the detected mutation will change amino acids in the protein

c. Indicates whether the mutation is a synonymous or non-synonymous mutation

d. Indicates whether the mutation is predicted to be damaging to the protein or tolerated

Chapter 3

Reduced Endocytosis and Transcytosis of APP and Lipoproteins Owing to Accumulation of β-CTF in Familial Alzheimer's Disease Mutations

3.1 Introduction

Alzheimer's Disease (AD) is a progressive neurodegenerative disease that affects more than 30 million people worldwide including 11% of those over 65 years of age and 32% of those over 85 (Fargo and Bleiler, 2014). The disease is characterized by progressive cerebral dysfunction, memory loss, and neuronal impairment leading to cell death. To date, there are no disease-modifying treatments that can cure or reduce the progression of AD. Genetically, AD is segmented into two populations: sporadic AD (sAD) where the underlying cause is not known and rare, autosomal-dominant mutations of familial AD (fAD) (Gatz et al., 2006). The common pathological features of the sAD and fAD patients are the accumulation of senile plaques composed of aggregated amyloid-β (Aβ) and neurofibrillary tangles (NFT), composed of hyper-phosphorylated tau (Spires-Jones and Hyman, 2014). The majority of clinical trials have focused largely on the amyloid cascade hypothesis of AD, which posits that extracellular Aβ fragments and intracellular tau accumulate abnormally in AD and drive cellular stress, neurotoxicity, and ultimately neurodegeneration. While considerable evidence exists to support the amyloid cascade model, clinical trials that rely on this model have been unsuccessful. In part, the high failure rate (99.6%) may be because the majority of clinical trials seek to reduce Aβ burden in the brain without considering the effects of candidate drugs on other amyloid precursor protein (APP) fragments and other AD-relevant pathways (Toyn and Ahlijanian, 2014).

APP is proteolytically cleaved in sequential steps by α-secretase and γ-secretase along the non-amyloidogenic pathway, and by β-secretase (BACE1) and γ-secretase along the amyloidogenic route. Prominent drug failures include the γ-

secretase inhibitors, Semagecestat and Avagacestat, both of which were terminated because of side effects, including worsened cognitive outcomes. This may be because γ-secretase inhibition, while reducing Aβ, also increases the levels of APP β-CTFs, which are known to have toxic effects and can severely impair neuronal function (Jin et al., 2002; Lu et al., 2000; Toyn and Ahlijanian, 2014; Weissmiller et al., 2015). Better drug candidates may be the class of BACE inhibitors that seek to shift processing of APP to the α-secretase pathway and inhibit production of β-CTFs (C-terminal fragments) and Aβ. BACE as a clinical target is also attractive because mutations that enhance BACE activity (APP Swedish KM670/671NL) are strongly pathogenic, while the protective APP mutation A673T reduces BACE processing, consequently reducing Aβ and β-CTF production and lowering AD risk (Jonsson et al., 2012; Stamford and Strickland, 2013; Vassar et al., 2014).

Despite the known cytotoxicity of β-CTFs, and their equimolar relationship to Aβ, studies of this immediate precursor to Aβ are incomplete. In large part, understanding the disease-relevant roles of β-CTFs is limited by the use of model systems that incompletely recapitulate AD (Balducci and Forloni, 2011; Braidy et al., 2012; Goldstein et al., 2014). For this reason, we sought to use a human system that expressed endogenous levels of human fAD mutations in Presenilin 1 (PS1) and APP that cause increased levels of β-CTFs. Beyond the consensus that APP and PS1 fAD mutations alter APP processing, increasing Aβ42/40 ratio and β-CTF levels, there is little agreement in the field about how these mutations initiate pathogenic events that eventually lead to neurodegeneration. Previous work suggested that β-CTF accumulation might cause defects in lipoprotein internalization, but how general this

defect might be and what cellular pathways might be dysregulated is not yet understood (Tamboli et al., 2008).

We tested whether isogenic iPSC-derived neurons with fAD mutations display early cellular phenotypes beyond the known effects on APP processing, including altered endocytosis and sorting of cargo (Von Bartheld, 2004; Cataldo et al., 2000; Ginsberg et al., 2010; Karch and Goate, 2014; Lee et al., 2010; Maxfield, 2014). We found that fAD mutant neurons alter subcellular distribution of APP and internalized lipoprotein, leading to elevated levels of APP in the soma and reduced levels in the axons. The redistribution of APP is accompanied by the concurrent accumulation of a Rab11 compartment in the soma and reduced axonal staining, suggesting that the reduction in axonal APP and lipoproteins can be partly explained by reduced Rab11-dependent soma-to-axon transcytosis (Ascaño et al., 2009; Von Bartheld, 2004; Buggia-Prévot et al., 2014). Knockdown of Rab11 causes similar phenotypes, which are also rescued by treatment with a β-Secretase inhibitor. In keeping with these data, these alterations are not accompanied by changes in lysosomal pH or bulk endocytosis. Our study thus reveals that a common defect among fAD mutations is βCTF accumulation-induced impairment of neuronal transcytosis of Rab11-cargoes such as APP and lipoproteins.

3.2 Results

The PS1$^{\Delta E9}$ Mutation Increases APP in the Soma of Human Neurons and Decreases APP in axons

PS1 has been reported to have a role in APP trafficking in primary neurons and in non-neuronal cell types (Burns et al., 2003; Cai et al., 2003; Gandy et al., 2007;

Zhang et al., 2006). PS1 knockout has been reported to increase cell surface APP (Leem et al., 2002), while PS1 FAD mutations have been shown to delay APP arrival at the cell surface (Cai et al., 2003; Gandy et al., 2007). To determine whether the $PS1^{\Delta E9}$ mutation affects APP localization in human neurons, we generated purified neurons from isogenic iPSC cell lines of controls and lines heterozygous and homozygous for the $PS1^{\Delta E9}$ mutation (Woodruff et al., 2013). We stained with an APP antibody, which has minimal staining in an APP knockout background in both mice (Guo et al., 2012; Weissmiller et al., 2015) and human iPSC-derived neurons (Figure 3.1). We found that $PS1^{wt/\Delta E9}$ and $PS1^{\Delta E9/\Delta E9}$ neurons exhibited increased APP staining in the cell body (Figure 3.2A), including increased APP puncta and APP puncta intensity (Figure 3.2B). To determine whether APP was also increased on the surface of $PS1^{\Delta E9}$ neurons, we stained unpermeabilized purified neurons with an N-terminal APP antibody that recognizes the extracellular portion of APP (22C11) (Figure 3.2C). We observed increased surface APP in the soma of $PS1^{\Delta E9}$ neurons (Figure 3.2C).

We previously published that $PS1^{\Delta E9}$ neurons do not exhibit changes in total levels of full-length APP though there are increases in the APP CTFs (Woodruff et al., 2013). The increase in soma APP suggests that APP CTFs are accumulating in the soma of purified neurons and/or that APP is missorted possibly at the expense of axonal APP. We therefore assessed APP staining in the axons of $PS1^{\Delta E9}$ neurons. To ensure that we were quantifying staining in axons and not dendritic processes, we made use of microfluidic compartments, which separate axons from the bulk somatodendritic population (See Figure 4.2A) (Niederst et al., 2015; Selfridge et al., 2015; Taylor et al., 2006). As shown in Figure 4.2B, differentiated neural progenitor

cells (NPCs) grown in microfluidic devices extend long processes into the axonal space that do not stain for the somatodendritic marker Map2 and that do stain for the axonal marker neurofilament-H (SMI31 clone). We observed that PS1$^{\Delta E9}$ axons grown in microfluidic devices have decreased axonal APP puncta with diminished APP puncta intensity (Figure 3.2D); this decrease is sensitive to PS1$^{\Delta E9}$ gene dose. To test whether the phenotypic differences that we observed in PS1$^{\Delta E9}$ neurons might be due to differences in neuronal subtypes in our cultures we stained neurons of each genotype with the neuronal subtype markers GABA, GAD65/67 and vGlut (Figure 3.3A). We found no significant differences in the proportion of cells that stained positive for GABA, GAD65/67 or vGlut between different genotypes (Figure 3.3B), which suggests that APP localization differences and other phenotypes we observed were not due to a difference in neuronal subtype.

Rab11 Distribution is Altered in PS1$^{\Delta E9}$ Neurons

There are at least two pathways by which APP can be delivered to the axon. The first is by direct delivery from the trans Golgi network (TGN) and the second is by an indirect pathway where APP first arrives at the cell surface of the somatodendritic compartment, then undergoes endocytosis and sorting to the axon. The indirect pathway is a process known as transcytosis and multiple cargo, including APP (Niederst et al., 2015), TrkA (Ascaño et al., 2009) and L1/NgCAM (Anderson et al., 2005; Yap et al., 2008) (among other proteins, trophic factors, tracers, and pathogens (Von Bartheld, 2004)) have been demonstrated to be sorted along this pathway in neurons.

One endocytic regulator that functions at the intersection of the TGN and transcytotic pathways is the Rab GTPase Rab11 (Welz et al., 2014). Rab11 has a well-established role in mediating recycling of many receptors including transferrin receptor (Ullrich et al., 1996), and LDL receptors (Sakane et al., 2010; Takahashi et al., 2007b). In addition to its role in recycling, Rab11 has also been shown to mediate transcytosis in epithelial cells and neurons. Specifically, in neurons, TrkA receptors undergo Rab11-dependent transcytosis to the axon (Ascaño et al., 2009; Lazo et al., 2013). Rab11 may also be involved in trafficking of BACE1 to the axon (Buggia-Prévot et al., 2014), colocalizes with APP in axons (Niederst et al., 2015), and was recently identified in an unbiased RabGTPase screen as a regulator of Aβ and sAPPβ production (Udayar et al., 2013). Intriguingly, presenilins have also been reported to interact directly with Rab11 through their hydrophilic loop (Dumanchin et al., 1999).

To determine if Rab11 could be playing a role in the reduction of axonal APP, we stained neurons with a Rab11 antibody and measured Rab11 in the somatodendritic and axonal compartments. The Rab11 staining was reminiscent of the altered APP distribution such that $PS1^{\Delta E9/\Delta E9}$ neurons exhibited increased soma Rab11 intensity, Rab11 puncta, and Rab11 puncta area (Figure 3.4A). In axons, both the $PS1^{wt/\Delta E9}$ and $PS1^{\Delta E9/\Delta E9}$ genotypes had decreased Rab11 puncta density and puncta intensity (Figure 3.4B). In support of a role in Rab11-dependent trafficking of APP to the axon, shRNA-mediated knockdown of Rab11 on the soma-side of neurons grown in microfluidic devices resulted in a dramatic reduction in APP axonal staining (data not shown)**.** In keeping with a transcytotic route of APP to the axon, somatodendritic inhibition of endocytosis with the dynamin-inhibitor, Dynasore led to reduced APP

and Rab11 density in axons (Figure 3.4C). These findings are consistent with a previous study from our lab using a different Rab11 antibody (Niederst et al., 2015).

We also tested the early endosome effector, EEA1, and the lysosomal marker, Lamp2, even though they are not thought to traffic substantially to axons (Wilson et al., 2000). In fact, though differences in EEA1 and Lamp2 size and puncta counts were previously reported in PS1 mutations (Lee et al., 2010; Neely and Green, 2011; Tarabal et al., 2001), in our $PS1^{\Delta E9}$ iPSC-derived neurons the stains were not dramatically different (though there were a tendency toward larger puncta) suggesting that they are not playing an active role in sorting APP to the axon. (data not shown)

The $PS1^{\Delta E9}$ Mutation Decreases Endocytosis and Transcytosis of APP and LDL

Since we observed alterations in the subcellular distribution of both APP and Rab11 in $PS1^{\Delta E9}$ neurons, we investigated whether endocytosis, recycling and/or transcytosis could account for the APP localization changes. To assess endocytosis of APP we treated purified neurons with an N-terminal APP antibody (22C11) and allowed cells to internalize antibody for 30 minutes, 120 minutes or 140 minutes and fixed cells at each of those timepoints. We then stained with a secondary antibody and quantified the amount of APP endocytosis at each timepoint (Figure 3.5A). We observed a decrease in APP puncta in the $PS1^{\Delta E9/\Delta E9}$ genotype starting at 30 minutes compared to $PS1^{wt/wt}$ and this decrease was more prominent at both the 2 and 4 hour timepoints (Figure 3.5A). The $PS1^{wt/\Delta E9}$ genotype also exhibited decreased APP puncta compared to $PS1^{wt/wt}$ at the 2 and 4 hour timepoints. To assess whether this endocytosis defect was specific to APP or common to other Rab11-dependent cargo,

we also measured uptake of fluorescently labeled LDL at 30 minutes, 1 hour, 2 hours and 4 hours (Figure 3.5B). Similar to what was observed with APP, LDL puncta intensity and LDL puncta density were reduced in $PS1^{wt/\Delta E9}$ and $PS1^{\Delta E9/\Delta E9}$ neurons at 2 hours and 4 hours (Figure 3.5B). To test if the differences observed were due to a non-specific defect in endocytosis, we also quantified uptake of fluorescently labeled dextran as a marker of bulk endocytosis. We did not observe any significant differences in dextran endocytosis at any timepoint (Figure 3.5E).

We measured transcytosis of APP and LDL by growing neurons in microfluidic compartments. The axon side of the compartment was kept in fluidic isolation from the soma side and APP antibody or labeled LDL was added only to the soma side. Transcytotic delivery of cargo from the axon to the soma is a relatively slow process since internalized cargo has to travel long distances (on the order of millimeters in cultured neurons). When we measured transcytosed LDL after 2 hours of continuous uptake in axons of differentiated NPCs grown in compartments, we saw minimal, if any, fluorescent labeling (data not shown). Therefore, we restricted our analysis to the 4 hour time point for transcytosis experiments. At 4 hours, cells were fixed and we quantified the amount of anterogradely transcytosed APP by using an anti-mouse secondary antibody; fluorescent LDL was measured directly (Figure 3.5C, D). We observed that both the $PS1^{wt/\Delta E9}$ and $PS1^{\Delta E9/\Delta E9}$ genotypes exhibited decreased APP axonal density and APP intensity after 4 hours of transcytosis (Figure 3.5C). Similarly, LDL axonal density and intensity were also decreased in $PS1^{wt/\Delta E9}$ and $PS1^{\Delta E9/\Delta E9}$ axons after 4 hours (Figure 3.5D).

In support of a role of Rab11-dependent route in sorting lipoproteins, when we used shRNA to knockdown Rab11 in $PS1^{wt/wt}$ neurons and measured LDL endocytosis, we found that endocytosis of LDL was severely impaired (Figure 3.6A). Axonal LDL was virtually undetectable with shRNA knockdown of Rab11. An example of the efficiency of the shRNA knockdown is shown in Figure 3.6B. Support for a role of Rab11 mediated transcytosis of APP comes from co-staining experiments where axonal transcytosed APP (22C11) were stained with Rab11 (Figure 3.6C). As seen in Figure 3.6D, 34.68% of Rab11 overlapped with transcytosed APP in $PS1^{wt/wt}$ axons and about 23.39% of transcytosed APP overlapped with Rab11 in $PS1^{wt/wt}$ axons.

The absence of a lipoprotein endocytic defect at early time-points suggested that transcription, levels, degradation, or recycling of the LDL receptor may be driving the reduction in transcyctosis. While there are many potential LDL receptors, LRP1 was an attractive candidate because of its high expression in brain and neuronal samples (Zhang et al., 2014)**.** To determine if transcription or degradation of LRP1 was affected in $PS1^{\Delta E9}$ mutations, we treated purified human neurons with unlabeled LDL and harvested neurons for mRNA and protein. We did not observe differences in APP or LRP1 mRNA or protein levels **(**Figure 3.7A, B**)** at baseline or after LDL treatment, suggesting that transcription, levels, or degradation of LRP1 are not playing a role in the reduced endocytosis of APP and LDL. Though PS1 has been hypothesized to drive reduced degradation of proteins because of alterations in lysosomal pH (Nixon and Mcbrayer, 2013; Nixon and Yang, 2011), we did not observe changes in lysosomal pH in the $PS1^{\Delta E9}$ mutations as assessed by the two

ratiometric pH probes LysoSensor Yellow/Blue Dextran and fluorescein-tetramethylrhodamine Dextran (Figure 3.8A).

In addition, degradation of full-length APP is not different in $PS1^{\Delta E9/\Delta E9}$ neurons treated with cycloheximide (Figure 3.8B) or when lysosome degradation is blocked with chloroquine. Activation of autophagy pathways as measured by chloroquine-induced changes in LC3 II/I ratio is also not altered in $PS1^{\Delta E9/\Delta E9}$ differentiated NPCs (Figure 3.8B). Interestingly, LRP1 protein levels are not reduced by cycloheximide treatment in the time points analyzed, suggesting LRP1 requires an external source of cholesterol to initiate degradation of the receptor (Figure 3.8C).

To determine if the amount of lipoprotein receptors at the somatodendritic surface are driving endocytosis defects, we measured LDL receptor number at baseline and after 4 hours of LDL treatment using two different methods. First, we incubated purified neurons under cold conditions with labeled LDL at 0 and 4 hours, and fixed, and imaged the neurons without permeabilization (Figure 3.7C and D). Under these conditions, we did not observe differences in surface LDL puncta counts in homozygous $PS1^{\Delta E9/\Delta E9}$ neurons compared to $PS1^{wt/wt}$ neurons. Since LDL could be binding non-specifically to the cell surface, we evaluated specific receptor populations by biotinylating the surface of neurons with a cleavable biotin (Sulfo-NHS-LS-Biotin, Pierce) and used streptavidin beads to pull down surface proteins before and after LDL treatment. Probing for LRP1 demonstrated that the surface levels of LRP1 receptor is not different at baseline but is decreased in $PS1^{\Delta E9/\Delta E9}$ differentiated NPCs after LDL treatment (Figure 3.7E and F). This indicates that LRP1 recycling back to the surface after LDL treatment is reduced in $PS1^{\Delta E9/\Delta E9}$ differentiated NPCs.

LDL Endocytosis Defects in PS1ΔE9 Neurons are Rescued by β-secretase Inhibition

PS1 is the catalytic core of the γ-secretase complex which cleaves the β-CTF fragment of APP that is generated by β-secretase cleavage of full-length APP. We previously demonstrated that the $PS1^{\Delta E9}$ mutation impairs γ-secretase activity and APP CTFs accumulate in $PS1^{\Delta E9}$ neurons (Woodruff et al., 2013). A previous study also demonstrated that γ-secretase inhibition in MEFs reduces LDL endocytosis (Tamboli et al., 2011). To determine if γ-secretase activity or if the β-CTF fragment might be responsible for the impaired LDL endocytosis in human neurons, we treated $PS1^{wt/wt}$ neurons with β- and γ-secretase inhibitors and measured LDL endocytosis (Figure 3.9A). Since the most robust difference in LDL internalization was seen at 4 hours, we restricted our data analysis to this last time point. γ-secretase inhibition severely decreased LDL endocytosis at 4 hours while β-secretase inhibitor had no significant effect (Figure 3.9A). Treatment with both β- and γ-secretase inhibitors caused a marked accumulation of α-CTFs while ablating β-CTFs (Figure 3.9D), but had no effect on LDL endocytosis at 4 hours (Figure 3.9A). These results suggest that the β-CTF fragment of APP is responsible for impairing LDL endocytosis in ΔE9 neurons. To further test this possibility, we treated $PS1^{\Delta E9}$ neurons with a β-secretase inhibitor and measured LDL endocytosis (Figure 3.9B). We observed that upon treatment with a β-secretase inhibitor, $PS1^{\Delta E9/\Delta E9}$ neurons were rescued in the ability to endocytose LDL (Figure 3.9B). Treatment of $PS1^{\Delta E9/\Delta E9}$ neurons with both β- and γ-secretase inhibitors also rescued the LDL endocytosis defect (Figure 3.9B), which

suggests that accumulation of only the β-CTF is responsible for impaired LDL endocytosis (Figure 3.9D)**.** Example images of the drug treatments analyzed are depicted in (Figure 3.9C).

LDL Endocytosis Defects are Common to Other FAD Mutations

Accumulation of APP β-CTFs is a phenotype shared by many APP and PS1 FAD mutations (Chang and Suh, 2005; Sinha and Lieberburg, 1999). To assess whether other PS1 mutations might share a common phenotype of impaired LDL endocytosis and transyctosis, we generated additional isogenic cell lines harboring either the $PS1^{A246E/null}$ mutation mutations (Table 1) (Sherrington et al., 1995). In $PS1^{A246E/null}$ mutant neurons we observed significantly decreased LDL endocytosis after 4 hours; this defect was rescued to near wild-type levels when neurons were treated with a β-secretase inhibitor **(**Figure 3.10A and B**)**. This finding demonstrates that the reduction in LDL endocytosis is not specific to the $PS1^{\Delta E9}$ mutation but may be a common feature of many PS1 mutations.

Since the combination of drugs we used are not specific to APP and can have a variety of other targets, we also tested if βCTFs alone are sufficient to drive reduced endocytosis of LDL by overexpressing GFP or βCTF-EGFP (C99-EGFP) in neurons (Rodrigues et al., 2012). After 48 hours of transfection, we incubated cultured neurons with labeled LDL for 4 hours and fixed cells for analysis. βCTF-EGFP transfected neurons had reduced LDL uptake compared to GFP-transfected alone at 4 hours **(**Figure 3.10C**)**.

In contrast, neurons that are haploinsufficient for PS1 ($PS1^{wt/null}$) do not have a defect in LDL internalization (not shown). This argues against a role for simple presenilin reduction of function in driving the observed LDL defect and supports the hypothesis that βCTF accumulation is the primary player. In further support of a βCTF-dependent effect on lipoprotein internalization, isogenic lines with $APP^{wt/V717F}$ and $APP^{V717F/V717F}$ mutations, which accumulate βCTFs **(Figure 3.10D)**, also drive reduced LDL endocytosis at 4 hours.

3.3 Discussion

Here we demonstrate that in human neurons with endogenous expression of fAD mutations increased β-CTF alters the subcellular localization of APP, the distribution of Rab11, and decrease endocytosis and transcytosis of APP and LDL through a common mechanism. The β-CTF induces reduced LDL endocytosis and transcytosis at least in part by impairing recycling of LRP1. These defects are rescued by β-Secretase inhibition. Our results show that impaired LDL endocytosis is present in multiple forms of FAD. The observation that the major risk factor for sAD is E4 allele of APOE, the major brain cholesterol carrier, raises the possibility that lipoprotein transcytosis defects could be a common defect present in multiple fAD and sAD forms. Epidemiologic evidence implicating cholesterol as a major player in AD also dovetails with these molecular and cellular findings (reviewed in Fonseca et al., 2010; Wolozin, 2004).

We demonstrate that β-CTFs cause impaired LDL uptake by reducing recycling of LDL receptors back to the cell surface. One possible mechanism is that β-

CTFs bind to LRP1 (Kounnas et al., 1995; Pietrzik et al., 2002), and retain LRP1 in a Rab11 containing compartment until the β-CTF is cleaved by γ-secretase. This idea would explain why γ-secretase inhibition impairs LDL uptake and why that defect can be rescued by β-Secretase inhibition. Another intriguing possibility is that APP, through its C-terminal domain, acts as a cholesterol sensing protein (Beel et al., 2010; Song et al., 2013). There is ample evidence linking elevated cholesterol levels with increased association of APP and β-CTFs to lipid rafts thus favoring amyloidogenic processing of APP (Beel et al., 2010; Bodovitz and Klein, 1996; Guardia-Laguarta et al., 2010; Grimm et al., 2008; Kojro et al., 2001; Simons et al., 1998; Wahrle et al., 2002). The finding that β-CTFs favors binding to cholesterol over homodimerization suggests that elevated levels of β-CTFs can drive retention of cholesterol in membrane-bound structures mimicking a cholesterol enriched state (Beel et al., 2010). This state could drive a negative feedback loop whereby high levels of APP or the proteolytic products of amyloidogenic APP processing, Aβ, β-CTFs, and AICD, downregulate intracellular cholesterol uptake, biosynthesis, and turnover (Pierrot et al., 2013).

Neurons are dependent on uptake of extracellular cholesterol from lipoprotein particles to perform functions such as axon elongation and synapse formation and maintenance (Lane-Donovan et al., 2014; Mauch et al., 2001; Nägler et al., 2001; Pfrieger, 2003; Pierrot et al., 2013). In fact, glia-derived cholesterol was reported to enhance synaptogenesis of adult rat CNS (Mauch et al., 2001; Nägler et al., 2001) suggesting that a defect in endocytosis and transcytosis of extracellularly-derived cholesterol could have long-term functional consequences leading to impaired

neurotransmitter release and synaptic function. Therefore the defects in LDL endocytosis and transcytosis described here for multiple fAD mutations could contribute to a wide array of phenotypes that have been associated with AD. For instance, the most consistently identified risk factor for sAD is the e4 allele of APOE, which confers the strongest risk for developing SAD (reviewed in Bertram et al., 2010). Though many studies of APOE function have focused on its potential role in mediating Aβ clearance, APOE has also been identified as the major lipoprotein carrier in the brain and the e4 allele is less efficient in transporting brain cholesterol (Liu et al., 2012). Interestingly, post-mortem studies comparing sAD patients to age-matched controls found that brain cholesterol levels are reduced in the areas of learning and memory, the hippocampus and cortex (Svennerholm and Gottfries, 1994).

Our finding that the reduction in LDL endocytosis and transyctosis is common to multiple fAD mutations that increase β-CTFs suggests that therapies should be focused on reducing these toxic APP fragments in addition to amyloid-β and/or modulating cholesterol homeostasis. Furthermore, the common impairment in axonal delivery of cholesterol has far-reaching consequences for maintenance of proper synaptic function and could explain why AD neurons exhibit multiple axonal defects associated with neurodegeneration.

3.4 Experimental Procedures

Cell Culture

Isogenic iPSCs and NPCs were derived as previously described (Israel et al., 2012; Woodruff et al., 2013; Yuan et al., 2011). Purified neurons were generated by differentiating NPCs for 3 weeks in medium containing DMEM:F12 + Glutamax, .5x N2 (Life Technologies), .5x B27 (Life Technologies), and 1x Pen/Strep on plates coated with 20ug/mL poly-ornithine and 5ug/mL laminin (both from Sigma). Media was replaced twice per week. After the 3-week differentiation, neurons were purified by fluorescence activated cell sorting (FACS, BD Biosciences). Cells were stained with CD184, CD44, CD24 (all from BD Bioscience) and cells that were CD184-, CD44- and CD24+ were selected and plated on poly-ornithine/laminin coated plates. Purified neurons were cultured in the same medium as above with the addition of 0.5mM decamp (Sigma), 20ng/mL brain-derived neurotrophic factor, and 20ng/mL glial cell line-derived neurotrophic factor (both from Peprotech). Cells that were grown in microfluidic compartments were differentiated for 3 weeks and then dissociated and the mixed culture was plated in compartments with medium and growth factors as above. Transcytosis experiments were performed after cells had been in microfluidic compartments for 7-10 days.

Statistical Methods

Statistics were performed using GraphPad Prism. Normality for each data set was assessed using D'Agostino-Pearson test. When data were normally distributed, a two-way ANOVA with a post hoc Tukey test was used to compare genotypes. Most immunofluorescence data were non-normally distributed and a nonparametric

Kruskal-Wallis test with Dunn's multiple comparison was used to compare genotype medians.

Immunofluorescence

Purified neurons were grown in 384-well imaging plates at a density of 25,000 cells per well for 7-9 days post-sort. For most experiments, neurons were fixed in 4% paraformaldehyde and PBS for 30 min at 37°C, permeabilized with 0.1% Triton X-100, and blocked in blocking media (10% donkey serum, 3% BSA, 0.1% Triton X-100 in PBS) (Szpankowski et al., 2012). For surface labeling experiments, neurons were not permeabilized and Triton X-100 was excluded from the experiment. For compartment experiments, PDMS microfluidic devices were plasma bonded directly onto 22x50 VWR glass coverslips (Niederst et al., 2015). Dissociated differentiated NPCs were seeded at a density of 1-3 million cells per compartment and grown for 7-10 days (until axons passed through the channels). At this point, compartments were fixed as above and imaged in PBS. Antibodies used for immunofluorescence experiments were rabbit anti-Rab11 (1:1000, Life Technologies 71-5300), rabbit anti-APP Y188 (1:200, Abcam ab32136), mouse anti-APP 22C11 (1:100, EMD Millipore, MAB348), mouse anti-TrkB (1:100, BD 610101), mouse anti-EEA1 (1:100, BD 610457), mouse anti-Lamp-2/CD107b (1:200, BD 555803), mouse anti-NF-H (1:1000, Biolegend SMI-31r), and chicken anti-Map2 (1:500, ab5392). Secondary antibodies were Alexa Fluor donkey anti-mouse and anti-rabbit IgG (Invitrogen) and Dylight 405 donkey anti-chicken IgY from (Jackson ImmunoResearch, 703-475-155) were used at 1:200. Images were acquired on a Zeiss confocal microscope.

Automated Image Analysis

In order to perform unbiased, quantitative analysis of fluorescent images, a series of ImageJ scripts were developed. In all soma immunofluorescence experiments, neurons were labeled with chicken anti-Map2 and stained with the secondary antibody Dylight 405 donkey anti-chicken IgY from (Jackson ImmunoResearch, 703-475-155). The blue Map2 channel served to delineate and identify soma borders (**Figure 2.1A).** The SomatoDendrite_ROI script used thresholding to generate black and white mask images, which was then used to identify soma bodies 50-200 um^2 in size. Zip files corresponding to the soma ROIs from each image were then used to quantify fluorescent intensity in unthresholded images from the other channels with MeasureIntensityinROI script (**Figure 2.1B).** To quantify neuronal puncta, a separate script, PunctaInROIAnalysis, was developed that used the thresholding and Analyze Particles features of ImageJ to automatically segment and count puncta in the ROIs generated from SomatoDendrite_ROI (**Figure 2.1C and D**). Example output text files can be seen for PunctaInROIAnalysis (C) and MeasureIntensityInROI (D) scripts.

Endocytosis, Recycling, and Transcytosis

For constitutive uptake endocytosis assays, neurons were incubated with LDL-Bodipy (20 ug/ml, Invitrogen L3483), Dextran-tetramethylrhodamine (TMR) (250 ug/ml, Invitrogen D1817), or Transferrin-647 (25 ug/ml, Invitrogen T-23366) at 37°C for indicated times, fixed, and imaged. For recycling assays, neurons were treated with Transferrin-647 at 37°C and allowed to internalize for 20 minutes. Neurons were

washed twice in warm media and then chased for the indicated amount of time. For all fixed endocytosis assays, a custom ImageJ program was used to identify Map2-positive soma and automatically generate region of interests (ROI) corresponding to soma. Mean intensity and puncta count per soma were then determined and averaged across images and experiments. All endocytosis assays were repeated at least three times.

For transcyctosis experiments, dNPCs were grown in compartments and treated on the soma side with LDL-Bodipy (20 ug/ml), LDL-DiI (12.5 ug/ml), or mouse anti-22C11 (1:100) for 4 hours with axons in fluidic isolation (Niederst et al., 2014). Axonal puncta analysis was done as previously described with modifications (Szpankowski et al., 2012) (See **Figure 2.5**) **.** Briefly, axons were imaged at 100x and a custom Guassian-fitting colocalization package in MATLAB (MathWorks) was used to calculate axonal density, mean puncta intensity, and percent colocalization per axon.

Lysosomal pH Measurements

To measure lysosomal pH by microscopy, NPCs or dNPCs were grown in 96 well imaging plates and incubated with Dextran, fluorescein and tetramethylrhodamine (Fl/TMR) (250 ug/ml, Invitrogen D1951) or Lysosensor Yellow/Blue Dextran (Invitrogen, L-22460) for 2-6 hours. Cells were then washed twice with warm media and dextran was chased into the lysosomes for >12 hours. Red/green or Yellow/Blue wavelengths were captured simultaneously in live cells. Cells incubated with dextran Fl/TMR were imaged on a confocal microscope in warm

media. Imaging time was limited to half an hour per plate. A custom ImageJ program identified all red puncta greater than 0.2 um in size (lysosomes, pH-insensitive dye) and then the ratio of green/red mean intensity per puncta was determined. Cells incubated with Lysosensor Yellow/Blue Dextran were imaged on a plate reader. Cells were excited at 352 nm and simultaneously measured for Yellow and Blue fluorescence. To generate a standard curve, wild-type cells were treated with pH-calibrated buffers and the average green/red or yellow/blue ratio per image was fit to a standard curve (See **Figure 2.3**) (Diwu et al., 1999; Lee et al., 2010).

Surface Biotinylation Assay

NPCs were grown in 6 well plates and differentiated down a neuronal lineage as described in the Cell Culture methods. At 5 weeks, neuronal media was changed to warm fresh media or media supplanted with 12.5 ug/ml of unlabeled LDL for 4 hours. At the end of the incubation, differentiated NPCs were washed twice with ice-cold PBS and then incubated at 4C with 2mM EZ-Link™ Sulfo-NHS-SS-Biotin (Life Technologies) in PBS for 30 minutes. Cells were then lysed in equal volumes of RIPA buffer. For pulldown experiments, 200 ug of harvested protein at 0.5 ug/ul was incubated with 50 ul of pre-washed Pierce Streptavidin Magnetic Beads (Life Technologies, 88817) overnight at 4C. The next day, a sample of input was saved for bookkeeping and beads were washed to remove residual, unbound proteins and biotinylated proteins were released from the streptavidin beads by boiling samples in loading buffer at 100C. Westerns were run with 5% of input, 5% of supernatant, and

50% of pull down. Quantification of recycling was determined based on input signal. (Pull down/Input)

Chapter 3 is currently being prepared for submission for publication. Reyna, S.M., Woodruff, G., and Goldstein, L.S. Reduced endocytosis and transcytosis of APP and lipoproteins owing to accumulation of APP β-CTFs in familial Alzheimer's disease mutations. (To be published). The dissertation author is a primary researcher and author of this work.

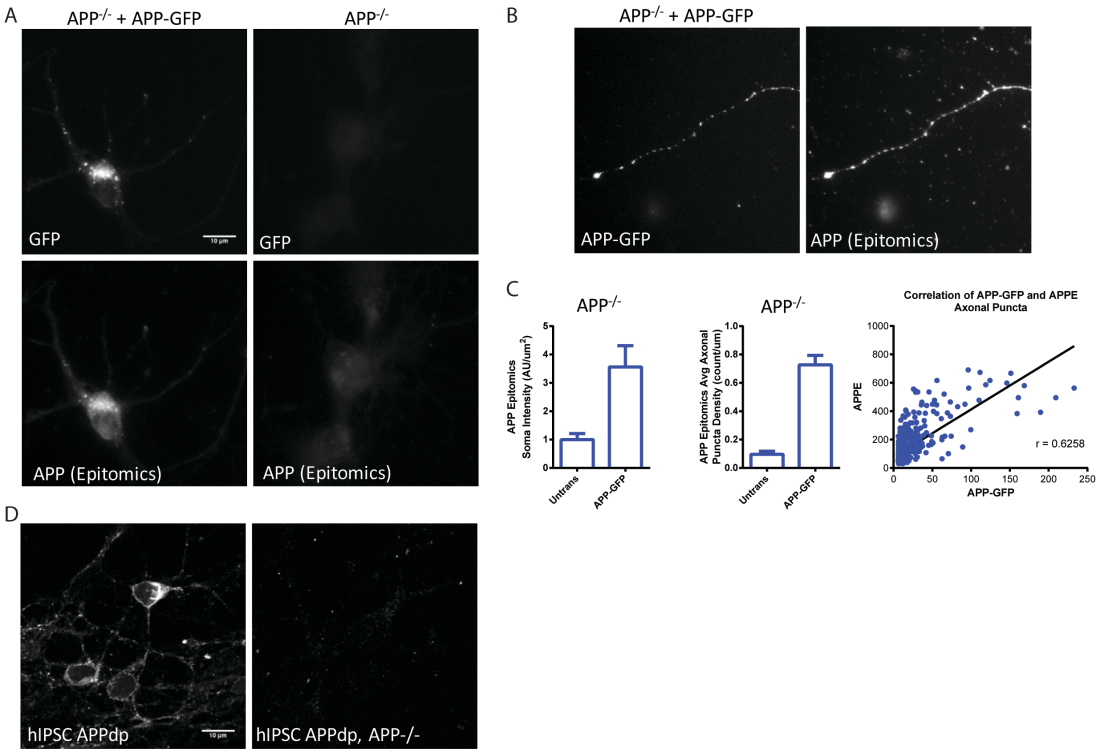

Figure 3.1 APP Epitomics Antibody is Specific to APP. A) APP$^{-/-}$ mouse neurons were stained with the APP Epitomics Y188 antibody with and without overexpression of an APP-GFP plasmid. Note the almost complete absence of APP staining in the untransfected cells and the extremely similar staining pattern of the APP-GFP and APP Epitomics stains. B) An example of axonal APP staining in APP$^{-/-}$ cells overexpressing APP-GFP and stained for APP Epitomics. Again, note the strongly similar distribution pattern. C) Quantification of APP Epitomics soma intensity from A and axonal APP Epitomics density in APP$^{-/-}$ untransfected and APP-GFP transfected cells. The third inset shows the strong correlation of axonal puncta APP-GFP and APP Epitomics intensities. D) APP Epitomics staining in hIPSC-derived neurons from an APP duplication patient and in a corresponding isogenic APP$^{-/-}$ clone.

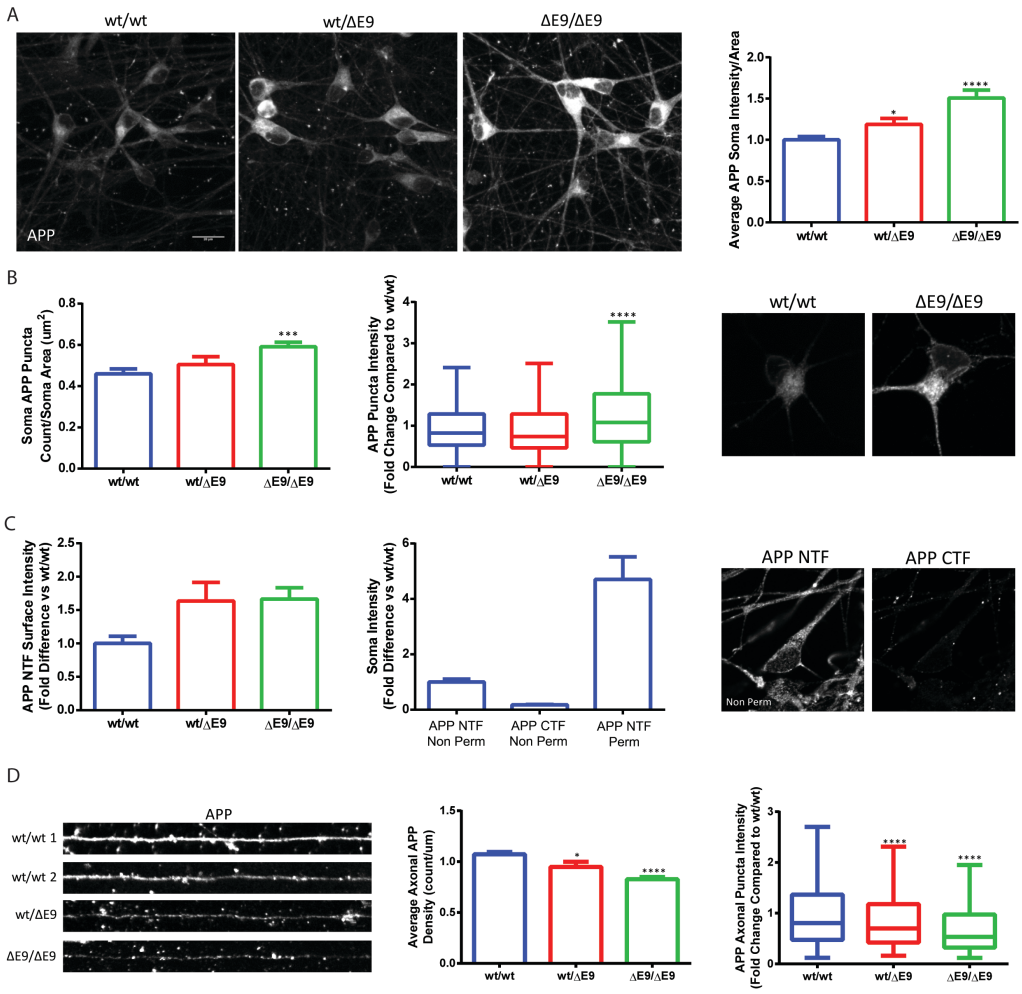

Figure 3.2 PS1$^{\Delta E9}$ iPSC-Derived Neurons Exhibit Altered Sub-cellular Distribution of APP. Purified iPSC-derived neurons were stained with a C-terminal APP antibody (Epitomics) and imaged for analysis. A) PS1$^{\Delta E9}$ neurons have a gene-dose dependent increase in soma APP intensity. Data represent a total of 5 immunofluorescence experiments from 5 differentiations. (Soma counts: wt/wt: 113; wt/ΔE9: 59; ΔE9/ΔE9: 109) B) High magnification analysis of APP puncta indicate that the increase in soma intensity is a combination of increased puncta counts and individual puncta intensity. Data represent 3 immunofluorescence experiments and over 4000 puncta per genotype. C) To evaluate surface APP, an antibody targeting the N-terminus of APP was used to probe unpermeabalized purified neurons. D) To evaluate axonal APP levels, axons from differentiated NPCs grown in microfluidic devices were stained with APP CTF antibody and imaged. Average density and individual puncta intensities were decreased in a gene-dose dependent manner in PS1$^{\Delta E9}$ axons. Data represent the pooled values of 3 immunofluorescence experiments and 2 NPC lines per genotype. wt/wt: 160 axons, 14238 puncta; wt/ΔE9: 36 axons, 2902 puncta; ΔE9/ΔE9: 161 axons, 10273 puncta.

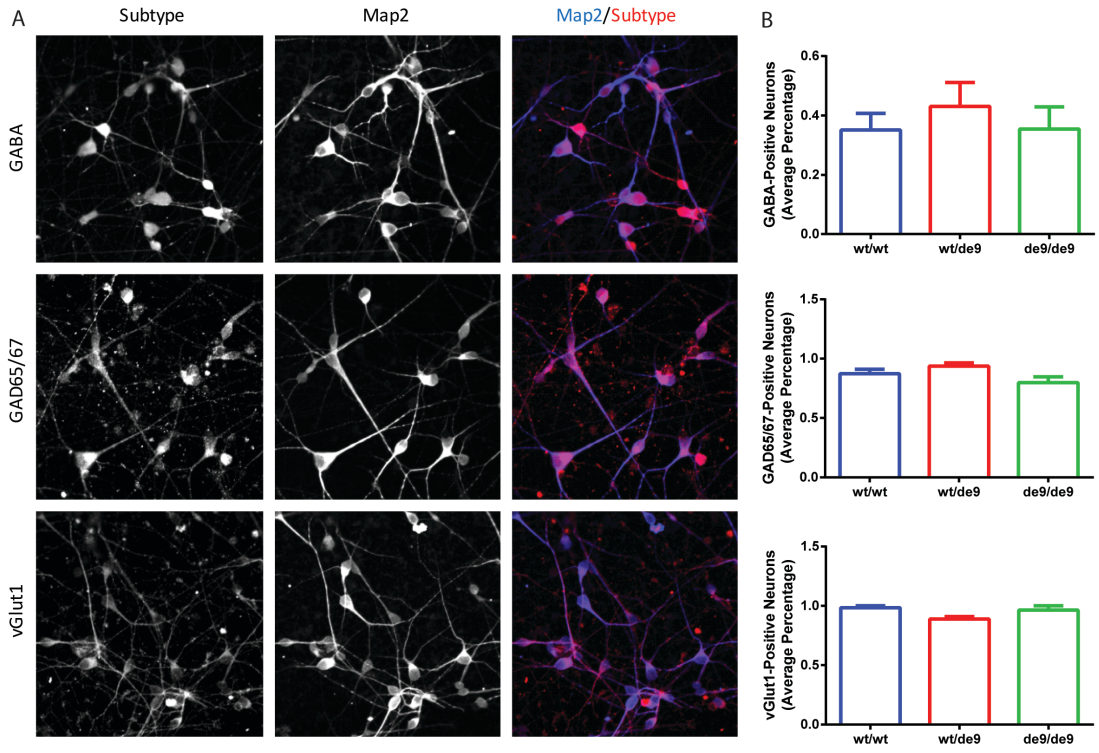

Figure 3.3 Neuronal Subtype Quantification in hIPSC-Derived PS1 Genotypes. A) Examples of purified neurons stained with Map2 and GABA, GAD65/67, or vGlut1. B) Quantification of neuronal subtype percentages. Data represent the average of 2 NPC lines per genotype, 2 differentiations, and multiple wells per differentiation.

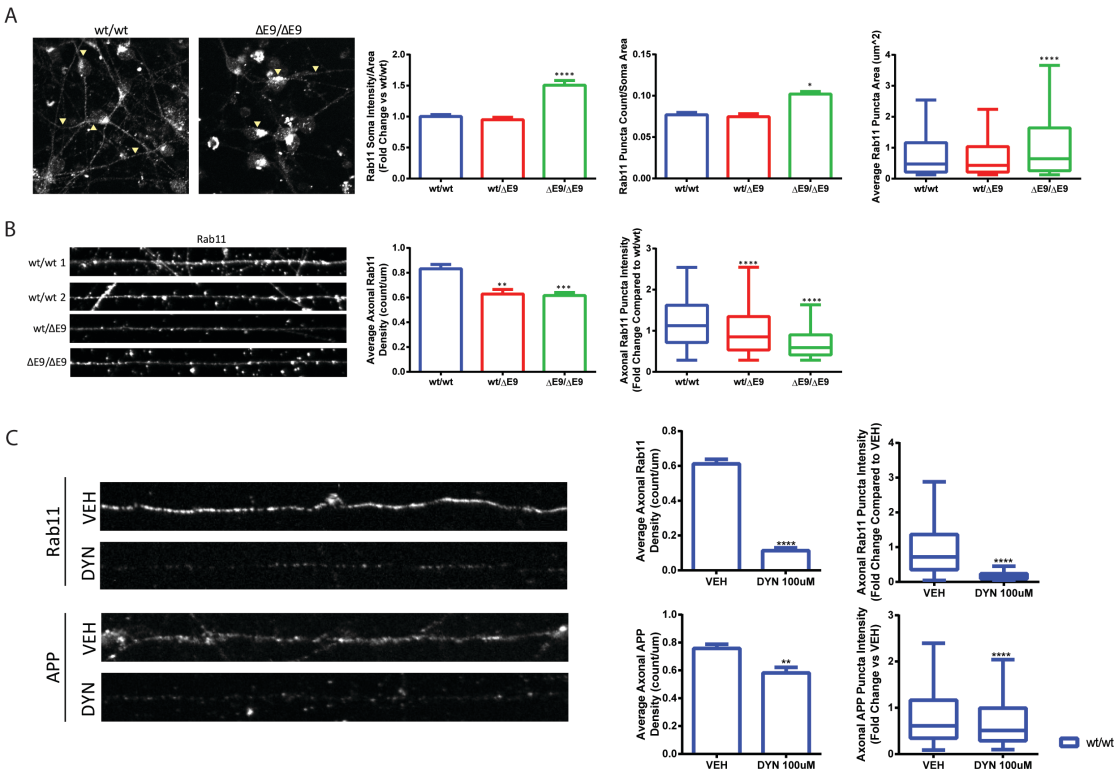

Figure 3.4 PS1$^{\Delta E9/\Delta E9}$ Neurons Exhibit Altered Rab11 Distribution. Purified iPSC-derived neurons were grown in 384 well imaging plates for 1 week after sorting and stained for Rab11a. A) While PS1$^{wt/wt}$ neurons exhibited distinct punctate pattern of Rab11 staining in soma, PS1$^{\Delta E9/\Delta E9}$ neurons had a marked accumulation of Rab11 in soma (arrows). Quantification of staining showed that soma Rab11 intensity, puncta count, and puncta area were all significantly increased in PS1$^{\Delta E9/\Delta E9}$ neurons (wt/wt: 87 neurons, 1099 puncta; wt/ΔE9: 79 neurons, 961 puncta; ΔE9/ΔE9: 62 neurons, 902 puncta). B) For quantification of Rab11 in axons, a purified population of axons was obtained by growing differentiated NPCs in microfluidic devices and stained for axonal Rab11a. Quantification of Rab11a staining in axons showed that Rab11 density and puncta intensity were reduced in a dose-dependent manner. (wt/wt: 57 images, 7373 puncta; wt/ΔE9: 33 images, 5312 puncta; ΔE9/ΔE9: 41 images, 5144 puncta). C) To estimate the percentage of Rab11 and APP in axons derived from transcytosis, PS1$^{wt/wt}$ were treated with the dynamin inhibitor 100uM Dynasore for 24 hours and subsequently stained for Rab11 and APP CTF. Inhibition of soma endocytosis resulted in almost complete ablation of axonal Rab11 density (first inset) and approximately a 20% decrease in APP density (second inset).

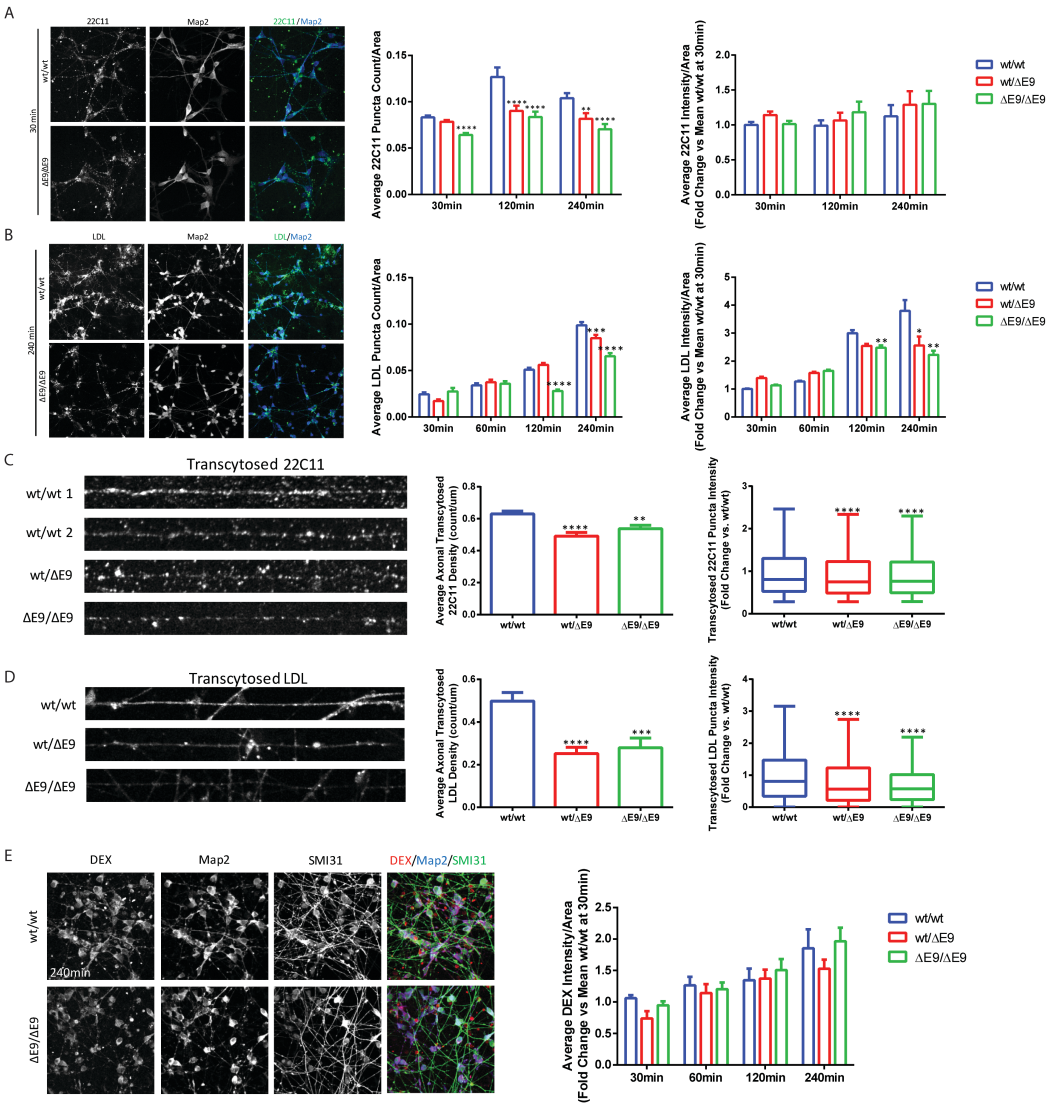

Figure 3.5 PS1 ΔE9 Neurons have Reduced Endocytosis and Transcytosis of APP and LDL. A) Example images of Internalization of APP 22C11 antibody at 30 minutes in $PS1^{wt/wt}$ and $PS1^{\Delta E9/\Delta E9}$ neurons. B) Example images of LDL-Bodipy labeling at 240min in $PS1^{wt/wt}$ and $PS1^{\Delta E9/\Delta E9}$ neurons, with intensity adjusted so that puncta are clearly visible in the $PS1^{\Delta E9/\Delta E9}$ neurons. Graphs depict quantification of LDL puncta count and intensity normalized to cell area at 30min, 60min, 120min, and 240min of LDL uptake. As evidenced, $PS1^{wt/\Delta E9}$ and $PS1^{\Delta E9/\Delta E9}$ neurons have reduced APP and LDL soma endocytosis, with the LDL effect appearing most prominently at 240min. C and D) differentiated NPCs were grown in microfluidic devices and then allowed to internalized either APP antibody (C) or LDL-Bodipy (D) on the soma side with the axons in fluidic isolation. Then axons that passed through the channels were imaged and puncta densities and intensities were evaluated. E) Example images and a graph of intensity quantification are depicted for endocytosis of the fluid phase fixable marker, Dextran-TetramethylRhodamine.

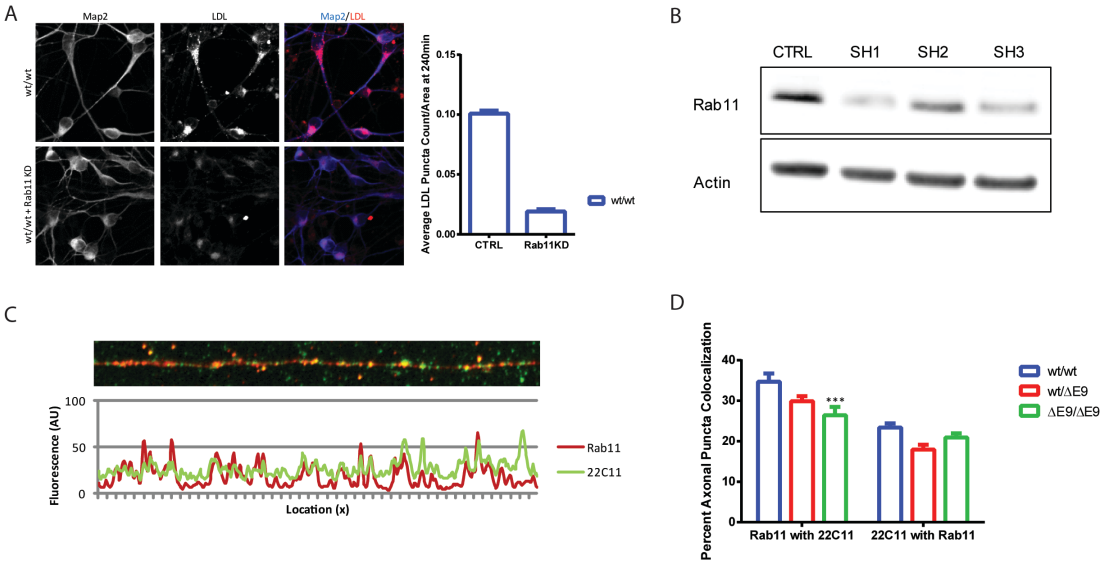

Figure 3.6 LDL and APP Use Rab11 for Transcytosis into Axons. A) Purified neurons stained were pre-treated with SH3 against Rab11a for 48h. At 48h, neurons were incubated with 12.5ug/ml of LDL-DiI for 4h before fixation. Note the strong reduction in LDL-DiI internalization after Rab11a knockdown in the soma. There was almost complete absence of axonal LDL staining in Rab11 shRNA-treated neurons. B) Differentiated NPCs were grown in microfluidic chambers and allowed to transcytose APP (22C11) for 4h with axons in fluidic isolation. Transcytosed 22C11 overlaps with Rab11 ~25% of the time in $PS1^{wt/wt}$ cells, indicating that at least 25% of internalized APP is transported via a transcytotic route.

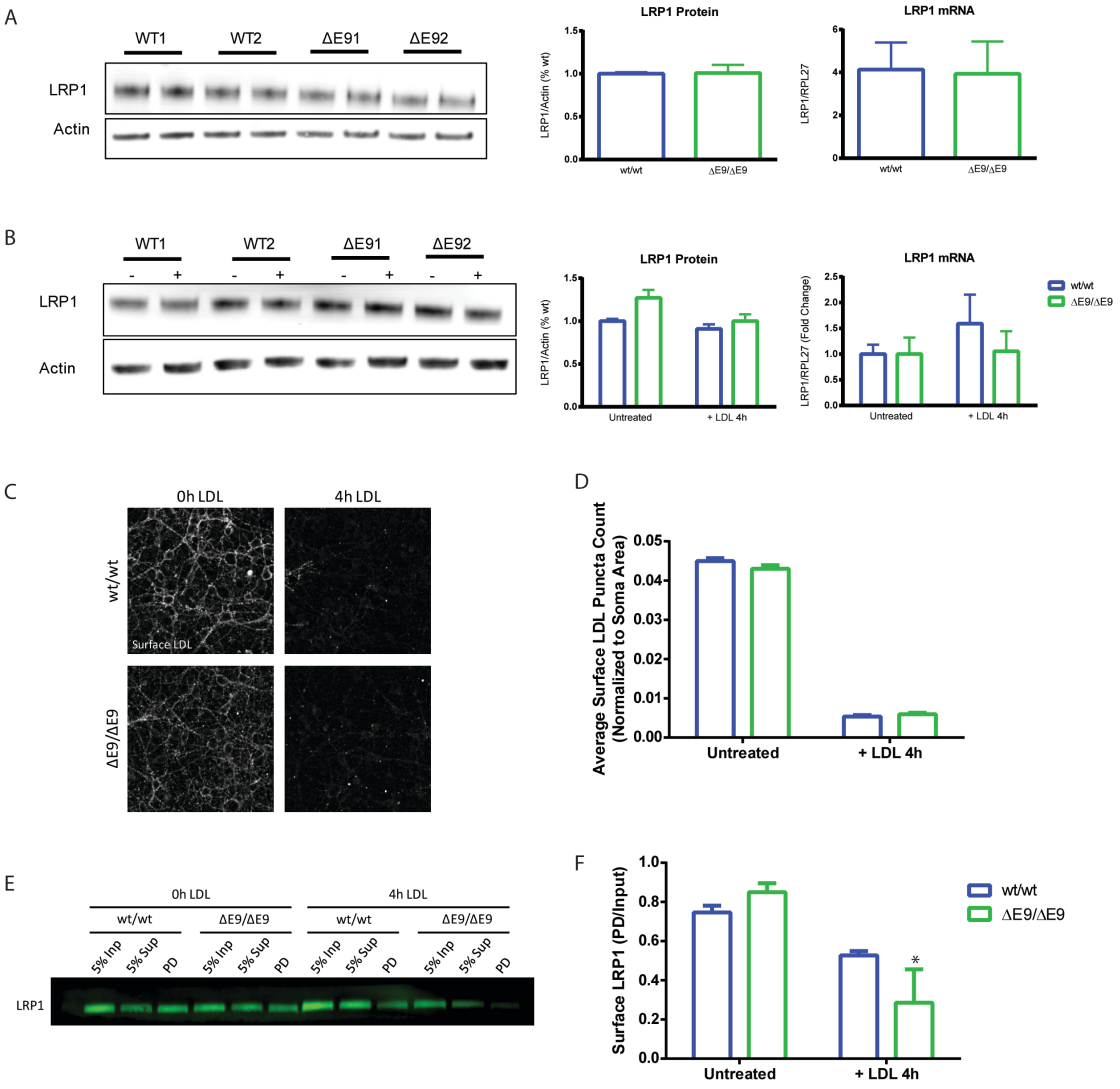

Figure 3.7 LRP1 Surface Recycling is Reduced in PS1$^{\Delta E9/\Delta E9}$ After 4h LDL Treatment. A) Purified neurons were harvested and LRP1 protein and mRNA levels were measured. PS1$^{\Delta E9}$ LRP1 levels were not different at baseline. B) LRP1 protein and mRNA levels were measured after purified neurons were treated with LDL for 4 hours. PS1$^{\Delta E9}$ LRP1 levels were not different after 4h LDL treatment. C) To measure surface LDL labeling and recycling, purified neurons were left untreated or treated with 12.5ug/ml of unlabeled LDL for 4h. At the end of 4h, purified neurons were incubated with LDL-Dial for 30 minutes at 4C to label surface LDL receptors. Neurons were then fixed and puncta counts were evaluated in unpermeabilized cells. Surface LDL levels were not different in PS1$^{\Delta E9}$ neurons. D) Differentiated NPCs were treated with a cell impermeant Biotin for 30 minutes at 4C with and without pre-treatment with 4h LDL. Streptavidin beads were then used to pull down biotinylated surface proteins and run on a gel.

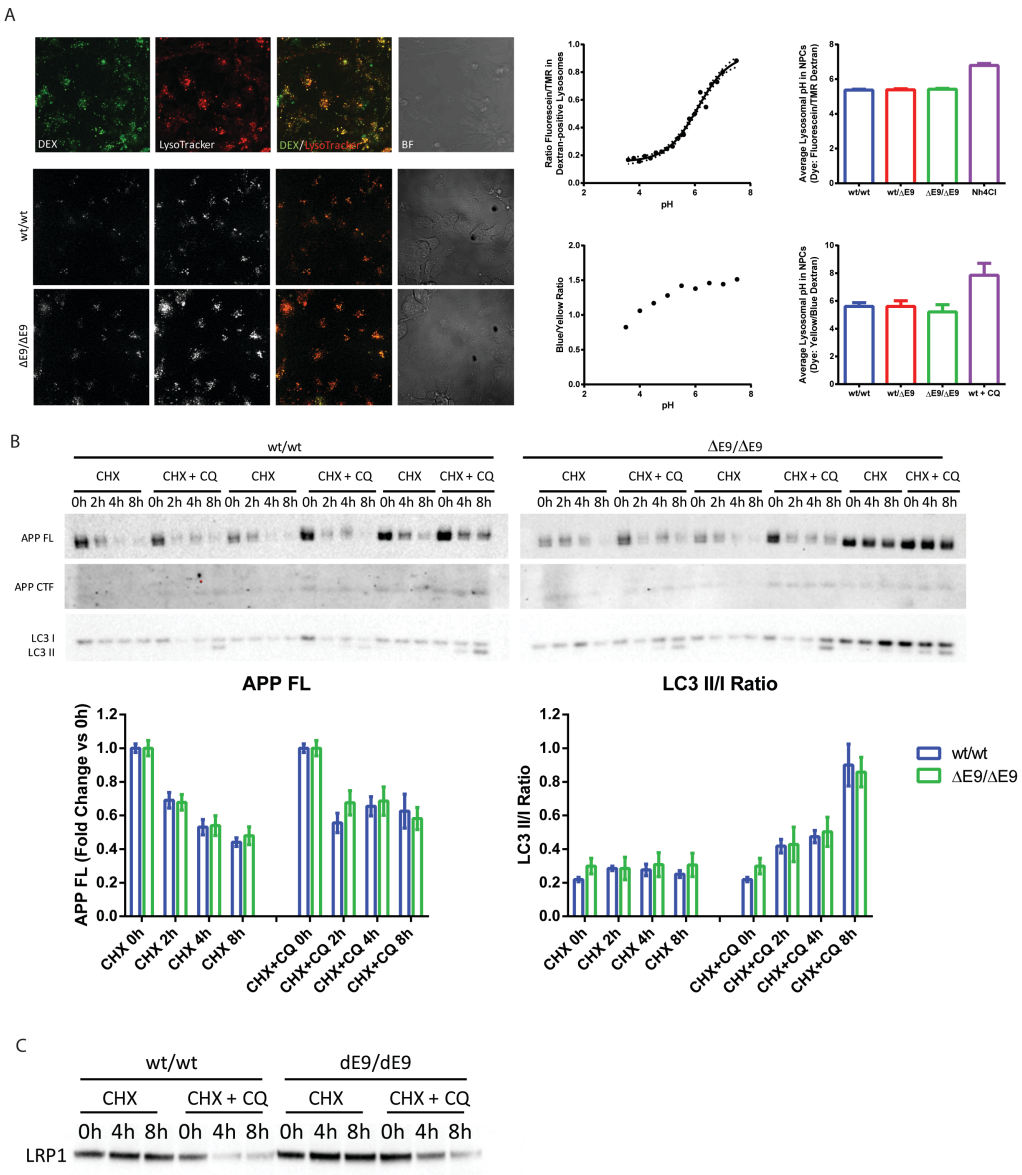

Figure 3.8 PS1$^{\Delta E9}$ Mutations do not have Altered Lysosomal pH, Protein Degradation, or Autophagy Activation. A) PS1$^{\Delta E9}$ NPCs were incubated with Fl/TMR Dextran or Lysosensor Yellow/Blue Dextran to label lysosomes. Example images of Fl/TMR Dextran are shown. Lysosomal pH was measured using these ratiometric probes and plotting the experimental values on a standard curve (shown in graphs). Data represent multiple NPC lines per genotype, multiple experiments, and many wells. B) NPCs were differentiated for 5 weeks and then treated with cycloheximide (CHX) with and without chloroquine (CQ) for the indicated times. Samples were harvested and run on a Western and probed for APP and LC3. As evidenced, neither APP degradation or LC3 II/I ratio (a measure of autophagy activation) were different in PS1$^{\Delta E9}$ dNPCs. C) LRP1 is not degraded in the time points analyzed.

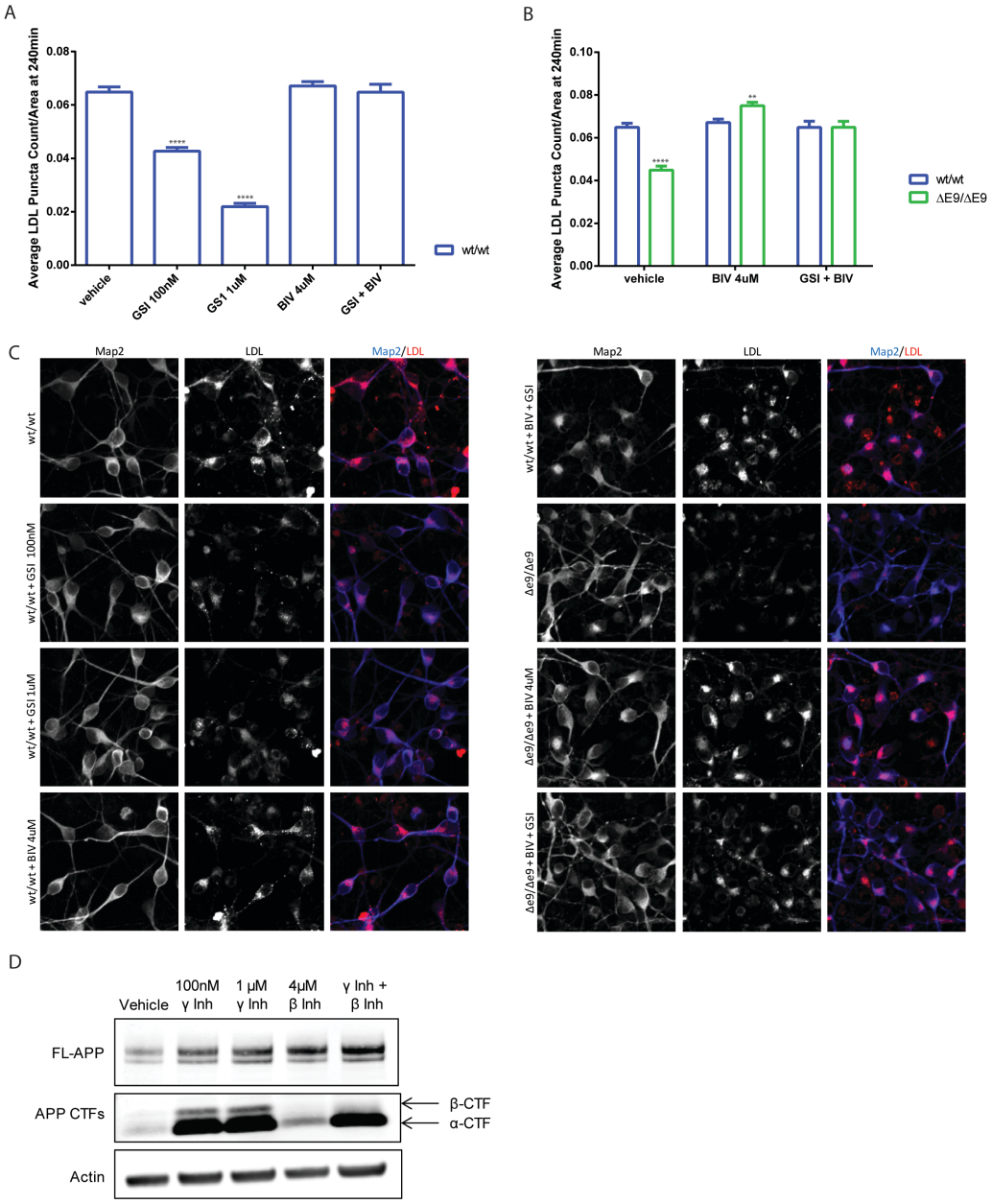

Figure 3.9 β-CTF Levels Inversely Affect LDL Uptake in Purified Human Neurons. A) Quantification of LDL puncta counts in 4 hour LDL-treated $PS1^{wt/wt}$ neurons. B) When β-CTF levels were ablated in $PS1^{\Delta E9/\Delta E9}$ neurons treated with a BIV, the reduction in LDL internalization at 4 hours was rescued to $PS1^{wt/wt}$ levels. Importantly, LDL endocytosis is rescued even in the presence of high levels α-CTFs when β-CTFs are reduced (GSI + BIV). Data represent 2 NPC lines per genotype, multiple wells, 2 separate experiments, and hundreds of neuronal soma. C) Example images for 5A and 5B. D) Example Western blot of neurons treated with the pharmacological modulators used in 3A-C. α-CTFs and β-CTFs are indicated by arrows.

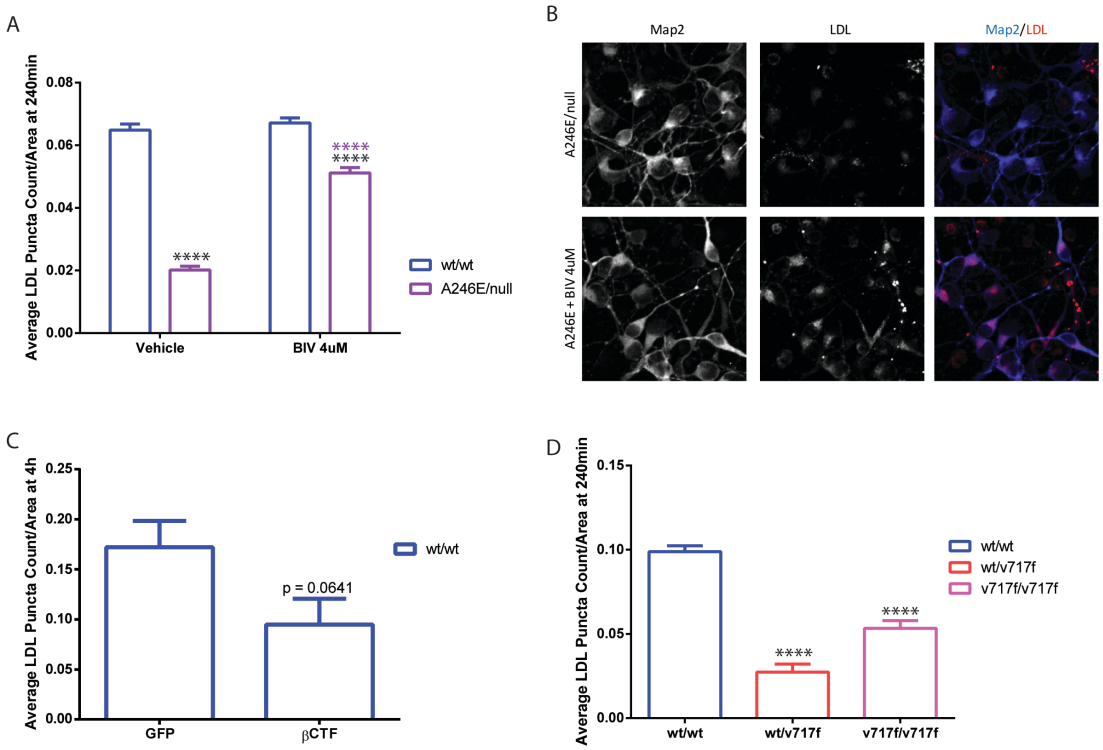

Figure 3.10 LDL Endocytosis is Reduced in hIPSC-Derived Neurons with Increased Levels of βCTF. A) PS1$^{A246E/null}$ mutants show reduced LDL uptake at 4h, which is partially rescued by 4h pre-treatment with 4uM BIV. B) Example LDL uptake images from PS1$^{A246E/null}$ with and without 4uM BIV. C) Purified neurons transfected with βCTF (C99-EGFP) exhibit a trend toward reduced LDL internalization at 4h. (n=1 experiment) D) hIPSC-derived neurons with APP^{V717F} mutations also exhibit reduced LDL endocytosis at 4h.

Chapter 4

Isogenic Human Neuronal Models of Multiple Familial Alzheimer's Disease Mutations Reveals Differences in Early Detectable Phenotypes

4.1 Introduction

Alzheimer's Disease (AD) is a devastating and incurable neurodegenerative disorder. AD brains are identified by characteristic extracellular plaques composed of amyloid-beta (Aβ) peptides and intracellular neurofibrillary tangles comprised of hyperphosphorylated tau protein. Aβ peptides are generated when the full length amyloid precursor protein (APP) undergoes amyloidogenic APP processing. Mutations in APP, presenilin 1 (PS1) and presenilin 2 (PS2) cause dominantly inherited AD, known as familial AD (FAD). Most mutations in APP that cause FAD either promote amyloidogenic processing of APP or increase longer forms of Aβ, which are more prone to aggregation. Mutations in the presenilin genes also increase longer forms of Aβ, which generally increase the Aβ 42/40 ratio.

The APP Indiana mutation (V717F) was one of the first described mutations in APP and shown to cause FAD (Murrell et al., 1991). The site of the mutation is just beyond the Aβ sequence of APP and near γ-secretase cleavage sites. Multiple reports show that the V717F mutation increases the Aβ 42/40 ratio (Roher et al., 2004; Wiley et al., 2005) and transgenic mice overexpressing the V717F mutation develop Alzheimer-type neuropathology (Games et al., 1995). Induced pluripotent stem cell technology (Takahashi et al., 2007a) has provided neuroscientists the opportunity to study disease-causing mutations in human neurons. This is important because studies in mice do not produce the full phenotypes that are observed in humans and studies in non-neuronal cells do not allow studies of tau pathology as tau is a neuron specific protein. Additionally, a single extra copy of the APP gene is sufficient to cause FAD (Rovelet-Lecrux et al., 2006), which raises the possibility that mice and cell culture

studies that overexpress FAD mutations are not an accurate representation of true AD pathophysiology. Induced pluripotent stem cells (iPSCs) provide neuroscientists the opportunity to study FAD mutations (Israel et al., 2012; Woodruff et al., 2013; Yagi et al., 2011) and AD risk factors (Young et al., 2015) in relevant human cell types. A recent study characterized iPSC-derived neurons from APP London mutation (V717I) patients and reported an increase in the Aβ 42/40 ratio, increased sAPPβ, and an increase in total and phosphorylated tau (Muratore et al., 2014). In general, most iPSC-derived neuron studies of APP mutations have reported some type of tau phenotype, while studies of PS1 and PS2 mutations either do not comment on tau, or report no differences.

Here we establish an iPSC model of FAD from patients harboring the APP V717F mutation and from CRISPR-mediated knockin of the V717F mutation into a "wt" genetic background. The comparison of patient and knockin lines with the V717F mutation reveals that the phenotypes observed in knockin lines are remarkably similar to the patient lines, but isogenic lines have considerably less variability. We report that the V717F mutation causes an increase in the Aβ 42/40 ratio caused by increased Aβ42 and decreased Aβ40, no change in the sAPP fragments, but interestingly, an increase in the β-CTF fragment of APP. Additionally, we report that the V717F mutation causes an increase in total levels of tau and phosphorylated tau at early time points, and an increase in the phospho-tau/total tau (p-tau/t-tau) ratio after 3 months of culture. Finally, we compare the early AD-related phenotypes in isogenic cells harboring either the APP V717F, or PS1 ΔE9 mutations and report that the PS1 ΔE9 mutation does not display tau phenotypes at early or late timepoints, despite

sharing the V717F phenotypes of an increased Aβ 42/40 ratio and increased APP CTFs.

4.2 Results

Reprogramming of V717F patient fibroblasts and CRISPR knocking of V717F mutation

Fibroblasts from two patients with the V717F mutation (V717F-1 and V717F-2) were reprogrammed to induced pluripotent stem cells (iPSCs) using the standard OSKM retroviral method. Each transcription factor was linked to a GFP tag so that silencing of the retroviral factors could be monitored. Multiple clones of IPSCs derived from each patient expressed the pluripotency markers Tra-1-60 and Tra-1-81 (Figure 4.1 A,B), and had no detectable GFP expression, indicating that the retroviruses were silenced (data not shown). To confirm that the reprogrammed cells possess the capacity to differentiate into the three germ layers, the iPSCs were grown in embryoid bodies for 14 days, followed by RNA extraction. The RNA was then used for multiplex qPCR detection of genes that are characteristic of each of the three germ layers. All clones tested for each patient were capable of differentiation to each of the three germ layers (data not shown).

To generate an isogenic model of the V717F mutation, we used CRISPR/Cas9 genome editing technology, to introduce the mutation into the genetic background of Craig Venter (CV). We used iPSCs from CV, along with a CRISPR-GFP plasmid, a guide-RNA plasmid designed to target the APP locus and a single-stranded oligo to serve as the donor template. CV iPSCs were nucleofected with the genome-editing

DNA and then plated at limiting dilutions so that clonal lines could be isolated. To detect which clones underwent successful genome-editing and integration of the V717F mutation, we used an allele-specific pcr. We isolated DNA from 150 clonal iPSC lines and of those 150, 1 cell line was confirmed to be heterozygous for the V717F mutation (wt/V717F) and 1 cell line was confirmed to be homozygous for the V717F mutation (V717F/V717F). Another 15 clones were also detected to have the V717F mutation, but also had an indel on the other allele that disrupted the APP gene.

Characterization of APP Aβ peptides from V717F patient and isogenic neurons

To characterize how the V717F mutation affects APP processing, we first differentiated the iPSCs to neural progenitor cells (NPCs) using a PA6 coculture and SMAD inhibition protocol (Yuan, et al. 2011). To generate a homogenous population of NPCs, we FACS purified the cultures. We did not detect any differences in the percentage of cells that stained positive for the NPC signature (data not shown) in any of the patient or isogenic cell lines. To further differentiate cells to a neuronal state, we removed FGF from the NPC cultures and differentiated the cells for 3 weeks. We specifically wanted to characterize APP processing changes from neurons, so to achieve this we FACS purified the cultures to obtain a purified neuronal population (Yuan et al, 2011). We did not detect any differences in the percentage of neurons between any of the patient or isogenic cell lines (data not shown).

We used a highly sensitive ELISA assay to measure secreted a-beta (Aβ) 38, 40, and 42 from the patient and isogenic cell lines. For comparison of the V717F patient lines, we used 2 non-demented control individuals (NDC1, NDC2) (Israel et

al., 2012). For comparison of the V717F isogenic lines we used 2 clonal cell lines that maintained 2 wild-type copies of APP (wt/wt). We first quantified the Aβ 42/40 ratio, as this is a phenotype associated with the V717F mutation and many other FAD mutations (ref). Both patient lines exhibited a significant ~2-fold increase in the Aβ 42/40 ratio when compared to NDC1 and NDC2 (Figure 4.2 A). In the isogenic cells, one copy of the V717F mutation was similar to the patient lines in that there was a 2-fold increase in the Aβ 42/40 ratio when compared to wild-type (Figure 4.2 B). Two copies of the V717F mutation further increased the Aβ 42/40 ratio to ~4-fold when compared to wild-type (Figure 4.2 B). To determine whether the ratio is altered due to a decrease in Aβ40, an increase in Aβ42, or both, we quantified the total amounts of each peptide. In the patient lines, one patient (V717F-2) exhibited a significant decrease in Aβ40 compared to NDCs, while the other patient (V717F-1) was not significantly different (Figure 4.2 C). Neurons from the isogenic cells both exhibited significantly decreased Aβ40 (Figure 4.2 D). Total levels of Aβ42 were significantly increased in one patient (V717F-1) and were not significantly different in the other patient (V717F-2) when compared to NDCs (Figure 4.2 E). The isogenic cells exhibited a dose-dependent increase in Aβ42 compared to wild-type (Figure 4.2 F). Thus, we conclude that the V717F mutation alters the Aβ 42/40 ratio by decreasing Aβ40 and increasing Aβ42. Finally, we quantified the total amounts of Aβ38, which has also been reported to be affected by the V717F mutation (Wiley et al., 2005). One of the patients (V717F-1) displayed a significant increase in Aβ38 compared to NDCs, while the other patient (V717F-2) was not significantly different (Figure 4.2 G). In the isogenic cells, there was a trend for wt/V717F to have an increase in Aβ38, and there

was significantly more Aβ38 in the V717F/V717F genotype when compared to wild-type (Figure 4.2 H). Since we observed variability between the 2 V717F patients with respect to Aβ (and some variability between NDCs), but much more clear dosage-dependent Aβ phenotypes in the isogenic cells, we proceeded forward by primarily analyzing the isogenic neurons for further characterization of AD-related phenotypes.

APP V717F mutation increases APP β-CTF fragments

A recent study of iPSC-derived neuron study of the APP London mutation (V717I) reported increased sAPPβ (Muratore et al., 2014). Additionally, many other APP and PS1 mutations have been reported to affect c-terminal fragments (CTFs) of APP (De Jonghe et al., 2001; McPhie et al., 1997; Wiley et al., 2005). To test if the V717F mutation affects the soluble fragments of APP, we utilized a highly sensitive ELISA assay to quantify both the sAPPα and sAPPβ fragments. We quantified the sAPPα/sAPPβ ratio from purified isogenic neurons, and observed no significant differences in the sAPPα/sAPPβ ratio (Figure 4.3 A). We also did not detect any differences in the total levels of sAPPα (Figure 4.3 B) or sAPPβ (Figure 4.3 C) between the wild-type and V717F genotypes.

To determine if the V717F mutation affects the levels of full-length APP (FL APP) or CTFs of APP, we performed a western blot from purified neurons. We did not observe any significant differences in FL APP between wild-type, wt/V717F and V717F/V717F genotypes (Figure 4.4 A). Likewise, there were no significant differences in the levels of α-CTF between genotypes (Figure 4.4 B). Interestingly, we did observe a significant increase in β-CTF in the V717F/V717F genotype compared

to wild-type, and a trend for increased β-CTF in the wt/V717F genotype (Figure 4.4 D). Both the α- and β-CTFs contain the mutated amino acid, which suggests that the trafficking of each fragment could be different and thus, only β-CTFs accumulate. Since we did not observe any differences in sAPPβ, we conclude that there is accumulation of β-CTFs in V717F neurons rather than enhanced β-secretase processing.

APP V717F mutation increases total and phosphorylated tau

Aggregates of hyperphosphorylated tau protein are one of the major pathologies found in AD brains. Recent studies of iPSC-derived neurons harboring APP mutations have shown that mutant APP neurons exhibit either increased total levels of tau and p-tau, an increase in the p-tau/t-tau ratio, or altered localization of tau. To test if the V717F mutation affects total levels or the p-tau/t-tau ratio, we utilized a highly sensitive ELISA assay that measure total and p-tau levels at the T231 phosphorylation site. We first tested neurons that were differentiated for 3 weeks, FACS sorted, and then harvested for tau analysis 5 days later. There were no significant differences in the p-tau/t-tau ratio, however, the levels of total tau and p-tau (T231) were significantly increased in both the wt/V717F and V717F/V717F genotypes compared to wild-type (Figure 4.5 A,B,C). In addition to increased p-tau at T231, V717F neurons also exhibited increased p-tau at other phosphorylation sites (data not shown). Next, we differentiated cells for a total of 3 months to determine if more mature neurons would have similar or different tau phenotype. At the 3 month

time point, both wt/V717F and V717F/V717F neurons displayed an increase in the p-tau/t-tau ratio (Figure 4.5 D).

APP V717F neurons respond to drug treatments

Human-derived models for AD present a new paradigm for drug testing. Drug testing can allow elucidation of pathways that may be affected or connected in AD and offer insight into whether human cells respond the same or different than murine models. The amyloid cascade hypothesis of AD posits that increased Aβ causes hyperphosphorylated tau and other downstream changes. To test this idea, we treated V717F neurons with inhibitors of α-secretase, β-secretase and γ-secretase and quantified the effect of these inhibitors on the p-tau/t-tau ratio. Additionally, we tested a recently published compound that stabilizes the retromer complex and decreases APP amyloidogenic processing (Mecozzi et al., 2014). The retromer stabilization compound (R33) was an ideal candidate to test in human cells, because previous studies were done in mouse hippocampal neurons. An inhibitor of α-secretase (TAPI) significantly decreased sAPPα with no significant affect on sAPPβ or Aβ40 (Figure 4.6 A, B, C). An inhibitor of β-secretase (βIV), and significantly increased sAPPα, significantly decreased sAPPβ and Aβ40 (Figure 4.6 A, B, C). A γ-secretase inhibitor (Comp E), was very similar to the β-secretase inhibitor in that it increased sAPPα, and decreased sAPPβ and Aβ40. Finally, the retromer stabilization compound (R33), did not significantly change sAPPα, but significantly decreased sAPPβ and Aβ40 (Figure 4.6 A, B, C). Interestingly, only the R33 compound significantly decreased the p-tau/t-

tau ratio (Figure 4.6 D), while α-, β-, and γ-secretase inhibitors had no significant affect (Figure 4.6 D).

APP mutations vs. PS1 mutations differ in tau phenotypes

We previously published that isogenic neurons harboring the PS1 ΔE9 mutation exhibit an increase in the Aβ42/40 ratio, increased APP CTFs, and interestingly, no change in the p-tau/t-tau ratio (Woodruff et al., 2013). When we directly compared the Aβ42/40 ratio in APP V717F and PS1 ΔE9 neurons, we observed that neurons heterozygous for either mutation increase the Aβ42/40 ratio ~2-fold when compared to wild-type and that neurons homozygous for either mutation increase the ratio ~4-fold (data not shown.). Both mutations alter the ratio by increasing Aβ42 and decreasing Aβ40. As we did not observe an increase in the p-tau/t-tau ratio at early time points in the APP V717F neurons, but rather an increase in total tau levels, we quantified the total tau and p-tau levels of PS1 ΔE9 neurons after 3 weeks of differentiation, followed by FACS purification and plating. We did not observe any significant differences in the total levels of tau or p-tau at T231 (Figure 4.7 A,B). We also quantified the p-tau/t-tau ratio in PS1 ΔE9 neurons cultured for 3 months, and while there was a slight increase in this ratio compared to wild-type (Figure 4.7 C), it was not as striking as the increase in the APP V717F homozygous neurons.

4.3 Discussion

Based on biochemical comparisons from a patient model and an isogenic model of the FAD APP V717F mutation, our results demonstrate that CRISPR-mediated knockin of this mutation is remarkably similar to the patient-derived lines. The isogenic system therefore allows more in-depth analysis of FAD mutations because a smaller number of lines and replicates are required to quantify phenotypes. We demonstrated that the APP V717F mutation affects multiple proteolytic fragments of APP. In both the patient and isogenic model, we observed an increase in the Aβ42/40 ratio that was due to a decrease in Aβ40 and an increase in Aβ42. Additionally, we observed an increase in Aβ37. There were no significant changes in the levels of sAPP fragments, which is in contrast to what was recently published for the APP V717I mutation. They reported an increase in sAPPβ (Muratore et al, 2014), which we did not observe. However, we did detect a significant increase in the levels of β-CTF. Thus, it seems that bot the APP V717I and V717F mutations may increase levels of β-CTF, although the process through which they are increased may be different between the two mutations.

In addition to testing how APP processing is altered by the APP V717F mutation, we also quantified total and phosphorylated levels of tau in the isogenic neurons. We found that in APP V717F neurons that were ~28 days old, there was a significant increase in the total levels of tau and in levels of phosphorylated tau at T231, but therefore no increase in the p-tau/t-tau ratio. However, APP V717F neurons that were ~3 months old displayed a significant increase in the p-tau/t-tau ratio, which is a phenotype observed in postmortem AD tissue. Interestingly, a recent study that characterized the APP V717I mutation in iPSC-derived neurons observed similar tau

phenotypes (Muratore et al., 2014). Specifically, they also initially observed an increase in total and phosphorylated tau at early timepoints, and also at 3 months observed a significant increase in the p-tau/t-tau ratio (Muratore et al., 2014). This suggests that increases in total and phosphorylated tau may be a precursor to later changes that cause an increase in the p-tau/t-tau ratio. Increased total and phosphorylated tau levels could be used as an early diagnostic, or an early marker to predict later tau phenotypes. It would be particularly interesting to quantify total and phosphorylated tau levels in SAD patients to determine if this is a phenotype that is also shared with SAD.

There are now in the literature multiple studies of iPSC-derived neurons from many different APP and PS1 mutations. These studies have revealed that APP mutations generate tau phenotypes, while PS1 mutations do not. Studies of APP duplication, both from SAD and Down's Syndrome, reported increases in the p-tau/t-tau ratio and increases in levels of tau and tau localization (Israel et al., Shi et al., 2012). A study of the APP V717F mutation reported increases in total and phosphorylated tau at earlier time points, an increase in the p-tau/t-tau ratio at later time points (Muratore et al., 2012). Studies of the PS1 mutations A246E, A79V and ΔE9 either did not report on whether a tau phenotype was present or did not observe a tau phenotype (Yagi et al., 2011; Woodruff et al., 2013). Finally, a recent study directly compared APP and PS1 mutations, the first study to do so (Moore et al., 2015). They compare the PS1 mutations Y115C, M146I and intron 4 to the APP V7171 mutation and APP duplication. They report an increase in total tau levels and phosphorylated tau at multiple sites (S202, T205, S396, and S404) only in the APP

V717I and APP duplication patient neurons, while the PS1 patient neurons were not significantly different from controls (Moore et al., 2015). These results are very similar to what we observed in our study, which is that APP V717F mutant neurons display tau phenotypes, while the PS1 ΔE9 mutant neurons do not. Importantly, our study was performed in isogenic neurons, which confirms that the differences in tau phenotypes are not due to differences in patient genetic backgrounds. Additionally, our data and others directly support the idea that tau phenotypes can not simply be caused by an increase in Aβ42. The APP V717I mutation and the PS1 ΔE9 mutation both increase the Aβ42/40 ratio by increasing Aβ42 and decreasing Aβ40, but only the APP V717F mutation displays a tau phenotype. The Moore, et al study suggested that APP mutations and APP duplication cause tau changes because these mutations also affect APP CTF accumulation. Our data do not support this idea because both APP V717F and PS1 ΔE9 cause accumulation of APP CTFs. Our data suggest that changes other than APP processing are responsible for tau accumulation. Future studies to further compare APP and PS1 mutations will shed light onto why and how APP mutations cause tau changes while PS1 mutations do not. One possibility is that PS1 mutations will display tau phenotypes when other cell types are present, such as astrocytes or microglia. Another possibility is that the early events that cause AD in APP vs. PS1 mutations are different, but the disease presents as the same once it has progressed far enough.

Important therapeutic implications from this work is that 1) APP and PS1 mutations may respond differently to therapeutics based on the early detectable phenotypes described here and 2) targeting the retromer complex may be a possible

treatment. Future studies will shed even more light on the similarities and differences of APP vs PS1 mutations. However, as the current literature has shown, APP and PS1 mutations do not produces equivalent phenotypes in iPSC-derived isogenic neurons. This suggest that the underlying cause of disease between APP and PS1 mutations may not be equivalent and therefore may require different intervention to halt the progression of disease. Given that there are such differences in dominantly-inherited FAD, it seems likely that SAD could have even more variability in the cause and initiation of disease. The iPSC system is ideal to test for these differences and to stratify patients into subsets that produce similar phenotypes. Drug screening studies could then predict which patients might respond to a specific therapeutic. As we identified here, targeting the retromer complex may be a therapeutic that both lowers Aβ and p-tau. SAD patients that share similar phenotypes as the APP V717F mutation then might also be ideal candidates for a retromer complex therapeutic.

2.4 Experimental Procedures

iPSC Culture

iPSCs were generated as previously described (Gore, et al., 2011; Israel, et al., 2012). iPSCs are cultured on an irradiated MEF feeder layer generated in-house. Cells are grown in medium containing KO DMEM (Gibco), 10% Plasmanate (Talecris Biotherapeutics), 10% KO Serum Replacement (Gibco), 20mM GlutaMax (Invitrogen), 20mM NEAA (Invitrogen), 20mM Pen/Strep (Invitrogen) and 20ng/uL

FGF (Millipore). Cells were passaged by dissociation with Accutase (Innovative Cell Technologies).

Isogenic iPSC Generation

iPSCs were pretreated with 10uM Rock Inhibitor (Ascent Scientific) for 1 hour prior to nucleofection. Cells were dissociated using accutase and passed through a 100uM filter to obtain single cells. Two million iPSCs were nucleofected using Amaxa Human Stem Cell Nucleofector Kit 1 (Lonza), with 5ug of each Cas9-GFP encoding plasmid, 3ug of gRNA (Lonza) and 30ug of ssODN (Integrated DNA Technologies). Cells were maintained in iPSC culture conditions with 10uM Rock inhibitor for 72 hours followed by FACS sorting (FACS Aria, BD Biosciences) for GFP+ cells. GFP-expressing cells were plated a $1x10^4$ cells per 10cm plate in the presence of Rock Inhibitor. Thereafter, media was changed every other day until isolated colonies grew. Isolated colonies were manually picked and grown in 96-well plates. Once cells were confluent, cells were split into a duplicate well and grown until confluent at which point they were harvested for DNA using DNA QuickExtract (Epicentre). DNA was amplified using allele specific primers to detect the APP V717F point mutation using Jump Start PCR Ready Mix (Sigma). To sequence the PCR products, we cloned them using the Zero Blunt PCR Cloning Kit (Invitrogen).

NPC Differentiation, Purification, and Culture

iPSCs were differentiated to NPCs as previously described (Yuan, et al., 2011). Briefly, $1x10^5$ iPSCs were seeded onto PA6 cells in PA6 differentiation medium:

Glasgow DMEM, 10% KOSR, 1mM Sodium Pyruvate, 0.1mM Nonessential Amino Acids and 0.1 mM β-Mercaptoethanol (all from Invitrogen). For the first 6 days media was not changed and also contained 500 ng/ml Noggin (R&D Systems) and 10 μM SB431542 (Tocris). After the first 6 days, medium was changed every other day until day 12. On day 12, cells were dissociated and stained with, CD184, CD44, CD271 and CD24 (all from BD Biosciences). CD184 +, CD24+, CD44-, CD271- cells were sorted (FACS Aria, BD Biosciences). NPC cultures were cultured on 20 μg/ml poly-L-ornithine and 5 μg/ml laminin (both from Sigma) coated plates in medium containing: DMEM:F12 + Glutamax, 0.5X N2, 0.5X B27 (both from Life Technologies), 1X P/S, and 20 ng/ml FGF (Millipore). Media was changed every other day.

Neuron Differentiation, Purification, and Culture

NPCs were expanded to 10cm plates and grown to confluency (3-4 days) at which point FGF was removed from the media. The medium was changed twice per week and the cells were differentiated for 21 days. After the 3 week differentiation, neurons were purified as previously described (Yuan, et al., 2011). Briefly, cells were dissociated using Accutase and Accumax (both from Innovative Cell Technologies) and then stained with CD184, CD44 and CD24 (all from BD Biosciences). CD184-, CD44-, CD24+ cells were sorted (FACS Aria, BD Biosciences) and then plated on poly-ornithine/laminin coated plates in NPC media + 0.5mM dbCAMP (Sigma), 20ng/uL BDNF and 20ng/uL GDNF (both from Peprotech).

Aβ Measurements

Neurons were plated at density of $2.0x10^5$ per 96 well in a 100uL volume of media. Media was harvested from purified neurons after 2 weeks. Aβ from the media was measured with MSD Human (6E10) Abeta3-Plex Kits (Meso Scale Discovery). For experiments with γ-secretase inhibitor, all media was changed on day 3 and replaced with 100uL of media either with Compound E or DMSO (vehicle). All media was harvested on day 5. Compound E (EMD Chemicals) was used at concentrations of 5nM and 200nM. 3-6 independent measurements were made per line. Each NPC line was differentiated twice in independent experiments for purified neurons.

Gel Elctrophoresis and Western Blot

Tissue culture lysates were prepared using RIPA lysis buffer (Millipore) supplemented with protease (cocktail set I, Calbiochem) and phosphatase (Halt, Pierce) inhibitors. The BCA assay (Pierce) was used to estimate the protein content. Equal protein amounts were separated in MES buffer alongside Novex Sharp prestained markers (Invitrogen) on NUPAGE 4–12% Bis-Tris precast gels (Invitrogen) and then transferred to polyvinylidene fluoride (PVDF) or nitrocellulose (0.45 μm pore size Immobilon Millipore). Membranes were blocked in 5% BSA in tris buffered saline with 0.1% Tween-20 or Odyssey Blocking Buffer (Li-Cor). Primary antibodies (Presenilin 1 c-loop 1:1000 Chemicon; Presenilin 1 N-term 1:1000 Santa Cruz; APP C-terminus 1:1000 Calbiochem; N-cadherin C-terminus 1:1000 BD Biosciences; Nicastrin 1:1000 Affinity BioReagents; Actin C4 1:100,000 Chemicon; Tubulin-alpha DM1A 1:50,000 Sigma) were prepared in 5% BSA. Fluorescent secondary antibodies (LiCor) were diluted 1:5000. LiCor Odyssey infrared imager was

used to measure pixel intensities of bands at detector settings set at the maximum or one half unit below saturation. For each protein band, background subtracted integrated intensity values were calculated using the Odyssey software. Since absolute integrated intensity values vary for the same samples on different blots, samples within a blot were plotted relative to control and these normalized values were used to average replicates from separate blots. To show protein bands in the conventional manner with dark bands on a light background, grayscale images were inverted in the figures. HRP-conjugated secondary antibodies (Invitrogen) were diluted 1:5000. Blots were developed using ECL Western Blotting Kit (Pierce).

Statistical Methods

All data was analyzed using GraphPad Prism Software (GraphPad). Statistical analysis comparing different genotypes was performed by Tukey's multiple comparison test. Drug responses were compared to controls by Dunnett's test.

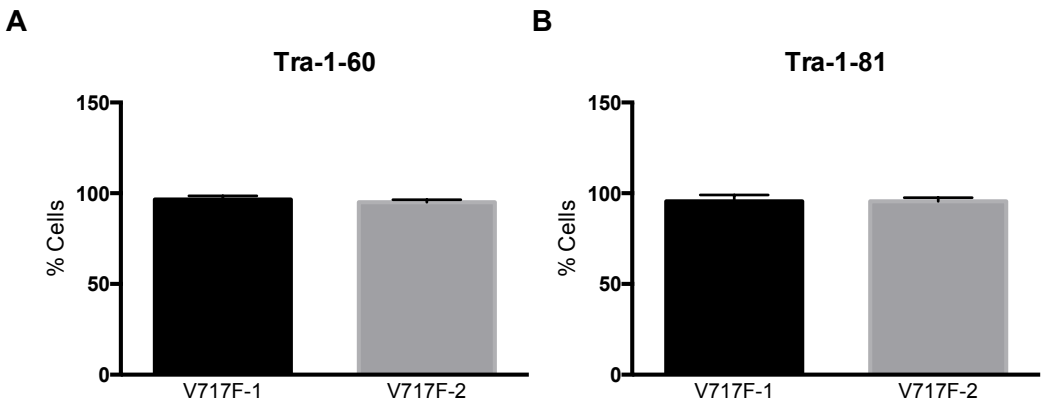

Figure 4.1. Reprogrammed Cells Express Pluirpotent Markers. (A) Percent of cells from each patient that express Tra-1-60. Error bars represent measurements from 3 iPSC lines per patient. (B) Percent of cells from each patient that express Tra-1-81. Error bars represent measurement from 3 iPSC lines per patient.

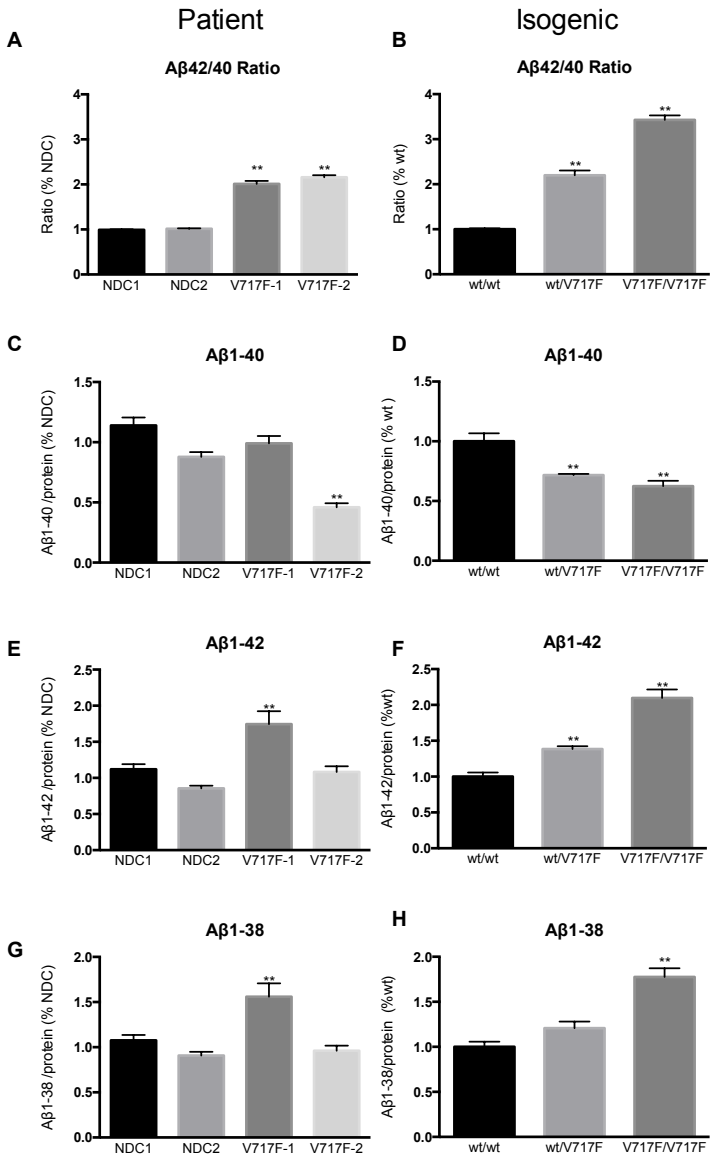

Figure 4.2. The APP V717F Mutation Increases Aβ 42 and 38 and Decreases Aβ40. (A) Aβ 42/40 ratio from purified neurons. (B) Aβ 42/40 ratio from isogenic neurons. (C) Aβ40 from patient purified neurons. (D) Aβ40 from isogenic purified neurons. (E) Aβ42 from patient purified neurons. (F) Aβ42 from isogenic purified neurons. (G) Aβ38 from patient purified neurons. (H) Aβ38 from isogenic purified neurons. For all patient graphs bars represent measurements from 2 lines per individual. Error bars represent SEM from 6 biological replicates per line. For all isogenic graphs, bars represent measurements from 2 lines from the wt/wt genotype and 1 line for the wt/V717F and V717F/V717F genotypes. Error bars represent SEM from 6-8 biological replicates per line.

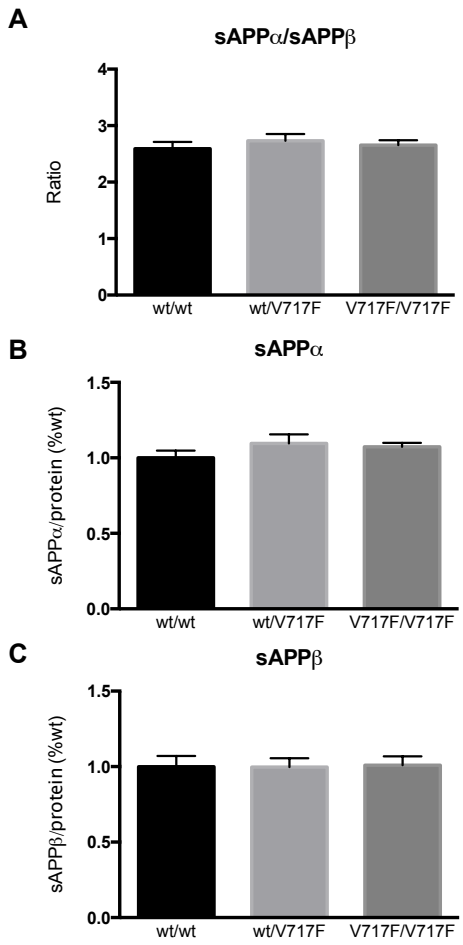

Figure 4.3. The APP V717F Mutation Does Not Alter sAPP Fragments. (A) sAPPα/sAPPβ ratio from purified isogenic neurons. (B) Total sAPPα levels normalized to protein from isogenic neurons. (C) Total sAPPβ levels normalized to protein from isogenic neurons. For all graphs, bars represent measurements from 2 lines from the wt/wt genotype and 1 line for the wt/V717F and V717F/V717F genotypes. Error bars represent SEM from 6-8 biological replicates per line.

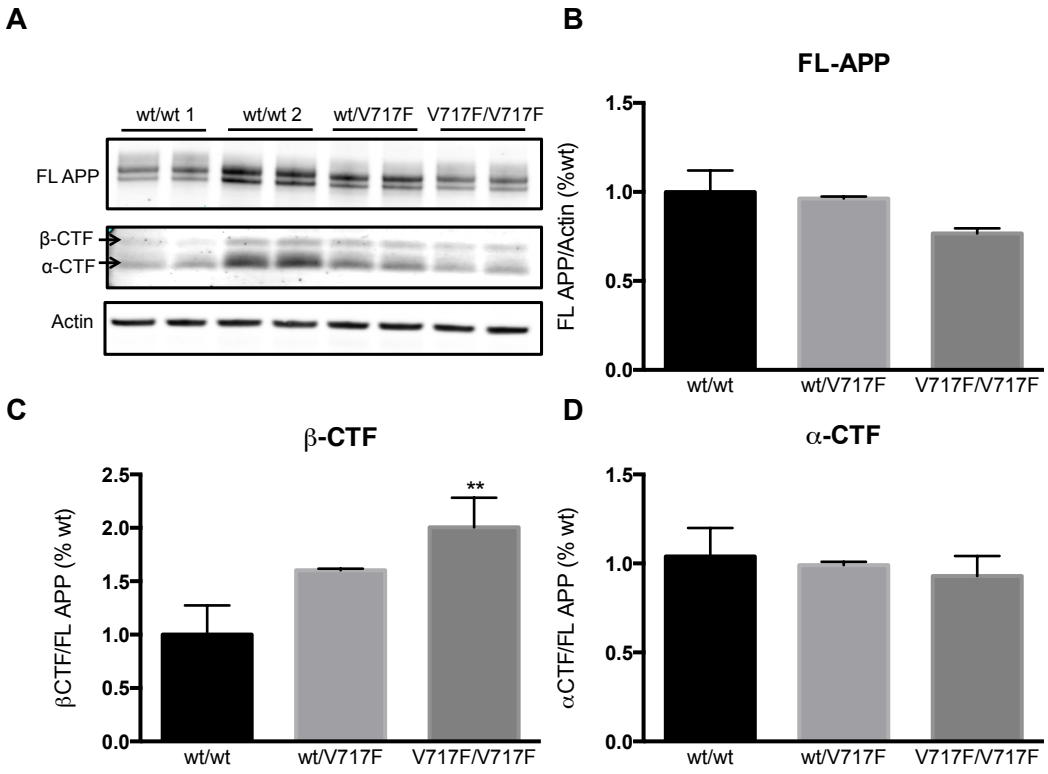

Figure 4.4. The APP V717F Mutation Increases β-CTF Levels but Does Not Affect FL-APP or α-CTF. (A) Representative western blots of FL-APP, APP CTFs and Actin from purified isogenic neurons. (B) Quantification of FL-APP normalized to Actin. (C) Quantification of β-CTF normalized to FL-APP. (D) Quantification of α-CTF normalized to FL-APP. For all graphs, bars represent measurements from 2 lines from the wt/wt genotype and 1 line for the wt/V717F and V717F/V717F genotypes. Error bars represent SEM from 4-6 biological replicates per line.

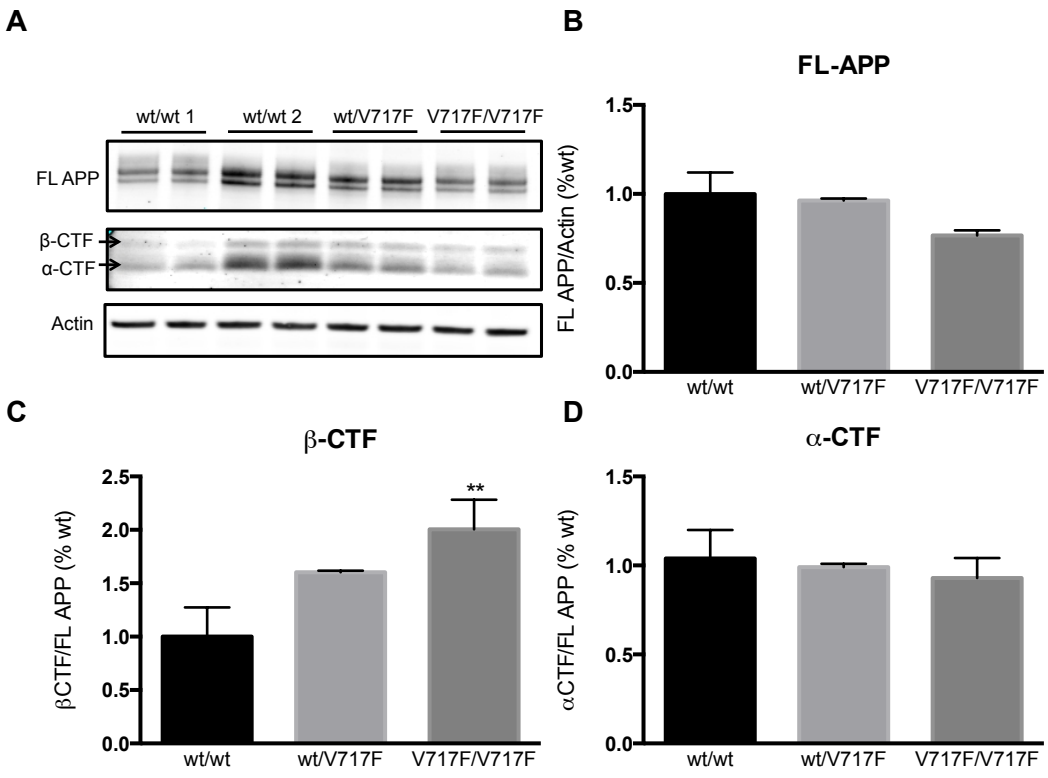

Figure 4.5. The APP V717F Mutation Increases Total and Phospho-tau Levels at Early Time Points and Increase the p-tau/t-tau Ratio after 3 Months. (A) The p-tau/t-tau ratio in purified isogenic neurons. (B) Total tau levels normalized to total protein in isogenic neurons. (C) Total p-tau levels (T231) in isogenic purified neurons. (D) The p-tau/t-tau ratio in isogenic purified neurons after 3 months of differentiation. For all graphs, bars represent measurements from 2 lines from the wt/wt genotype and 1 line for the wt/V717F and V717F/V717F genotypes. Error bars represent SEM from 4-6 biological replicates per line.

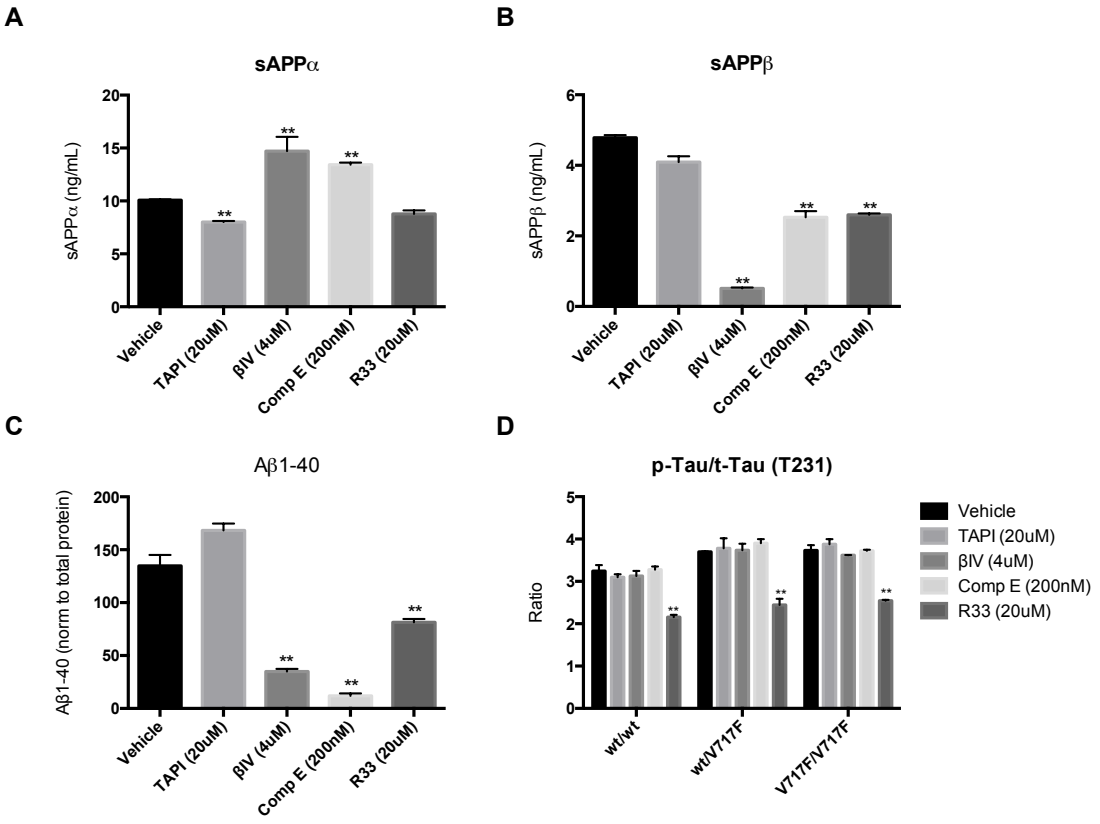

Figure 4.6. APP V717F Neurons Respond to Drug Treatments. (A) Secreted sAPPα from control neurons treated with α-secretase inhibitor (TAPI 20μM), β-secretase inhibitor (βIV 4μM), γ-secretase inhibitor (Comp E 200nM), and retromer complex stabilizer (R33 20μM). (B) Secreted sAPPβ from control neurons treated with drugs. (C) Secreted Aβ40 from control neurons treated with drugs. (D) The p-tau/t-tau ratio in isogenic purified neurons treated with drugs. For all graphs, bars represent measurements from 2 lines from the wt/wt genotype and 1 line for the wt/V717F and V717F/V717F genotypes. Error bars represent SEM from 3 biological replicates per line.

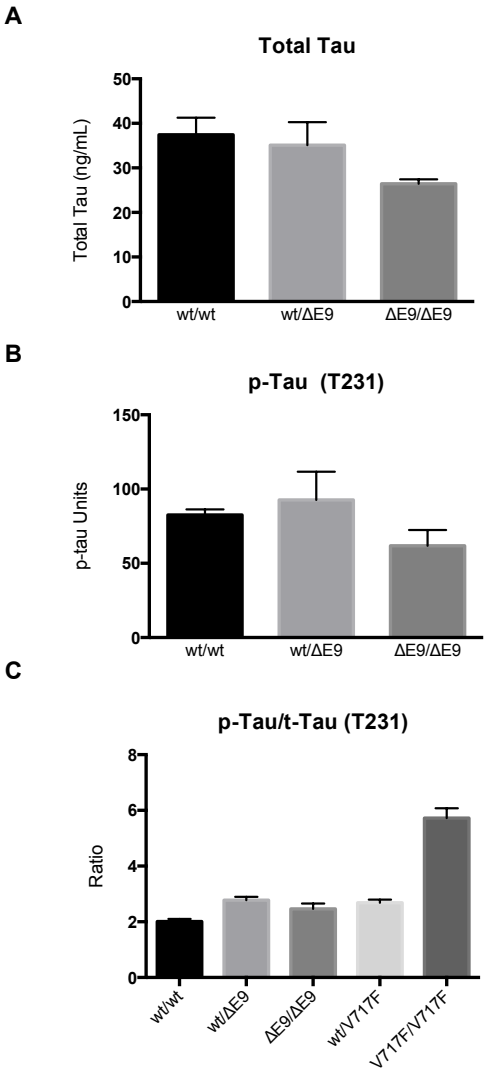

Figure 4.7. PS1 ΔE9 Neurons Do Not Alter Tau Levels. (A) Total tau levels normalized to protein in isogenic neurons. (B) Phospho-tau levels (T231) normalized to protein in isogenic neurons. (C) p-tau/t-tau ratio from isogenic neurons that were grown for 3 months. For all graphs, bars represent measurements from 2 lines from the wt/wt genotype, 2 lines for both the wt/ΔE9 and ΔE9/ΔE9 genotypes, and 1 line for the wt/V717F and V717F/V717F genotypes. Error bars represent SEM from 3 biological replicates per line.

Chapter 5

Conclusions

The human iPSC system is a valuable tool for studying human development, genetics, and cell types and diseases for which there is not an ideal animal model. AD, which is a particularly complex disorder with many genetic and environmental risk factors, has already benefited from iPSC modeling. Researchers can now study the cell types of interest, neurons and glia, with human genetic backgrounds and the proteins of interest expressed at endogenous levels. Particularly for SAD, the iPSC system is ideal for generating a model, as there is no animal model for sporadic disease.

Many research groups have reported AD-related phenotypes from iPSC-derived neurons that harbor APP, PS1 and PS2 mutations and several groups were able to shed light on pathways that may be disrupted in AD. Israel et al., reported that β-secretase inhibition, but not γ-secretase inhibition, reduced the p-tau/t-tau ratio in APP duplication neurons. This result suggests that increased levels of p-tau are at least in part mediated by the APP β-CTF. Muratore at al, reported that increased levels of total and phosphorylated tau observed in APP V717I neurons could be rescued by treatment with an antibody against Aβ. This result suggests that levels of total tau and p-tau can also be affected by levels of extracellular Aβ. Although, another interpretation of this result is that the Aβ antibody could be binding non-specifically on the cell surface or to APP at the cell surface and affecting endocytosis. Young et al., reported a mechanism by which haplotypes associated with SAD in the SORL1 gene could be contributing to AD. Specifically, they revealed that individuals that were homozygous for a risk haplotype were unable to induce SORL1 expression upon BDNF treatment, while individuals with even 1 protective haplotype were able to upregulate SORL1. SORL1 has been shown to traffic APP away from amyloidogenic

cleavage, thus individuals with the risk haplotype had increased Aβ compared to individuals with the protective haplotype when treated with BDNF.

My work was focused on further elucidating mechanisms of neuronal dysfunction caused by APP and PS1 FAD mutations. As described above, many studies have successfully recapitulated aspects of AD pathology through modeling with iPSC-derived neurons. However, most of these studies did not characterize phenotypes beyond changes in APP processing and tau phosphorylation. The iPSC system is ideal for discovering early detectable changes that are caused by FAD mutations. For over 100 years, researchers have known the end point of pathology in AD brains, but a major unanswered question is the early changes that lead to the Aβ plaques and tau tangles. Thus, my work sought to characterize how APP and PS1 mutations cause neuronal dysfunction and compared the similarities and differences between APP and PS1 mutations.

Presenilin-1 Mutations are not Simple Loss-of-Function

Since the first PS1 mutation was identified to cause dominantly inherited FAD, there have been many studies investigating whether PS1 mutations are gain or loss-of-function, with evidence for both sides of the debate. However, a limitation of previous studies has been the lack of an appropriate model. Studies utilizing overexpression of mutant PS1, and in many cases are accompanied by over expression of APP, do not accurately portray what occurs in AD. A single extra copy of the APP gene is sufficient to cause FAD, thus vast overexpression of APP in a model system makes it difficult to interpret the results. Mouse models with mutant PS1 recapitulate certain

aspects of AD, but lack key phenotypes such as neurofibrillary tangles. Finally, studying PS1 mutations in non-neuronal cells can provide some information on the nature of dysfunction, but again cannot be used as the only tool as neurons are highly complex cells with many specialized functions. Finally, most studies of PS1 mutations have focused primarily on the γ-secretase function of PS1, which may indeed be the primary defect that causes FAD, but cannot be the only function investigated.

In our study, we generated and allelic series of PS1 mutations to determine whether the PS1 ΔE9 mutation is a gain or loss-of-function mutation when expressed at endogenous levels in human neurons. This was the first study to address this question in human neuronal cells, and to investigate both γ-secretase dependent and γ-secretase independent functions. We clearly demonstrated that the PS1 ΔE9 mutation appears to impair γ-secretase activity as evidenced by increased levels of APP CTFs and n-cadherin CTFs, which are both γ-secretase substrates. We also demonstrated that the PS1 ΔE9 mutation maintains some normal PS1 function as evidenced by no significant differences in the relative amount of mature nicastrin. To further make these claims, we also measured γ-secretase substrates and mature nicastrin in a cell line that is haploinsuficient for PS1. PS1 haploinsuficiency did not significantly affect γ-secretase substrate accumulation, but did significantly impair the maturation of nicastrin. Taken together, these results clearly demonstrate that the PS1 ΔE9 mutation is not just a simple loss-of-function mutation. Thus, we can conclude that not all PS1 mutations are loss-of-function.

A recent study that made knock-in mice harboring two different FAD mutations found that these mice shared similar phenotypes to the PS1 conditional

knockout mice, which led the authors to conclude that FAD mutations are loss-of-function (Xia et al., 2015). However, a limitation of this study was that the authors did not measure phenotypes that are both γ-secretase dependent and γ-secretase independent functions of PS1. It may indeed be the case that impaired γ-secretase activity is the main function of PS1 that ultimately causes AD, but this has not yet been exclusively determined. PS1 has been reported to have a vast array of functions and dissecting which function or functions are disrupted in FAD are vital for future studies. In addition to all of the phenotypes that are present in FAD, patients with PS1 mutations have also been documented to have other phenotypes including spastic paraparesis, lewy bodies and others. It could be possible that γ-secretase independent functions of PS1 could be responsible for causing other phenotypes. This has already been documented to some extent with the Ca^{2+} channel function of PS1. Thus, moving forward studies of PS1 mutations should document both γ-secretase dependent and independent functions of PS1.

APP and PS1 FAD Mutations Reduce Endocytosis and Transcytosis of APP and Lipoproteins Owing to β-CTF Accumulation

APP and PS1 are well documented to alter the cleavage of APP such that there is an increase in the total levels of Aβ or that there is an increase in the total levels of Aβ42. Indeed, much of the AD literature has focused on this feature and is the basis for the Amyloid Cascade Hypothesis. However, in addition to alterations in Aβ caused by both APP and PS1 mutations, they also share the common feature of increasing amounts of APP CTFs. This feature has not gone completely unnoticed and recent

literature has reported on the potentially deleterious effects of increased APP CTFs (Rodrigues et al., 2012; Weissmiller et al., 2015). In our study, we sought to determine whether the PS1 ΔE9 mutation causes changes in vesicle trafficking that could be contributing to the development of FAD.

We demonstrated that the PS1 ΔE9 mutation causes altered localization of APP, such that APP accumulates in the cell soma and is decreased in axons. The mechanism for altered APP localization arises from a decrease in endocytosis of APP and subsequent transcytosis of APP to the axon. We also demonstrated that the endocytosis and transcytosis changes were not specific to APP, but also affected the endocytosis and transcytosis of lipoproteins. To determine the mechanism by which the PS1 ΔE9 mutation is causing reduced endocytosis, we investigated whether γ-secretase activity, which is impaired by the PS1 ΔE9 mutation, might be playing a role. We found that when control neurons were treated with a γ-secretase inhibitor, the endocytosis of lipoproteins was significantly reduced, but this defect could be rescued when control neurons were co-treated with a β-secretase inhibitor. This result suggested that accumulation of APP β-CTFs was driving the endocytosis defects. To further test this, we treated PS1 ΔE9 neurons with a β-secretase inhibitor and observed that the endocytosis defects were rescued under this condition. To determine the mechanism by which β-CTF accumulation could be causing reduced endocytosis, we stained PS1 ΔE9 neurons with an array of endocytic markers and found that there was significantly more Rab11 staining in the soma of PS1 ΔE9 neurons. In non-neuronal cells, Rab11 has a well established role in mediating recycling of membrane receptors, including lipoprotein receptors (Ullrich et al., 1996). Additionally, in neurons Rab11

has been shown to mediate transcytosis of multiple cargo including TrkA receptors (Ascaño et al., 2009). We therefore decided to measure whether recycling of lipoprotein receptors was impaired in the PS1 ΔE9 neurons and whether it was dependent on β-CTFs. We demonstrated that PS1 ΔE9 neurons displayed significantly less lipoprotein receptor, at the cell surface, after 4 hours of lipoprotein treatment. Additionally we determined that the decrease in cell surface lipoprotein receptors after 4 hours was not due to changes in degradation or transcription of lipoprotein receptors, thus we concluded that recycling of lipoprotein receptors was decreased in PS1 ΔE9 neurons. To show that this affect was dependent on β-CTF accumulation, we transfected control neurons with a construct to overexpress β-CTF. Under these conditions, we observed decreased endocytosis of lipoproteins and accumulation of Rab11. Taken together, these results demonstrate that the APP β-CTF affects endocytosis and transcytosis of lipoproteins. Finally, as most FAD mutations increase APP CTF levels, we asked whether other FAD mutations shared the lipoprotein endocytosis defects. We utilized isogenic lines containing the APP V717F mutation and found that this mutation also increases APP β-CTFs and reduced lipoprotein uptake. This defect could once again be rescued by treatment with β-secretase inhibitor.

This work describes for the first time a possible link between not only APP and PS1 mutations, but also between FAD and SAD. The genetic variant that confers the highest risk for developing SAD is the e4 allele of the APOE gene. APOE is a lipoprotein carrier and is the major carrier in the brain. Studies investigating the role of APOE in AD have suggested that the e4 allele could have altered binding to

lipoprotein receptors and that the e4 variant is trafficked more slowly through the endocytic system. Our results suggest that reduced uptake of lipoproteins could play a role in development of FAD, and therefore suggest that a similar phenotype could be caused by the e4 allele.

Therapeutically, our results suggest that β-secretase inhibition could be a favorable therapeutic for AD. Not only does β-secretase inhibition reduce Aβ, but it also inhibits production of APP β-CTFs, which we demonstrated to be the cause of reduced lipoprotein endocytosis. A recent study reported an increase in β-CTFs in brains from SAD patients (Kim et al., 2015), which further suggests that β-secretase inhibition could be an ideal candidate for both FAD and SAD.

APP and PS1 Mutations Differ in Early Detectable AD-Related Phenotypes

A long-standing assumption in the FAD field is that APP and PS1 mutations initiate disease through a common pathway, namely an increase in Aβ42. We compared isogenic cells harboring the PS1 ΔE9 mutation or the APP V717F mutation and measured the affect of these mutations of APP processing and tau protein accumulation and phosphorylation. We found that both the PS1 ΔE9 mutation and the APP V717F mutation increase the Aβ42/40 ratio by increasing Aβ42 and by decreasing Aβ40. Neither mutation affects the sAPP fragments, but both mutations increase APP β-CTFs (the PS1 ΔE9 also increases APP α-CTFs). When we measured total and phosphorylated levels of tau, we observed that only the APP V717F mutation increased the total and phosphorylated levels of tau. After 3 months of neuronal differentiation, the APP V717F mutation also increased the ratio of p-tau to t-tau.

Interestingly, the PS1 ΔE9 mutation did not affect tau accumulation or the p-tau/t-tau ratio at early or late time points. This result suggests that there are differences between APP and PS1 mutations in how they initiate disease phenotypes.

A recent study compared APP processing and total and phosphorylated tau levels in neurons from multiple APP and PS1 mutations, and similar to our work, found that only APP mutations produced a tau phenotype (Moore et al., 2015). The conclusion of this study was that APP CTFs are the cause of increased levels of tau because treatment of control neurons with a γ-secretase inhibitor increased tau. However, the authors did not measure basal APP CTF levels in both the PS1 and APP mutant neurons. As there is now somewhat of a consensus that PS1 mutations decrease γ-secretase activity, and therefore increase APP CTFs, the explanation provided by Moore et al., does not seem viable. Rather, there must be some other factor that influences tau levels that is different between APP and PS1 mutation. One possible factor could be the presence of other cells types such as astrocytes or microglia. Perhaps PS1 mutations require glial cells to produce tau phenotypes, and future studies should investigate this possibility. Another possibility is that APP and PS1, which have roles in development, could affect that maturity of neurons that are produced by each mutation. Perhaps extended culture of PS1 mutant neurons, beyond the 3 month time point investigated in our study, would induce further maturation and a induce a tau phenotype.

The differences that we, and others, have observed between APP and PS1 mutations also suggests that APP and PS1 patients may respond differently to therapeutics. The iPSC system will be a powerful tool moving forward to identify

subsets of patients that respond positively to a particular therapeutic and will also help to identify subsets of patients with similar early detectable phenotypes.

Future Studies

Since the first report of iPSCs in 2007 (Takahashi et al., 2007a), the field has made many exciting advances in stem cell differentiation and disease modeling. The AD-field in general will be able to increase the complexity of in vitro iPSC modeling by utilizing 3D culture protocols that generate mature neurons and astrocytes (Paşca et al., 2015). Studies investigating the interaction of multiple cell types will shed light on to the cell autonomous or non-cell autonomous mechanisms that may be at play in AD. In particular, PS1 is highly expressed in microglia (Zhang et al., 2014), which suggests that the addition of microglia expressing mutant PS1 to the culture could alter the neuronal phenotypes that have already been observed. Additionally, reactive astrocytes are a feature of the AD brain, thus studies investigating the contribution of astrocyte-mediated neuronal dysfunction will clearly be of value.

My work reported a connection between altered APP processing, caused by both PS1 and APP mutations, and decreased lipoprotein endocytosis. While this is an exciting new phenotype described in iPSC-derived neurons, future studies should work to investigate downstream consequences of decreased lipoprotein endocytosis and transcytosis. Lipoproteins are essential for neurite extension and many aspects of synapse formation and maintenance, therefore, phenotypes of decreased neurite elongation or synapse dysfunction would be ideal candidates to investigate. Another avenue of investigation should be to look at a link between altered lipoprotein

homeostasis and tau. A link between the two already exists as treatment with statins, inhibitors of cholesterol synthesis, decrease phosphorylated tau (Kurata et al., 2011). Finally, a recent study described a mechanism by which increased APP β-CTFs induce dysfunction of Rab5 positive endosomes (Kim et al., 2015). Enlarged early endosomes have been described in postmortem AD tissue from both SAD and APP FAD brains, but is absent in PS1 FAD brains (Cataldo et al., 2003). Thus, looking at similarities and differences between APP and PS1 mutations with respect to other endocytic markers will help to identify which parts of the pathway are disrupted by FAD mutations and the sequence in which the disruptions occur.

Finally, my work described that not all PS1 mutations are not simple loss-of-function mutations. Future studies should aim towards determining which function or functions of PS1 are responsible for causing AD-related pathology. PS1 has been reported to have a wide variety of functions from γ-secretase activity, regulation of lysosomal protein turnover (Lee et al., 2010), and acting as Ca^{2+} channels in the ER (Tu et al, 2006). While any or all of these functions could be contributing to AD pathology, future studies need to elucidate whether this is the case. Additionally, different PS1 mutations could affect PS1 functions differently, and this also needs to be elucidated by future studies.

References

Anderson, E., Maday, S., Sfakianos, J., Hull, M., Winckler, B., Sheff, D., Fölsch, H., and Mellman, I. (2005). Transcytosis of NgCAM in epithelial cells reflects differential signal recognition on the endocytic and secretory pathways. J. Cell Biol. *170*, 595–605.

Ascaño, M., Richmond, A., Borden, P., and Kuruvilla, R. (2009). Axonal targeting of Trk receptors via transcytosis regulates sensitivity to neurotrophin responses. J. Neurosci. *29*, 11674–11685.

Ashe, K.H., and Zahs, K.R. (2010). Probing the Biology of Alzheimer's Disease in Mice. Neuron *66*, 631–645.

Balducci, C., and Forloni, G. (2011). App transgenic mice: Their use and limitations. NeuroMolecular Med. *13*, 117–137.

Barnes, D.E., and Yaffe, K. (2011). The projected effect of risk factor reduction on Alzheimer's disease prevalence. Lancet Neurol. *10*, 819–828.

Von Bartheld, C.S. (2004). Axonal Transport and Neuronal Transcytosis of Trophic Factors, Tracers, and Pathogens. J. Neurobiol. *58*, 295–314.

Beel, A.J., Sakakura, M., Barrett, P.J., and Sanders, C.R. (2010). Direct binding of cholesterol to the amyloid precursor protein: An important interaction in lipid-Alzheimer's disease relationships? Biochim. Biophys. Acta - Mol. Cell Biol. Lipids *1801*, 975–982.

Bennett, D.A., Schneider, J.A., Arvanitakis, Z., Kelly, J.F., Aggarwal, N.T., Shah, R.C., and Wilson, R.S. (2006). Neuropathology of older persons without cognitive impairment from two community-based studies. Neurology *66*, 1837–1844.

Bentahir, M., Nyabi, O., Verhamme, J., Tolia, A., Horré, K., Wiltfang, J., Esselmann, H., and De Strooper, B. (2006). Presenilin clinical mutations can affect gamma-secretase activity by different mechanisms. J. Neurochem. *96*, 732–742.

Bertram, L., Lill, C.M., and Tanzi, R.E. (2010). The genetics of Alzheimer disease: back to the future. Neuron *68*, 270–281.

Bodovitz, S., and Klein, W.L. (1996). Cholesterol modulates alpha-secretase cleavage of amyloid precursor protein. J. Biol. Chem. *271*, 4436–4440.

Braidy, N., Muñoz, P., Palacios, A.G., Castellano-Gonzalez, G., Inestrosa, N.C., Chung, R.S., Sachdev, P., and Guillemin, G.J. (2012). Recent rodent models for Alzheimer's disease: Clinical implications and basic research. J. Neural Transm. *119*, 173–195.

Buerger, K., Ewers, M., Pirttilä, T., Zinkowski, R., Alafuzoff, I., Teipel, S.J., DeBernardis, J., Kerkman, D., McCulloch, C., Soininen, H. (2006). CSF phosphorylated tau protein correlates with neocortical neurofibrillary pathology in Alzheimer's disease. Brain *129*, 3035–3041.

Buggia-Prévot, V., Fernandez, C.G., Riordan, S., Vetrivel, K.S., Roseman, J., Waters, J., Bindokas, V.P., Vassar, R., and Thinakaran, G. (2014). Axonal BACE1 dynamics and targeting in hippocampal neurons: a role for Rab11 GTPase. Mol. Neurodegener. *9*, 1.

Burns, M., Gaynor, K., Olm, V., Mercken, M., LaFrancois, J., Wang, L., Mathews, P.M., Noble, W., Matsuoka, Y., and Duff, K. (2003). Presenilin redistribution associated with aberrant cholesterol transport enhances beta-amyloid production in vivo. J. Neurosci. *23*, 5645–5649.

Cai, D., Leem, J.Y., Greenfield, J.P., Wang, P., Kim, B.S., Wang, R., Lopes, K.O., Kim, S.H., Zheng, H., Greengard, P. (2003). Presenilin-1 regulates intracellular trafficking and cell surface delivery of beta-amyloid precursor protein. J. Biol. Chem. *278*, 3446–3454.

Calhoun, M.E., Wiederhold, K.H., Abramowski, D., Phinney, a L., Probst, A., Sturchler-Pierrat, C., Staufenbiel, M., Sommer, B., and Jucker, M. (1998). Neuron loss in APP transgenic mice. Nature *395*, 755–756.

Cataldo, A., William Rebeck, G., Ghetti, B., Hulette, C., Lippa, C., Van Broeckhoven, C., Van Duijn, C., Cras, P., Bogdanovic, N., Bird, T. (2001). Endocytic disturbances distinguish among subtypes of Alzheimer's disease and related disorders. Ann. Neurol. *50*, 661–665.

Cataldo, A.M., Peterhoff, C.M., Troncoso, J.C., Gomez-Isla, T., Hyman, B.T., and Nixon, R.A. (2000). Endocytic Pathway Abnormalities Precede Amyloid β Deposition in Sporadic Alzheimer's Disease and Down Syndrome. Am. J. Pathol. *157*, 277–286.

Cataldo, A.M., Petanceska, S., Peterhoff, C.M., Terio, N.B., Epstein, C.J., Villar, A., Carlson, E.J., Staufenbiel, M., and Nixon, R. a (2003). App gene dosage modulates endosomal abnormalities of Alzheimer's disease in a segmental trisomy 16 mouse model of down syndrome. J. Neurosci. *23*, 6788–6792.

Chambers, S.M., Fasano, C.A., Papapetrou, E.P., Tomishima, M., Sadelain, M., and Studer, L. (2009). Highly efficient neural conversion of human ES and iPS cells by dual inhibition of SMAD signaling. Nat. Biotechnol. *27*, 275–280.

Chang, K.-A., and Suh, Y.-H. (2005). Pathophysiological roles of amyloidogenic carboxy-terminal fragments of the beta-amyloid precursor protein in Alzheimer's disease. J. Pharmacol. Sci. *97*, 461–471.

Chartier-Hariln, M.-C., Parfitt, M., Legrain, S., Pérez-Tur, J., Brousseau, T., Evans, A., Berr, C., Vldal, O., Roques, P., Gourlet, V. (1994). Apolipoprotein-E, Epsilon-4 Allele As a Major Risk Factor for Sporadic Early and Late-Onset Forms of Alzheimers-Disease - Analysis of the 19Q13.2 Chromosomal Region. Hum. Mol. Genet. *3*, 569–574.

Chávez-Gutiérrez, L., Bammens, L., Benilova, I., Vandersteen, A., Benurwar, M., Borgers, M., Lismont, S., Zhou, L., Van Cleynenbreugel, S., Esselmann, H. (2012). The mechanism of γ-Secretase dysfunction in familial Alzheimer disease. EMBO J. *31*, 2261–2274.

Chen, F., Pruett-Miller, S.M., Huang, Y., Gjoka, M., Duda, K., Taunton, J., Collingwood, T.N., Frodin, M., and Davis, G.D. (2011). High-frequency genome editing using ssDNA oligonucleotides with zinc-finger nucleases. Nat. Methods *8*, 753–755.

Coen, K., Flannagan, R.S., Baron, S., Carraro-Lacroix, L.R., Wang, D., Vermeire, W., Michiels, C., Munck, S., Baert, V., Sugita, S. (2012). Lysosomal calcium homeostasis defects, not proton pump defects, cause endo-lysosomal dysfunction in PSEN-deficient cells. J. Cell Biol. *198*, 23–35.

Corder, E.H., Saunders, A.M., Strittmatter, W.J., Schmechel, D.E., Gaskell, P.C., Small, G.W., Roses, A.D., Haines, J.L., and Pericak-Vance, M.A. (1993). Gene dose of apolipoprotein E type 4 allele and the risk of Alzheimer's disease in late onset families. Science *261*, 921–923.

Ding, Q., Lee, Y.K., Schaefer, E.A.K., Peters, D.T., Veres, A., Kim, K., Kuperwasser, N., Motola, D.L., Meissner, T.B., Hendriks, W.T. (2013). A TALEN genome-editing system for generating human stem cell-based disease models. Cell Stem Cell *12*, 238–251.

Diwu, Z., Chen, C.-S., Zhang, C., Klaubert, D.H., and Haugland, R.P. (1999). A novel acidotropic pH indicator and its potential application in labeling acidic organelles of live cells. Chem. Biol. *6*, 411–418.

Donoviel, D.B., Hadjantonakis, A.-K., Ikeda, M., Zheng, H., Hyslop, P.S.G., and Bernstein, A. (1999). Mice lacking both presenilin genes exhibitearlyembryonic patterningdefects. Genes Dev. *13*, 2801–2810.

Duan, L., Bhattacharyya, B.J., Belmadani, A., Pan, L., Miller, R.J., and Kessler, J. a (2014). Stem cell derived basal forebrain cholinergic neurons from Alzheimer's disease patients are more susceptible to cell death. Mol. Neurodegener. *9*, 3.

Dumanchin, C., Czech, C., Campion, D., Cuif, M.H., Poyot, T., Martin, C., Charbonnier, F., Goud, B., Pradier, L., and Frebourg, T. (1999). Presenilins interact with Rab11, a small GTPase involved in the regulation of vesicular transport. Hum. Mol. Genet. *8*, 1263–1269.

Dumanchin, C., Tournier, I., Martin, C., Didic, M., Belliard, S., Carlander, B., Rouhart, F., Duyckaerts, C., Pellissier, J.-F., Latouche, J.B. (2006). Biological effects of four PSEN1 gene mutations causing Alzheimer disease with spastic paraparesis and cotton wool plaques. Hum. Mutat. *27*, 1063.

Edbauer, D., Winkler, E., Regula, J.T., Pesold, B., Steiner, H., and Haass, C. (2003). Reconstitution of gamma-secretase activity. Nat. Cell Biol. *5*, 486–488.

Extance, A. (2010). Alzheimer's failure raises questions about disease-modifying strategies. Nat. Rev. Drug Discov. *9*, 749–751.

Fargo, K. and, and Bleiler, L. (2014). Alzheimer's Association Report: 2014 Alzheimers disease facts and figures. Alzheimer's Dement. *10*, e47–e92.

Fonseca, A.C.R.G., Resende, R., Oliveira, C.R., and Pereira, C.M.F. (2010). Cholesterol and statins in Alzheimer's disease: current controversies. Exp. Neurol. *223*, 282–293.

Games, D., Adams, D., Alessandrini, R., Barbour, R., Berthelette, P., Blackwell, C., Carr, T., Clemens, J., Donaldson, T., and Gillespie, F. (1995). Alzheimer-type neuropathology in transgenic mice overexpressing V717F beta-amyloid precursor protein. Nature *373*, 523–527.

Gandy, S., Zhang, Y.W., Ikin, A., Schmidt, S.D., Levy, E., Sheffield, R., Nixon, R. a., Liao, F.F., Mathews, P.M., Xu, H. (2007). Alzheimer's presenilin 1 modulates sorting of APP and its carboxyl-terminal fragments in cerebral neurons in vivo. J. Neurochem. *102*, 619–626.

Gatz, M., Reynolds, C.A., Fratiglioni, L., Johansson, B., Mortimer, J.A., Berg, S., Fiske, A., and Pedersen, N.L. (2006). Role of genes and environments for explaining Alzheimer disease. Arch. Gen. Psychiatry *63*, 168–174.

Ginsberg, S.D., Alldred, M.J., Counts, S.E., Cataldo, A.M., Neve, R.L., Jiang, Y., Wuu, J., Chao, M. V, Mufson, E.J., Nixon, R.A. (2010). Microarray analysis of hippocampal CA1 neurons implicates early endosomal dysfunction during Alzheimer's disease progression. Biol. Psychiatry *68*, 885–893.

Goldstein, L.S.B., Reyna, S., and Woodruff, G. (2014). Probing the Secrets of Alzheimer's Disease Using Human-induced Pluripotent Stem Cell Technology. Neurotherapeutics *12*, 121–125.

Gore, A., Li, Z., Fung, H.-L., Young, J.E., Agarwal, S., Antosiewicz-Bourget, J., Canto, I., Giorgetti, A., Israel, M.A., Kiskinis, E. (2011). Somatic coding mutations in human induced pluripotent stem cells. Nature *471*, 63–67.

Grimm, M.O.W., Grimm, H.S., Tomic, I., Beyreuther, K., Hartmann, T., and Bergmann, C. (2008). Independent inhibition of Alzheimer disease β- and γ-secretase cleavage by lowered cholesterol levels. J. Biol. Chem. *283*, 11302–11311.

Guardia-Laguarta, C., Coma, M., Pera, M., Clarimón, J., Sereno, L., Agulló, J.M., Molina-Porcel, L., Gallardo, E., Deng, A., Berezovska, O. (2010). Mild Cholesterol Depletion Reduces Amyloid-β Production by Impairing APP Trafficking to the Cell Surface. *110*, 220–230.

Gunawardena, S., and Goldstein, L.S.B. (2001). Disruption of axonal transport and neuronal viability by amyloid precursor protein mutations in Drosophila. Neuron *32*, 389–401.

Guo, Q., Li, H., Gaddam, S.S.K., Justice, N.J., Robertson, C.S., and Zheng, H. (2012). Amyloid precursor protein revisited: Neuron-specific expression and highly stable nature of soluble derivatives. J. Biol. Chem. *287*, 2437–2445.

Haapasalo, A., and Kovacs, D.M. (2011). The many substrates of presenilin/??-secretase. J. Alzheimer's Dis. *25*, 3–28.

Hall, A.M., and Roberson, E.D. (2012). Mouse models of Alzheimer's disease. Brain Res. Bull. *88*, 3–12.

Heilig, E.A., Xia, W., Shen, J., and Kelleher, R.J. (2010). A presenilin-1 mutation identified in familial Alzheimer disease with cotton wool plaques causes a nearly complete loss of γ-secretase activity. J. Biol. Chem. *285*, 22350–22359.

Herreman, A., Hartmann, D., Annaert, W., Saftig, P., Craessaerts, K., Serneels, L., Umans, L., Schrijvers, V., Checler, F., Vanderstichele, H. (1999). Presenilin 2 deficiency causes a mild pulmonary phenotype and no changes in amyloid precursor protein processing but enhances the embryonic lethal phenotype of presenilin 1 deficiency. Proc. Natl. Acad. Sci. U. S. A. *96*, 11872–11877.

Hockemeyer, D., Wang, H., Kiani, S., Lai, C.S., Gao, Q., Cassady, J.P., Cost, G.J., Zhang, L., Santiago, Y., Miller, J.C. (2011). Genetic engineering of human pluripotent cells using TALE nucleases. Nat. Biotechnol. *29*, 731–734.

Hornsten, A., Lieberthal, J., Fadia, S., Malins, R., Ha, L., Xu, X., Daigle, I., Markowitz, M., O'Connor, G., Plasterk, R. (2007). APL-1, a Caenorhabditis elegans protein related to the human beta-amyloid precursor protein, is essential for viability. Proc. Natl. Acad. Sci. U. S. A. *104*, 1971–1976.

Hussein, S.M., Batada, N.N., Vuoristo, S., Ching, R.W., Autio, R., Närvä, E., Ng, S., Sourour, M., Hämäläinen, R., Olsson, C. (2011). Copy number variation and selection during reprogramming to pluripotency. Nature *471*, 58–62.

Israel, M. a., Yuan, S.H., Bardy, C., Reyna, S.M., Mu, Y., Herrera, C., Hefferan, M.P., Van Gorp, S., Nazor, K.L., Boscolo, F.S. (2012). Probing sporadic and familial Alzheimer's disease using induced pluripotent stem cells. Nature *482*, 216–220.

Jiang, Y., Mullaney, K. a, Peterhoff, C.M., Che, S., Schmidt, S.D., Boyer-Boiteau, A., Ginsberg, S.D., Cataldo, A.M., Mathews, P.M., and Nixon, R. a (2010). Alzheimer's-related endosome dysfunction in Down syndrome is Abeta-independent but requires APP and is reversed by BACE-1 inhibition. Proc. Natl. Acad. Sci. U. S. A. *107*, 1630–1635.

Jin, L.-W., Hua, D.H., Shie, F.-S., Maezawa, I., Sopher, B., and Martin, G.M. (2002). Novel tricyclic pyrone compounds prevent intracellular APP C99-induced cell death. J. Mol. Neurosci. *19*, 57–61.

De Jonghe, C., Esselens, C., Kumar-Singh, S., Craessaerts, K., Serneels, S., Checler, F., Annaert, W., Van Broeckhoven, C., and De Strooper, B. (2001). Pathogenic APP mutations near the gamma-secretase cleavage site differentially affect Abeta secretion and APP C-terminal fragment stability. Hum. Mol. Genet. *10*, 1665–1671.

Jonsson, T., Atwal, J.K., Steinberg, S., Snaedal, J., Jonsson, P. V., Bjornsson, S., Stefansson, H., Sulem, P., Gudbjartsson, D., Maloney, J. (2012). A mutation in APP protects against Alzheimer's disease and age-related cognitive decline. Nature *488*, 96–99.

Karch, C.M., and Goate, A.M. (2014). Alzheimer's Disease Risk Genes and Mechanisms of Disease Pathogenesis. Biol. Psychiatry *77*, 43–51.

Killick, R., Pollard, C.C., Asuni, A.A., Mudher, A.K., Richardson, J.C., Rupniak, H.T., Sheppard, P.W., Varndell, I.M., Brion, J.P., Levey, A.I. (2001). Presenilin 1 independently regulates beta-catenin stability and transcriptional activity. J. Biol. Chem. *276*, 48554–48561.

Kim, M., Suh, J., Romano, D., Truong, M.H., Mullin, K., Hooli, B., Norton, D., Tesco, G., Elliott, K., Wagner, S.L. (2009). Potential late-onset Alzheimer's disease-associated mutations in the ADAM10 gene attenuate α-secretase activity. Hum. Mol. Genet. *18*, 3987–3996.

Kim, S., Sato, Y., Mohan, P.S., Peterhoff, C., Pensalfini, a, Rigoglioso, a, Jiang, Y., and Nixon, R. a (2015). Evidence that the rab5 effector APPL1 mediates APP-βCTF-induced dysfunction of endosomes in Down syndrome and Alzheimer's disease. Mol. Psychiatry 1–10.

Koch, P., Tamboli, I.Y., Mertens, J., Wunderlich, P., Ladewig, J., Stüber, K., Esselmann, H., Wiltfang, J., Brüstle, O., and Walter, J. (2012). Presenilin-1 L166P mutant human pluripotent stem cell-derived neurons exhibit partial loss of γ-secretase activity in endogenous amyloid-β generation. Am. J. Pathol. *180*, 2404–2416.

Kojro, E., Gimpl, G., Lammich, S., Marz, W., and Fahrenholz, F. (2001). Low cholesterol stimulates the nonamyloidogenic pathway by its effect on the alpha - secretase ADAM 10. Proc. Natl. Acad. Sci. U. S. A. *98*, 5815–5820.

Kondo, T., Asai, M., Tsukita, K., Kutoku, Y., Ohsawa, Y., Sunada, Y., Imamura, K., Egawa, N., Yahata, N., Okita, K. (2013). Modeling Alzheimer's disease with iPSCs reveals stress phenotypes associated with intracellular Aβ and differential drug responsiveness. Cell Stem Cell *12*, 487–496.

Kounnas, M.Z., Moir, R.D., Rebeck, G.W., Bush, A.I., Argraves, W.S., Tanzi, R.E., Hyman, B.T., and Strickland, D.K. (1995). LDL receptor-related protein, a multifunctional ApoE receptor, binds secreted β-amyloid precursor protein and mediates its degradation. Cell *82*, 331–340.

Kuhn, P.-H., Wang, H., Dislich, B., Colombo, A., Zeitschel, U., Ellwart, J.W., Kremmer, E., Rossner, S., and Lichtenthaler, S.F. (2010). ADAM10 is the physiologically relevant, constitutive alpha-secretase of the amyloid precursor protein in primary neurons. EMBO J. *29*, 3020–3032.

Kumar-Singh, S., Theuns, J., Van Broeck, B., Pirici, D., Vennekens, K., Corsmit, E., Cruts, M., Dermaut, B., Wang, R., and Van Broeckhoven, C. (2006). Mean age-of-onset of familial Alzheimer disease caused by presenilin mutations correlates with both increased A??42 and decreased A??40. Hum. Mutat. *27*, 686–695.

Kurata, T., Miyazaki, K., Kozuki, M., Panin, V.L., Morimoto, N., Ohta, Y., Nagai, M., Ikeda, Y., Matsuura, T., and Abe, K. (2011). Atorvastatin and pitavastatin improve cognitive function and reduce senile plaque and phosphorylated tau in aged APP mice. Brain Res. *1371*, 161–170.

Lambert, J.C., Ibrahim-Verbaas, C. a, Harold, D., Naj, a C., Sims, R., Bellenguez, C., DeStafano, a L., Bis, J.C., Beecham, G.W., Grenier-Boley, B. (2013). Meta-analysis of 74,046 individuals identifies 11 new susceptibility loci for Alzheimer's disease. Nat. Genet. *45*, 1452–1458.

Lane-Donovan, C., Philips, G.T., and Herz, J. (2014). More than cholesterol transporters: lipoprotein receptors in CNS function and neurodegeneration. Neuron *83*, 771–787.

Larner, A.J., and Doran, M. (2006). Clinical phenotypic heterogeneity of Alzheimer's disease associated with mutations of the presenilin-1 gene. J. Neurol. *253*, 139–158.

Lazo, O.M., Gonzalez, a., Ascano, M., Kuruvilla, R., Couve, a., and Bronfman, F.C. (2013). BDNF Regulates Rab11-Mediated Recycling Endosome Dynamics to Induce Dendritic Branching. J. Neurosci. *33*, 6112–6122.

Lee, J.H., Yu, W.H., Kumar, A., Lee, S., Mohan, P.S., Peterhoff, C.M., Wolfe, D.M., Martinez-Vicente, M., Massey, A.C., Sovak, G. (2010). Lysosomal proteolysis and autophagy require presenilin 1 and are disrupted by Alzheimer-related PS1 mutations. Cell *141*, 1146–1158.

Leem, J.Y., Saura, C.A., Pietrzik, C., Christianson, J., Wanamaker, C., King, L.T., Veselits, M.L., Tomita, T., Gasparini, L., Iwatsubo, T. (2002). A Role for Presenilin 1 in Regulating the Delivery of Amyloid Precursor Protein to the Cell Surface. Neurobiol. Dis. *11*, 64–82.

Levitan, D., Doyle, T.G., Brousseau, D., Lee, M.K., Thinakaran, G., Slunt, H.H., Sisodia, S.S., and Greenwald, I. (1996). Assessment of normal and mutant human presenilin function in Caenorhabditis elegans. Proc. Natl. Acad. Sci. U. S. A. *93*, 14940–14944.

Levy, S., Sutton, G., Ng, P.C., Feuk, L., Halpern, A.L., Walenz, B.P., Axelrod, N., Huang, J., Kirkness, E.F., Denisov, G. (2007). The diploid genome sequence of an individual human. PLoS Biol. *5*, 2113–2144.

Lister, R., Pelizzola, M., Kida, Y.S., Hawkins, R.D., Nery, J.R., Hon, G., Antosiewicz-Bourget, J., O'Malley, R., Castanon, R., Klugman, S. (2011). Hotspots of aberrant epigenomic reprogramming in human induced pluripotent stem cells. Nature *471*, 68–73.

Liu, C.-C., Kanekiyo, T., Xu, H., and Bu, G. (2012). Apolipoprotein E and Alzheimer disease: risk, mechanisms, and therapy. Changes *29*, 997–1003.

Liu, Q., Waltz, S., Woodruff, G., Ouyang, J., Israel, M.A., Herrera, C., Sarsoza, F., Tanzi, R.E., Koo, E.H., Ringman, J.M. (2014). Effect of Potent γ -Secretase

Modulator in Human Neurons Derived From Multiple Presenilin 1–Induced Pluripotent Stem Cell Mutant Carriers. JAMA Neurol. *71*, 1481–1489.

Lu, D.C., Rabizadeh, S., Chandra, S., Shayya, R.F., Ellerby, L.M., Ye, X., Salvesen, G.S., Koo, E.H., and Bredesen, D.E. (2000). A second cytotoxic proteolytic peptide derived from amyloid beta-protein precursor. Nat. Med. *6*, 397–404.

Mali, P., Yang, L., Esvelt, K.M., Aach, J., Guell, M., DiCarlo, J.E., Norville, J.E., and Church, G.M. (2013). RNA-guided human genome engineering via Cas9. Science *339*, 823–826.

Mauch, D.H., Nägler, K., Schumacher, S., Göritz, C., Müller, E.C., Otto, a, and Pfrieger, F.W. (2001). CNS synaptogenesis promoted by glia-derived cholesterol. Science *294*, 1354–1357.

Maxfield, F.R. (2014). Role of endosomes and lysosomes in human disease. Cold Spring Harb. Perspect. Biol. *6*.

McPhie, D.L., Lee, R.K., Eckman, C.B., Olstein, D.H., Durham, S.P., Yager, D., Younkin, S.G., Wurtman, R.J., and Neve, R.L. (1997). Neuronal expression of beta-amyloid precursor protein Alzheimer mutations causes intracellular accumulation of a C-terminal fragment containing both the amyloid beta and cytoplasmic domains. J. Biol. Chem. *272*, 24743–24746.

Mecozzi, V.J., Berman, D.E., Simoes, S., Vetanovetz, C., Awal, M.R., Patel, V.M., Schneider, R.T., Petsko, G. a, Ringe, D., and Small, S. a (2014). Pharmacological chaperones stabilize retromer to limit APP processing. Nat. Chem. Biol. *10*, 443–449.

Miller, J.C., Tan, S., Qiao, G., Barlow, K.A., Wang, J., Xia, D.F., Meng, X., Paschon, D.E., Leung, E., Hinkley, S.J. (2011). A TALE nuclease architecture for efficient genome editing. Nat. Biotechnol. *29*, 143–148.

Moore, S., Evans, L.D.B., Andersson, T., Portelius, E., Smith, J., Dias, T.B., Saurat, N., McGlade, A., Kirwan, P., Blennow, K. (2015). APP Metabolism Regulates Tau Proteostasis in Human Cerebral Cortex Neurons. Cell Rep. *11*, 689–696.

Muratore, C.R., Rice, H.C., Srikanth, P., Callahan, D.G., Shin, T., Benjamin, L.N.P., Walsh, D.M., Selkoe, D.J., and Young-Pearse, T.L. (2014). The familial alzheimer's disease APPV717I mutation alters APP processing and Tau expression in iPSC-derived neurons. Hum. Mol. Genet. *23*, 3523–3536.

Murrell, J., Farlow, M., Ghetti, B., and Benson, M.D. (1991). A mutation in the amyloid precursor protein associated with hereditary Alzheimer's disease. Science (80-.). *254*, 97–99.

Nägler, K., Mauch, D.H., and Pfrieger, F.W. (2001). Glia-derived signals induce synapse formation in neurones of the rat central nervous system. J. Physiol. *533*, 665–679.

Naruse, S., Thinakaran, G., Luo, J.J., Kusiak, J.W., Tomita, T., Iwatsubo, T., Qian, X., Ginty, D.D., Price, D.L., Borchelt, D.R. (1998). Effects of PS1 deficiency on membrane protein trafficking in neurons. Neuron *21*, 1213–1221.

Neely, K.M., and Green, K.N. (2011). Presenilins mediate efficient proteolysis via the autophagosome-lysosome system. Autophagy *7*, 664–665.

Neely, K.M., Green, K.N., and LaFerla, F.M. (2011). Presenilin is necessary for efficient proteolysis through the autophagy-lysosome system in a γ-secretase-independent manner. J. Neurosci. *31*, 2781–2791.

Niederst, E.D., Reyna, S.M., and Goldstein, L.S.B. (2014). Axonal amyloid precursor protein and its fragments undergo somatodendritic endocytosis and processing. Mol. Biol. Cell *26*, 205–217.

Nixon, R. a., and Mcbrayer, M. (2013). Lysosome and Calcium Dysregulation in Alzheimer's disease - Partners in Crime. Biochem Soc Trans *41*, 1495–1502.

Nixon, R.A., and Yang, D.-S. (2011). Autophagy failure in Alzheimer's disease--locating the primary defect. Neurobiol. Dis. *43*, 38–45.

Oddo, S., Caccamo, A., Kitazawa, M., Tseng, B.P., and LaFerla, F.M. (2003). Amyloid deposition precedes tangle formation in a triple transgenic model of Alzheimer's disease. In Neurobiology of Aging, pp. 1063–1070.

Opar, A. (2008). Mixed results for disease-modification strategies for Alzheimer's disease. Nat. Rev. Drug Discov. *7*, 717–718.

Paşca, A.M., Sloan, S. a, Clarke, L.E., Tian, Y., Makinson, C.D., Huber, N., Kim, C.H., Park, J.-Y., O'Rourke, N. a, Nguyen, K.D. (2015). Functional cortical neurons and astrocytes from human pluripotent stem cells in 3D culture. Nat. Methods *12*.

Perez-Tur, J., Froelich, S., Prihar, G., Crook, R., Baker, M., Duff, K., Wragg, M., Busfield, F., Lendon, C., and Clark, R.F. (1995). A mutation in Alzheimer's disease destroying a splice acceptor site in the presenilin-1 gene. Neuroreport *7*, 297–301.

Pfrieger, F.W. (2003). Role of cholesterol in synapse formation and function. Biochim. Biophys. Acta - Biomembr. *1610*, 271–280.

Pierrot, N., Tyteca, D., D'auria, L., Dewachter, I., Gailly, P., Hendrickx, A., Tasiaux, B., Haylani, L. El, Muls, N., N'Kuli, F. (2013). Amyloid precursor protein controls cholesterol turnover needed for neuronal activity. EMBO Mol. Med. *5*, 608–625.

Pietrzik, C.U., Busse, T., Merriam, D.E., Weggen, S., and Koo, E.H. (2002). The cytoplasmic domain of the LDL receptor-related protein regulates multiple steps in APP processing. EMBO J. *21*, 5691–5700.

Qiang, L., Fujita, R., Yamashita, T., Angulo, S., Rhinn, H., Rhee, D., Doege, C., Chau, L., Aubry, L., Vanti, W.B. (2011). Directed conversion of Alzheimer's disease patient skin fibroblasts into functional neurons. Cell *146*, 359–371.

Radde, R., Duma, C., Goedert, M., and Jucker, M. (2008). The value of incomplete mouse models of Alzheimer's disease. Eur. J. Nucl. Med. Mol. Imaging *35*.

Refolo, L.M., Eckman, C., Prada, C.M., Yager, D., Sambamurti, K., Mehta, N., Hardy, J., and Younkin, S.G. (1999). Antisense-induced reduction of presenilin 1 expression selectively increases the production of amyloid ??42 in transfected cells. J. Neurochem. *73*, 2383–2388.

Rockenstein, E., Mallory, M., Mante, M., Sisk, A., and Masliaha, E. (2001). Early formation of mature amyloid-β protein deposits in a mutant APP transgenic model depends on levels of Aβ1-42. J. Neurosci. Res. *66*, 573–582.

Rodrigues, E.M., Weissmiller, A.M., and Goldstein, L.S.B. (2012). Enhanced ??-secretase processing alters APP axonal transport and leads to axonal defects. Hum. Mol. Genet. *21*, 4587–4601.

Rogaeva, E., Meng, Y., Lee, J.H., Gu, Y., Kawarai, T., Zou, F., Katayama, T., Baldwin, C.T., Cheng, R., Hasegawa, H. (2007). The neuronal sortilin-related receptor SORL1 is genetically associated with Alzheimer disease. Nat. Genet. *39*, 168–177.

Roher, A.E., Kokjohn, T.A., Esh, C., Weiss, N., Childress, J., Kalback, W., Luehrs, D.C., Lopez, J., Brune, D., Kuo, Y.M. (2004). The Human Amyloid-?? Precursor Protein770 Mutation V717F Generates Peptides Longer Than Amyloid-??-(40-42) and Flocculent Amyloid Aggregates. J. Biol. Chem. *279*, 5829–5836.

Rovelet-Lecrux, A., Hannequin, D., Raux, G., Le Meur, N., Laquerrière, A., Vital, A., Dumanchin, C., Feuillette, S., Brice, A., Vercelletto, M. (2006). APP locus duplication causes autosomal dominant early-onset Alzheimer disease with cerebral amyloid angiopathy. Nat. Genet. *38*, 24–26.

Sakane, H., Yamamoto, H., and Kikuchi, A. (2010). LRP6 is internalized by Dkk1 to suppress its phosphorylation in the lipid raft and is recycled for reuse. J. Cell Sci. *123*, 360–368.

Sander, J.D., Cade, L., Khayter, C., Reyon, D., Peterson, R.T., Joung, J.K., and Yeh, J.-R.J. (2011). Targeted gene disruption in somatic zebrafish cells using engineered TALENs. Nat. Biotechnol. *29*, 697–698.

Sato, T., Dohmae, N., Qi, Y., Kakuda, N., Misonou, H., Mitsumori, R., Maruyama, H., Koo, E.H., Haass, C., Takio, K. (2003). Potential link between amyloid beta-protein 42 and C-terminal fragment gamma 49-99 of beta-amyloid precursor protein. J. Biol. Chem. *278*, 24294–24301.

Sato, T., Diehl, T.S., Narayanan, S., Funamoto, S., Ihara, Y., De Strooper, B., Steiner, H., Haass, C., and Wolfe, M.S. (2007). Active γ-secretase complexes contain only one of each component. J. Biol. Chem. *282*, 33985–33993.

Saura, C.A., Choi, S.Y., Beglopoulos, V., Malkani, S., Zhang, D., Rao, B.S.S., Chattarji, S., Kelleher, R.J., Kandel, E.R., Duff, K. (2004). Loss of presenilin function causes impairments of memory and synaptic plasticity followed by age-dependent neurodegeneration. Neuron *42*, 23–36.

Scheuner, D., Eckman, C., Jensen, M., Song, X., Citron, M., Suzuki, N., Bird, T.D., Hardy, J., Hutton, M., Kukull, W. (1996). Secreted amyloid beta-protein similar to that in the senile plaques of Alzheimer's disease is increased in vivo by the presenilin 1 and 2 and APP mutations linked to familial Alzheimer's disease. Nat. Med. *2*, 864–870.

Schor, N.F. (2011). What the halted phase III ??-secretase inhibitor trial may (or may not) be telling us. Ann. Neurol. *69*, 237–239.

Selfridge, A., Hyun, N., Chiang, C.-C., Reyna, S.M., Weissmiller, A.M., Shi, L.Z., Preece, D., Mobley, W.C., and Berns, M.W. (2015). Rat embryonic hippocampus and induced pluripotent stem cell derived cultured neurons recover from laser-induced subaxotomy. Neurophotonics *2*, 015006.

Shen, J., and Kelleher, R.J. (2007). The presenilin hypothesis of Alzheimer's disease: evidence for a loss-of-function pathogenic mechanism. Proc. Natl. Acad. Sci. U. S. A. *104*, 403–409.

Shen, J., Bronson, R.T., Chen, D.F., Xia, W., Selkoe, D.J., and Tonegawa, S. (1997). Skeletal and CNS defects in Presenilin-1-deficient mice. Cell *89*, 629–639.

Shepherd, C.E., Gregory, G.C., Vickers, J.C., Brooks, W.S., Kwok, J.B.J., Schofield, P.R., Kril, J.J., and Halliday, G.M. (2004). Positional effects of presenilin-1 mutations on tau phosphorylation in cortical plaques. Neurobiol. Dis. *15*, 115–119.

Sherrington, R., Rogaev, E.I., Liang, Y., Rogaeva, E. a, Levesque, G., Ikeda, M., Chi, H., Lin, C., Li, G., Holman, K., et al. (1995). Cloning of a gene bearing missense mutations in early-onset familial Alzheimer's disease. Nature *375*, 754–760.

Shi, Y., Kirwan, P., Smith, J., MacLean, G., Orkin, S.H., and Livesey, F.J. (2012). A human stem cell model of early Alzheimer's disease pathology in Down syndrome. Sci. Transl. Med. *4*, 124ra29.

Simons, M., Keller, P., De Strooper, B., Beyreuther, K., Dotti, C.G., and Simons, K. (1998). Cholesterol depletion inhibits the generation of beta-amyloid in hippocampal neurons. Proc. Natl. Acad. Sci. U. S. A. *95*, 6460–6464.

Sinha, S., and Lieberburg, I. (1999). Cellular mechanisms of beta-amyloid production and secretion. Proc. Natl. Acad. Sci. U. S. A. *96*, 11049–11053.

Soldner, F., Laganière, J., Cheng, A.W., Hockemeyer, D., Gao, Q., Alagappan, R., Khurana, V., Golbe, L.I., Myers, R.H., Lindquist, S. (2011). Generation of isogenic pluripotent stem cells differing exclusively at two early onset parkinson point mutations. Cell *146*, 318–331.

Song, Y., Hustedt, E.J., Brandon, S., and Sanders, C.R. (2013). Competition between homodimerization and cholesterol binding to the C99 domain of the amyloid precursor protein. Biochemistry *52*, 5051–5064.

Spires-Jones, T.L., and Hyman, B.T. (2014). The intersection of amyloid beta and tau at synapses in Alzheimer's disease. Neuron *82*, 756–771.

Sproul, A.A., Jacob, S., Pre, D., Kim, S.H., Nestor, M.W., Navarro-Sobrino, M., Santa-Maria, I., Zimmer, M., Aubry, S., Steele, J.W. (2014). Characterization and molecular profiling of PSEN1 familial alzheimer's disease iPSC-Derived neural progenitors. PLoS One *9*.

Stamford, A., and Strickland, C. (2013). Inhibitors of BACE for treating Alzheimer's disease: a fragment-based drug discovery story. Curr. Opin. Chem. Biol. *17*, 320–328.

Svennerholm, L., and Gottfries, C.G. (1994). Membrane lipids, selectively diminished in Alzheimer brains, suggest synapse loss as a primary event in early-onset form (type I) and demyelination in late-onset form (type II). J. Neurochem. *62*, 1039–1047.

Szpankowski, L., Encalada, S.E., and Goldstein, L.S.B. (2012). Subpixel colocalization reveals amyloid precursor protein-dependent kinesin-1 and dynein association with axonal vesicles. Proc. Natl. Acad. Sci. *109*, 8582–8587.

Takahashi, K., Tanabe, K., Ohnuki, M., Narita, M., Ichisaka, T., Tomoda, K., and Yamanaka, S. (2007a). Induction of Pluripotent Stem Cells from Adult Human Fibroblasts by Defined Factors. Cell *131*, 861–872.

Takahashi, M., Murate, M., Fukuda, M., Satoshi, S.B., Ohta, A., and Kobayashi, T. (2007b). Cholesterol Controls Lipid Endocytosis through Rab11. Mol. Biol. Cell *18*, 2667–2677.

Takahashi, R.H., Milner, T.A., Li, F., Nam, E.E., Edgar, M.A., Yamaguchi, H., Beal, M.F., Xu, H., Greengard, P., and Gouras, G.K. (2002). Intraneuronal Alzheimer abeta42 accumulates in multivesicular bodies and is associated with synaptic pathology. Am. J. Pathol. *161*, 1869–1879.

Tamboli, I.Y., Prager, K., Thal, D.R., Thelen, K.M., Dewachter, I., Pietrzik, C.U., St George-Hyslop, P., Sisodia, S.S., De Strooper, B., Heneka, M.T. (2008). Loss of gamma-secretase function impairs endocytosis of lipoprotein particles and membrane cholesterol homeostasis. J. Neurosci. *28*, 12097–12106.

Tamboli, I.Y., Hampel, H., Tien, N.T., Tolksdorf, K., Breiden, B., Mathews, P.M., Saftig, P., Sandhoff, K., and Walter, J. (2011). Sphingolipid storage affects autophagic metabolism of the amyloid precursor protein and promotes Abeta generation. J. Neurosci. *31*, 1837–1849.

Tarabal, O., Calderó, J., Lladó, J., Oppenheim, R.W., and Esquerda, J.E. (2001). Long-lasting aberrant tubulovesicular membrane inclusions accumulate in developing motoneurons after a sublethal excitotoxic insult: a possible model for neuronal pathology in neurodegenerative disease. J. Neurosci. *21*, 8072–8081.

Taylor, A.M., Blurton-jones, M., Rhee, S.W., Cribbs, D.H., and Carl, W. (2006). A Microfluidic Culture Platform for CNS Axonal Injury, Regeneration, and Transport. Nat. Methods *2*, 599–605.

Thinakaran, G., Borchelt, D.R., Lee, M.K., Slunt, H.H., Spitzer, L., Kim, G., Ratovitsky, T., Davenport, F., Nordstedt, C., Seeger, M., et al. (1996). Endoproteolysis of presenilin 1 and accumulation of processed derivatives in vivo. Neuron *17*, 181–190.

Torroja, L., Chu, H., Kotovsky, I., and White, K. (1999). Neuronal overexpression of APPL, the Drosophila homologue of the amyloid precursor protein (APP), disrupts axonal transport. Curr. Biol. *9*, 489–492.

Toyn, J.H., and Ahlijanian, M.K. (2014). Interpreting Alzheimer's disease clinical trials in light of the effects on amyloid-β. Alzheimers. Res. Ther. *6*, 14.

Tu, H., Nelson, O., Bezprozvanny, A., Wang, Z., Lee, S.F., Hao, Y.H., Serneels, L., De Strooper, B., Yu, G., and Bezprozvanny, I. (2006). Presenilins Form ER Ca2+ Leak Channels, a Function Disrupted by Familial Alzheimer's Disease-Linked Mutations. Cell *126*, 981–993.

Udayar, V., Buggia-Prévot, V., Guerreiro, R.L., Siegel, G., Rambabu, N., Soohoo, A.L., Ponnusamy, M., Siegenthaler, B., Bali, J., Simons, M. (2013). A Paired RNAi and RabGAP overexpression screen identifies Rab11 as a regulator of β-amyloid production. Cell Rep. *5*, 1536–1551.

Ullrich, O., Reinsch, S., Urbé, S., Zerial, M., and Parton, R.G. (1996). Rab11 regulates recycling through the pericentriolar recycling endosome. J. Cell Biol. *135*, 913–924.

Vassar, R., Kuhn, P.H., Haass, C., Kennedy, M.E., Rajendran, L., Wong, P.C., and Lichtenthaler, S.F. (2014). Function, therapeutic potential and cell biology of BACE proteases: Current status and future prospects. J. Neurochem. *130*, 4–28.

Vieira, S.I., Rebelo, S., Esselmann, H., Wiltfang, J., Lah, J., Lane, R., Small, S.A., Gandy, S., da Cruz E Silva, E.F., and da Cruz E Silva, O.A. (2010). Retrieval of the Alzheimer's amyloid precursor protein from the endosome to the TGN is S655 phosphorylation state-dependent and retromer-mediated. Mol. Neurodegener. *5*, 40.

Wahrle, S., Das, P., Nyborg, A.C., McLendon, C., Shoji, M., Kawarabayashi, T., Younkin, L.H., Younkin, S.G., and Golde, T.E. (2002). Cholesterol-dependent gamma-secretase activity in buoyant cholesterol-rich membrane microdomains. Neurobiol. Dis. *9*, 11–23.

Wang, B., Yang, W., Wen, W., Sun, J., Su, B., Liu, B., Ma, D., Lv, D., Wen, Y., Qu, T. (2010). γ-Secretase Gene Mutations in Familial Acne Inversa. Science (80-.). *330*, 1065–1065.

Weissmiller, A.M., Natera-Naranjo, O., Reyna, S.M., Pearn, M.L., Zhao, X., Nguyen, P., Cheng, S., Goldstein, L.S.B., Tanzi, R.E., Wagner, S.L. (2015). A γ-Secretase Inhibitor, but Not a γ-Secretase Modulator, Induced Defects in BDNF Axonal Trafficking and Signaling: Evidence for a Role for APP. PLoS One *10*, e0118379.

Welz, T., Wellbourne-Wood, J., and Kerkhoff, E. (2014). Orchestration of cell surface proteins by Rab11. Trends Cell Biol. *24*, 407–415.

Wiley, J.C., Hudson, M., Kanning, K.C., Schecterson, L.C., and Bothwell, M. (2005). Familial Alzheimer's disease mutations inhibit gamma-secretase-mediated liberation of beta-amyloid precursor protein carboxy-terminal fragment. J. Neurochem. *94*, 1189–1201.

Wilson, J.M., de Hoop, M., Zorzi, N., Toh, B.H., Dotti, C.G., and Parton, R.G. (2000). EEA1, a tethering protein of the early sorting endosome, shows a polarized distribution in hippocampal neurons, epithelial cells, and fibroblasts. Mol. Biol. Cell *11*, 2657–2671.

Wolfe, D.M., Lee, J. hyun, Kumar, A., Lee, S., Orenstein, S.J., and Nixon, R.A. (2013). Autophagy failure in Alzheimer's disease and the role of defective lysosomal acidification. Eur. J. Neurosci. *37*, 1949–1961.

Wolozin, B. (2004). Cholesterol and the Biology of Alzheimer's Disease. Neuron *41*, 7–10.

Woodruff, G., Young, J.E., Martinez, F.J., Buen, F., Gore, A., Kinaga, J., Li, Z., Yuan, S.H., Zhang, K., and Goldstein, L.S.B. (2013). The Presenilin-1 δE9 Mutation Results in Reduced γ-Secretase Activity, but Not Total Loss of PS1 Function, in Isogenic Human Stem Cells. Cell Rep. *5*, 974–985.

Wu, L., Rosa-Neto, P., Hsiung, G.-Y.R., Sadovnick, A.D., Masellis, M., Black, S.E., Jia, J., and Gauthier, S. (2012). Early-onset familial Alzheimer's disease (EOFAD). Can. J. Neurol. Sci. *39*, 436–445.

Xia, D., Watanabe, H., Wu, B., Lee, S.H., Li, Y., Tsvetkov, E., Bolshakov, V.Y., Shen, J., and Kelleher, R.J. (2015). Presenilin-1 Knockin Mice Reveal Loss-of-Function Mechanism for Familial Alzheimer's Disease. Neuron *85*, 967–981.

Yagi, T., Ito, D., Okada, Y., Akamatsu, W., Nihei, Y., Yoshizaki, T., Yamanaka, S., Okano, H., and Suzuki, N. (2011). Modeling familial Alzheimer's disease with induced pluripotent stem cells. Hum. Mol. Genet. *20*, 4530–4539.

Yap, C.C., Wisco, D., Kujala, P., Lasiecka, Z.M., Cannon, J.T., Chang, M.C., Hirling, H., Klumperman, J., and Winckler, B. (2008). The somatodendritic endosomal regulator NEEP21 facilitates axonal targeting of L1/NgCAM. J. Cell Biol. *180*, 827–842.

Young, J.E., Boulanger-Weill, J., Williams, D.A., Woodruff, G., Buen, F., Revilla, A.C., Herrera, C., Israel, M.A., Yuan, S.H., Edland, S.D. (2015). Elucidating Molecular Phenotypes Caused by the SORL1 Alzheimer's Disease Genetic Risk Factor Using Human Induced Pluripotent Stem Cells. Cell Stem Cell *16*, 373–385.

Yuan, S.H., Martin, J., Elia, J., Flippin, J., Paramban, R.I., Hefferan, M.P., Vidal, J.G., Mu, Y., Killian, R.L., Israel, M.A. (2011). Cell-surface marker signatures for the Isolation of neural stem cells, glia and neurons derived from human pluripotent stem cells. PLoS One *6*.

Zhang, M., Haapasalo, A., Kim, D.Y., Ingano, L. a M., Pettingell, W.H., and Kovacs, D.M. (2006). Presenilin/gamma-secretase activity regulates protein clearance from the endocytic recycling compartment. FASEB J. *20*, 1176–1178.

Zhang, Y., Chen, K., Sloan, S. a, Bennett, M.L., Scholze, A.R., Keeffe, S.O., Phatnani, H.P., Guarnieri, X.P., Caneda, C., Ruderisch, N. (2014). An RNA-Sequencing Transcriptome and Splicing Database of Glia , Neurons , and Vascular Cells of the Cerebral Cortex. *34*, 1–19.

Zheng, H., Jiang, M., Trumbauer, M.E., Sirinathsinghji, D.J., Hopkins, R., Smith, D.W., Heavens, R.P., Dawson, G.R., Boyce, S., Conner, M.W. (1995). beta-Amyloid precursor protein-deficient mice show reactive gliosis and decreased locomotor activity. Cell *81*, 525–531.